ENERGY SPECTRA OF ALPHA PARTICLES EMITTED FROM ^{27}Al, ^{54}Fe, ^{63}Cu, ^{64}Zn and ^{107}Ag IRRADIATED WITH FAST NEUTRONS

by

M. IRFAN

Department of Natural Philosophy,

University of Glasgow

PRESENTED AS A THESIS FOR THE DEGREE OF Ph.D.

IN THE UNIVERSITY OF GLASGOW, JANUARY, 1962.

PREFACE

This thesis is based on the work carried out in the Department of Natural Philosophy of Glasgow University during the period June 1960 - December 1961, after two years of preliminary experimentation with the research group working on Fast Neutron Physics utilising the beam of a 1 MeV deuteron accelerator. Energy distributions of alpha particles emitted, in a forward direction, from ^{27}Al, ^{54}Fe, ^{63}Cu, ^{64}Zn and ^{107}Ag on bombardment with 14.8 MeV neutrons have been studied using a proportional counter - scintillation counter telescope. Neutrons were obtained from the nuclear reaction $^{3}H(d,n)^{4}He$ for which deuterons were accelerated using a 160 KV Cockroft-Walton accelerator. The counter telescope was designed primarily to obtain good statistics for the energy spectra even at some sacrifice of angular resolution. However an attempt was later made to modify this telescope to obtain good angular resolution, and results for the angular distributions of alpha particles from ^{27}Al are also presented.

Since the reactions studied here fall within the general scheme of reactions at intermediate energies with medium weight nuclei, Chapter 1 has been devoted

to a review of this field. The limited work done so far on (n,α) energy and angular distributions by other investigators has been surveyed in Chapter 2.

After an introduction explaining the principle of the experimental technique employed, Chapter 3 describes the design and development of counter telescopes for the measurement of energy spectra and angular distributions of alpha particles emitted from thin targets bombarded with fast neutrons. The chapter concludes with a description of the experimental procedure. Part of this work was done in collaboration with Dr. W. Jack, the joint contributions being, the evolution of the principle of the technique and the design and development of the counter telescope used in measuring the energy spectra. The author is solely responsible for the modifications to the apparatus which were required in the studies of the angular distributions, and for the application of both telescopes to obtaining the final data - upon energy spectra and angular distributions.

After presenting the basic results in Chapter 4, their detailed analysis and interpretation have been given in Chapter 5. The material presented in these two chapters is entirely due to the author but he is grateful to Dr. W. Jack for many helpful suggestions and

discussions. Chapter 5 is followed by a brief narration of suggestions for improvements and future programme.

Two appendices are attached to the thesis. One describes and discusses the study, carried out by the author in connection with this work, of the luminescent response of CsI(Tl) to alpha particles. The other gives some elaborations of the mathematics used in Chapter 1.

It gives the author great pleasure in offering sincere thanks to Professor P.I. Dee for the encouragement that the author derived from his sustained interest in this work at all stages. Thanks are also due to several other colleagues and technical and workshop staff.

CONTENTS

CHAPTER 1. NUCLEAR REACTIONS AT INTERMEDIATE ENERGIES WITH MEDIUM WEIGHT NUCLEI

1.1 Introduction

The occurrence of sharp resonance peaks in the excitation functions and the predominance of absorption over scattering in low energy nuclear reactions (ref. 1) led Bohr to put forward his 'compound nucleus model' for nuclear reaction mechanism in 1936 (ref. 2). Breit and Wigner derived an expression, in the same year, for cross sections (ref. 3). They did it by an adaptation of the time-dependent perturbation theory of resonance absorption and subsequent emission of optical radiation by an atomic system. The Breit and Wigner expression gives excellent fits to observed cross-sections but the interpretation of values of the parameters obtained from such fittings presents difficulties. The 'form' of the expression appears to be correct because this (the form) depends only on the condition that the reaction proceeds through a long lived intermediate state - the compound nucleus picture of Bohr. The otherwise failure of this expression is due to the fact that nuclear forces cannot be treated as perturbation. Bethe in 1937 gave a quantitative discussion of nuclear

reactions in terms of the compound nucleus mechanism using time-independent perturbation theory (ref. 4). Later on, Weisskopf (ref. 5), Bethe and Placzek (ref. 6) and Weisskopf and Ewing (ref. 7) investigated the detailed consequences of Bohr's theory. All these discussions were in terms of compound nucleus model and were of limited applicability and non-rigorous. In 1938 Kapur and Peierls (ref. 8) presented their theory of nuclear reactions which was not dependent on any idealized model and which was also mathematically rigorous. During the next few years Breit and collaborators as well as Wigner and collaborators also presented papers on the general and rigorous theory of nuclear reactions, with different approaches. In 1947 Wigner and Eisenbud formulated their R-matrix theory (ref. 9). In principle, R-matrix formalism or Kapur-Peierls formalism or any other rigorous formalism of the same generality should be individually sufficient for a complete treatment of nuclear reactions. R-matrix theory, however, is more suited to compound nucleus type of reactions, specially where relatively low level densities are involved. On the other hand, Kapur-Peierls formalism is better suited for higher excitation energies where level densities are, on the average, higher. But, in any case,

the application of formalisms of such generality to practical problems is somewhat formidable. To 'visualize' reaction mechanism through experiments, it is quite profitable to use more simplified (and thus more restricted) theories based on idealized models. The 'Statistical Model' and some of the 'Direct Interaction' theories will be discussed at some length later in this chapter. The 'Optical Model' (also called 'complex potential model' or 'cloudy crystal ball model') will also be referred to at appropriate points. We shall conclude this introductory section by giving a physical picture of the processes involved.

The Compound nucleus model is a 'strong absorption' model. The incident particle is immediately absorbed after its arrival at the target nucleus and its energy (incident particle's) is very quickly shared by other nucleons. The compound state is long lived and its decay is independent of its particular mode of formation. (Conservation laws are, of course, obeyed.) Nuclear levels are of the order of electron volts wide - these being, well separated at low energies, wider and closer at higher energies and eventually overlapping. For very high excitation energies ($\gtrsim$ 100 MeV) the levels are too wide, and 'compound state' is too short lived to

be a meaningful intermediate state at all. At intermediate energies and for not too light nuclei, transitions between levels can be treated with methods analogous to statistical thermodynamics (assuming random phase relationship between various levels) and 'statistical model' of Weisskopf and Ewing is developed for such cases (ref. 7).

The optical model is essentially a 'weak absorption' model. Motion of the incident particle is described by replacing the target nucleus with a complex potential well. The imaginary part of the potential is needed to account for the disappearance of the incident particle from the 'entrance channel'; otherwise only potential (or shape-elastic) scattering will take place. The complex potential thus endows the target nucleus with a sort of diffuseness. What happens after the particle is absorbed is not a direct concern of the optical model. The compound system formed in this picture offers much wider possibilities than the 'compound nucleus' of Bohr, which is included in optical model as a special case when the imaginary part is too high and the absorbed particle loses its energy very quickly. The emergent particle, when the compound system has broken up, will be moving in the potential well of the residual nucleus. The

most important aspect of the whole picture is the appearance of 'single particle states' due to the motion of the particle in a potential well. These states (or levels) are of the order of MeV wide and their resonances can yield broad maxima in excitation functions, in contrast with the sharp maxima of compound nucleus model. The averaging over many sharp resonance maxima, on the compound nucleus basis, predicts a smooth (average) variation. When the experiments proved contrary to this prediction and instead 'giant maxima' were observed even at low energies in 1952 (ref. 10), the single particle states were identified as the origin of these broad maxima (superimposed on sharp maxima). Thus the concept of optical model describing the 'average' behaviour was established by Feshbach, Porter and Weisskopf in 1953 (ref. 11). This picture also accommodates several other modes of nuclear reactions contradictory to the compound nucleus model by allowing a direct 'knockout' process or excitation of some kind of 'collective' states, or of 'rotational' or 'vibrational states etc. These non-compound nucleus processes are generally termed as 'direct nuclear reactions'. They generally start showing up above~10 MeV ~~or so~~ incident energy, and are normally found to be restricted to transitions to low lying states

of the residual nucleus.

In 1955, Lane, Thomas and Wigner formulated an 'Intermediate Coupling Model' (ref. 12). This is a step towards compromise between the two extremes - the use of either single particle states only or of compound states only. This, also, is a potential well description but instead of including the non-elastic processes by ascribing an imaginary part to the potential 'to do the absorption' they use a real potential well and nuclear reactions are explained by considering the effect of the replacement of the average potential by the sum of the potentials of the individual nucleons of the target nucleus.

The extent of success and limitations of various models will be more closely examined in another section of this chapter dealing with the experimental evidence about nuclear reaction mechanisms.

According to the basic assumptions of various models the (n,d) reactions in medium weight nuclei, even with such a high neutron energy as 15 MeV, are expected to proceed mainly according to the statistical model. However, the possibility of departures from theoretical predictions cannot be excluded in this very interesting energy region where direct interactions are known to play an important role

in certain types of reactions.

1.2 The Statistical Model

(a) General Considerations

Consider the nuclear reaction X(a,b)Y, which proceeds via an intermediate compound state. The cross section for the reaction can be expressed as

$$\sigma(a,b) = \sigma_c(a)\, G_c(b) \qquad (1)$$

where σ_c (a) is the cross section for the formation of the compound nucleus by particle 'a' incident upon the target nucleus X, and $G_c(b)$ is the probability of the 'disintegration' of the compound nucleus into particle 'b' and the residual nucleus Y.

If the compound nucleus is formed with sufficiently high excitation energy, then its decay can be studied by statistical methods. The evaporation model of Weisskopf, 1937 (ref. 5 & 7) does this. σ_c can be estimated on the basis of the 'continuum model' (also called the 'schematic model') developed by Feshbach and Weisskopf, 1949 (ref. 13 & 14). This strong coupling model is based upon a very simplified picture of nuclear structure and the only information employed about the internal

structure of the nucleus is its radius R (a well defined one) and the wave number K of particle 'a' within the nucleus. It is assumed that the particle 'a', after it has penetrated in the nucleus, does not reappear in the incident channel. It is further assumed that the average kinetic energy of 'a' is the sum of its incident kinetic energy and the kinetic energy of the intra nuclear motion.

σ_c has also been calculated, for some cases, from the weak coupling model of the 'complex potential'.

The expression obtained from evaporation model for the probability of decay of the compound nucleus by the emission of particle 'b' of energy E_b, (leaving an excited nucleus Y), contains the cross-section for the inverse process of formation of a compound nucleus by a collision with energy E_b between particle 'b' and the excited residual nucleus Y. At the moment values for this cross-section have not been calculated for the excited nucleus case and in practical problems the values which are used are those for the ground state. (Identical with σ_c, calculated for the appropriate particle and the target).

Before going into some details of the expressions for σ_c and the decay of compound nucleus etc, we think it is appropriate to say a few words about the physical aspects of the concept of nuclear level and its properties.

For a level of width Γ , the probability of decay of that level per unit time is $\Gamma/\hbar$. The reciprocal quantity $\frac{\hbar}{\Gamma}$ gives the mean life of the level τ . A level of width Γ having a number of possible competing modes of decay, has a corresponding number of 'partial widths' Γ_i , and $\Gamma = \sum_i \Gamma_i$. The levels are not uniformly spaced in energy, but it is convenient to think of an average level distance D in any particular region of excitation energy. Weisskopf, 1950 (ref. 15) has given a simple semiclassical picture connecting Γ and D, and the transparency T of the nuclear barrier at this excitation energy. According to this description, any particular configuration of the compound nucleus repeats itself with a recurrence time $\Delta t = (2\pi\hbar)/D$. Thus, after entering the nucleus the particle 'a' comes back to the surface after time 'Δt' with its energy re-established, and ready to leave the compound nucleus. However, due to a large potential step at the nuclear surface the particle is reflected back into the nucleus and it starts its motion inside all over again. This repetition of the motion is essential for the existence of well-defined compound states. But we know that the compound states do decay. This is taken into account by introducing a certain probability of leakage through the barrier. For an emission of the

particle with angular momentum ℓ, this leakage probability is given by the 'partial' transmission coefficient T_ℓ. The partial width of the level is $\Gamma_\ell \simeq T_\ell \frac{D_\ell}{2\pi}$. Thus $\Gamma_\ell \ll D_\ell$ i.e. discrete spectrum of levels requires T_ℓ to be very small, and the particle suffers several thousands or millions reflections before re-emission. This is the situation applicable to low energies. It has been established experimentally that D_ℓ of the levels decreases with increasing excitation energy and this might have made Γ_ℓ also smaller for higher energies but for the overriding effect of increase in T_ℓ. In fact, the widths of the level increase and eventually they overlap. The situation in this region of excitation energy corresponds to the mean life time of the compound being smaller than the repitition time. This makes it unlikely for the particle 'a' to reappear in the incident channel. If the excitation energy is too high then, of course, the too short mean life of the compound state invalidates the use of the picture of a proper intermediate state. The energy region of our interest is described by $\tau < \Delta t$ but not $\tau \ll \Delta t$

(b) <u>Formation of the Compound Nucleus. (based on the continuum model)</u>.

We wish to derive an expression for σ_c. To do

this we first write down the expression for the total reaction cross section σ_r.

$$\sigma_r = \pi \lambda^2 \sum_l (2l+1)(1 - |\eta_l|^2) \qquad (1.2)$$

This expression for σ_r has been obtained by taking a plane incident wave; expanding it into spherical harmonics; and then including the effect of the disturbance due to the nuclear interaction, by introducing complex ~~nucleons~~ numbers η_l, $(|\eta_l| \ll 1)$ as the coefficients to the outgoing sub-waves of angular momenta l (from zero to infinity). $\lambda = \frac{1}{k}$ where k is the wave number in the incident channel.

The continuum model makes certain assumptions about the conditions at the nuclear surface and then relates η_l to them. We consider the logarithmic derivative f_l, of the radial wave function $u_l(r)$ evaluated at the nuclear surface $r = R$

$$\text{ie,} \qquad f_l \equiv R\left[\frac{du_l}{dr} \Big/ u_l\right]_{r=R} \qquad (1.3)$$

For $r > R$, $u_l(r)$ can be separated into ingoing and outgoing waves. We write down,

$$u_l(r) = A\, u_l^{(-)}(r) + B\, u_l^{(+)}(r) \qquad (1.4)$$

where A and B are constants. It follows that $\eta_l = -\frac{B}{A}$

We introduce two quantities S_l and P_l by the relation,

$$R\left[\frac{d u_\ell^{(+)}(r)}{dr} \Big/ u_\ell^{(+)}(r)\right]_{r=R} \equiv S_\ell + i P_\ell \qquad (1.5)$$

The real numbers S_ℓ and P_ℓ are completely determined from conditions outside the nucleus, and depend on k, R, ℓ, and on a parameter which determines the importance of the coulomb effects.

We also define the phase constant ξ_ℓ by the equation,

$$\exp(2i\xi_\ell) = u_\ell^{(-)}(R) / u_\ell^{(+)}(R) \qquad (1.6)$$

It can be shown that,

$$\eta_\ell = \frac{f_\ell - S_\ell + i P_\ell}{f_\ell - S_\ell - i P_\ell} \exp(2i\xi_\ell) \qquad (1.7)$$

Two assumptions of the continuum model are now introduced. Firstly, for $r<R$, $u_\ell(r)$ will be assumed to be of the form of an ingoing wave only, that is, $u_\ell(r) \sim \exp(-iKr)$ inside the nucleus, which in view of the continuity of f_ℓ at the nuclear surface gives,

$$f_\ell = -iKR \qquad (1.8)$$

Secondly, the wave number K for the particle 'a' after it has entered the nucleus will be assumed to be given by

$$K^2 = k^2 + k_o^2 \qquad (1.9)$$

where k_o is the contribution from the intra-nuclear motion, i.e. it is the value of 'K' when the incident particle

enters with zero energy.

Since it is implied that the incident particle does not reappear in the incident channel (after having entered the nucleus), $\sigma_c = \sigma_r$.

Using equations 1.2, 1.7 and 1.8, it can be shown that,

$$\sigma_c = \pi \lambda^2 \sum_l (2l+1) \frac{4 P_l KR}{S_l^2 + (KR + P_l)^2} \qquad (1.10)$$

An alternative description of σ_c is in terms of the penetrability of the nuclear surface,

$$\sigma_c = \pi \lambda^2 \sum_l (2l+1) \; T_l \qquad (1.11)$$

where T_l , the partial wave transmission coefficient can be identified with the quantity $[1 - |\eta_l|^2]$

The transmission coefficients T_l can be calculated exactly for neutrons but for charged particles approximations have to be made. (Ref. 16) gives tables of σ_c calculated by Shapiro, (ref. 54) for alpha particles (and protons) for a range of energy and Z number; and values for other energies and Z can be determined by interpolation.

(c) <u>Formation of the Compound Nucleus (based on the optical model)</u>.

Feshbach, Porter and Weisskopf 1954, (ref. 11) have derived an expression for σ_c for neutrons, using a square

well complex potential. For more recent modifications of the optical model potential, the complexity of calculations requires electronic computer techniques. For alpha particles, Igo, 1959 (ref. 17), has calculated σ_c, for a potential $V+iW$ whose shape is exponential at the nuclear surface. The potential which was obtained from the analysis of the data on the elastic scattering of alpha particles, is given by

$$V+iW = \left\{-1100 \exp\left[-\left(\frac{r-1.17A^{1/3}}{0.574}\right)\right] - 45.7i \exp\left[-\left(\frac{r-1.40A^{1/3}}{0.578}\right)\right]\right\}_{\text{Mev.}} \quad (1.12)$$

Tables are given for some values of σ_c and others can be obtained by interpolation.

(d) Nuclear Level Densities and Nuclear Temperature

The nuclear level density, which we shall denote by ω, plays an important role in the statistical theory. We shall briefly discuss it before we come to the decay of the compound nucleus (next section).

First we shall describe the expression for 'ω', due to Bethe, 1936,37 (ref. 18,19). He used an approach analogous to the statistical thermodynamics and assumed that the nucleus was a Fermi-gas of A particles. He found,

$$\omega(E) = \frac{e^{S(E)}}{\Theta \left(2\pi \frac{dE}{d\Theta}\right)^{1/2}} \qquad (1.13)$$

where E is the energy of the system; S the entropy; and Θ, the nuclear temperature measured in energy units and equivalent to the usual 'kT' term of statistical thermodynamics. ω depends on 'A' too, and by $\omega(E)$, we mean $\omega(A,E)$.

To calculate 'ω' from equation 13, either some model has to be adopted for the 'heat content' of the system, or some general assumption has to be made for relating E and Θ, (the constants to be determined by fitting the data). For a general power law dependence $E = a\Theta^n$, Bethe obtained,

$$\omega(E) = (2\pi n)^{-\frac{1}{2}} \left[a/E^{n+1} \right]^{+\frac{1}{2}n} \cdot \exp\left[\frac{n}{n-1} a^{\frac{1}{n}} E^{\frac{n-1}{n}} \right] \qquad (1.14)$$

For the Fermi-gas model n = 2; and for the liquid drop model n = $^7/_3$ and 4 at low and high excitation energies, respectively.

If the coefficient can be considered constant, then for the Fermi-gas model

$$\omega(E) = C \exp\left[2(aE)^{1/2}\right] \qquad (1.15)$$

It has been realized that the odd-even character of the nucleus affects the level density, and it is explained

in terms of a shift in the position of the effective ground state of a nucleus caused by nucleon pairing. Lang and Le Couteur, 1954 (ref. 21) have also calculated ω for a Fermi gas nucleus. They derive the equation

$$\omega = \frac{\pi^{1/2}}{12}\left(\frac{f}{A}\right)^{3/2}\theta^{-5/2}\exp 2\left(\frac{AE}{f}\right)^{1/2} \qquad (1.16)$$

for which they used the following relation between E and θ,

$$E = \frac{A}{f}\theta^2 - \theta \qquad (1.17)$$

where 'f' is an adjustable parameter. They have also pointed out how to take "nuclear surface waves" effect into consideration.

Newton, 1956 (ref. 22) has considered the shell effects in a Fermi-gas model. An approximate relationship for θ , on that basis is given by,

$$\theta \cong 3.2\, A^{-1/2} E^{1/2} \qquad (1.18)$$

When we speak of the density of levels of a particular angular momentum J, and denote it by $\omega(J)$, then the total level density is obtained by the relation,

$$\omega = \sum_J (2J+1)\,\omega(J)$$

Now we give the definition of an approximate nuclear temperature, denoted by T, which is more commonly used in deducing conclusions from the experiments. Reverting to equation 1.13, we write it down in an alternative form,

$$\frac{d}{dE}\left(\log_e \omega\right) = \frac{1}{\theta} - \frac{1}{2}\frac{d}{dE}\left(\log_e\left[\theta^2 \frac{dE}{d\theta}\right]\right) \qquad \text{SEE APPENDIX.II} \qquad (1.19)$$

For practical purposes the second term on the R.H.S. of eq. 1.19, can be neglected and an approximate nuclear temperature 'T' is obtained,

$$\frac{d}{dE}\left(\log_e \omega\right) = \frac{1}{T} \quad , \quad T, \text{always} > \theta \qquad (1.20)$$

(e) Decay of the Compound Nucleus

Now we consider the factor $G_c(b)$ in the relation $\sigma(a,b) = \sigma_c(a) G_c(b)$ If the particle 'b' is emitted into a specific channel β, with the corresponding partial width Γ_β, then the branching ratio $G_c(\beta)$ is equal to $\frac{\Gamma_\beta}{\sum_i \Gamma_i}$, where Γ_i is the partial width for any possible exit channel. From the reciprocity theorem of nuclear reactions, Weisskopf (ref. 5) has shown that the ratio $\frac{\sigma_c(\rho)}{\lambda_\rho^2 \Gamma_\rho}$ is independent of the channel 'ρ'. Using this property it can be shown that $G_c(\beta) = \frac{\Gamma_\beta}{\Gamma} = \frac{k_\beta^2 \sigma_c(\beta)}{\sum_\rho k_\rho^2 \sigma_c(\rho)}$. It may be noted that σ_c in the expression for $G_c(\beta)$ refers to the exit channels (i.e. it is for the inverse process). Taking into account the density of the levels of the residual nucleus into which the decay may proceed, one obtains

$$\sigma(a,b) = \sigma_c(a) \frac{F_b}{\sum_i F_i}$$

$$\text{with, } F_b = F(E_a+Q_{ab}) = \frac{2M_b}{\hbar^2}\int_0^{E_a+Q_{ab}} E_b \cdot \sigma_c(E_b)\cdot \omega_Y(E_a+Q_{ab}-E_b)\cdot dE_b \qquad (1.21)$$

SEE APPENDIX II

and similar expressions for F_i for the competing reactions $X(a,i)W$, where i and W stand for the general case of emitted particle i and the corresponding residual nucleus W.

E_a is the energy of a; Q_{ab} the Q-value for the reaction X(a,b)Y; M_b is reduced mass; $\sigma_c(E_b)$ is the cross section for the formation of compound nucleus by 'b' (with energy E_b) on the excited residual nucleus Y (with excitation energy $E_a + Q_{ab} - E_b$); and $\omega_Y(E_a + Q_{ab} - E_b)$ is the level density of excited Y nucleus at the energy of excitation.

If the residual nucleus is left with sufficiently high excitation energy, it may de-excite by an emission of another particle. The 'secondary reaction' can be, in principle, treated as the 'decay' of the residual nucleus.

(f) <u>The Evaporation Spectrum and the Statistical Plot</u>.

Consider the compound nucleus at excitation energy E_c. The probability that it decays by emission of the particle b, having spin s, with kinetic energy in the range E_b and $E_b + dE_b$, leaving the residual nucleus Y with the excitation energy in the range E_y and dE_y is given by Weisskopf as,

$$P(E_b)\,dE_b = \frac{(2S+1)\,M_b}{\pi^2 \hbar^3} \cdot \sigma_c(E_b) \cdot E_b \cdot \frac{\omega_y(E_y)}{\omega_c(E_c)}\, dE_y \qquad (1.22)$$

$E_c = E_b + E_y + B_{bc}$, where B_{bc} is the binding energy of b to the compound nucleus. σ_c is for the inverse process. The spectrum of the particle 'b' will be given by

$$\frac{dN(E_b)}{dE_b} \propto E_b \cdot \sigma_c(E_b) \cdot \omega_y(E_y) \qquad (1.23)$$

where $dN(E_b)$ is the number of particles b with the energy within E_b and $E_b + dE_b$.

From 1.23 we can write

$$\frac{d}{dE_b}\left[\log_e\left(\frac{dN(E_b)}{dE_b} \Big/ E_b \cdot \sigma_c(E_b)\right)\right] = \frac{d}{dE_y}\left(\log_e \omega_y(E_y)\right) \qquad (1.24)$$

But according to eq. 1.20, $\frac{d}{dE}(\log_e \omega) = \frac{1}{T}$, where T is the approximate nuclear temp.

Hence 1.24 leads to

$$\frac{d}{dE_b}\left[\log_e\left(\frac{dN(E_b)}{dE_b} \Big/ E_b \cdot \sigma_c(E_b)\right)\right] = \frac{1}{T} \qquad (1.25)$$

The temperature T obtained from 1.25 will be for the residual nucleus at the excitation energy E_y.

If the quantity $\mathrm{Log}_e\left(\frac{dN(E_b)}{dE_b} \Big/ E_b \cdot \sigma_c(E_b)\right)$ is plotted against E_b the slope of the curve at every point will give the temperature T for the corresponding energy of excitation of the residual nucleus. This plot is called the

statistical plot.

For E_b much less than $(E_c - B_{bc})$, it can be shown that

$$\frac{dN(E_b)}{dE_b} \propto E_b \cdot \sigma_c(E_b) \cdot \exp\left(-\frac{E_b}{T_m}\right) \qquad \text{SEE APPENDIX II} \quad (1.26)$$

where T_m is the value of T for maximum excitation energy of the residual nucleus. If particle 'b' is a neutron then σ_c does not change much with the energy and shape of the spectrum will be nearly maxwellian. For charged particles due to strong dependence of σ_c on energy the shape will depart from Maxwellian nature according to the extent of coulomb effects.

(g) The Angular Distributions

It would appear that if the decay of compound nucleus is independent of its mode of formation, the reaction products should be isotropically distributed. However, the conservation of the angular momentum affects the distribution as if the compound nucleus 'remembers' the direction of incidence. To derive the expression for the spectrum of the emitted particle, when spins are involved, the principle of 'detailed balancing' is employed.

Wolfenstein 1951 (ref. 41), and later Hauser and Feshbach, 1952 (ref. 42) showed that when statistical assumptions are applied to the compound nucleus as well as residual nucleus, a level density expression for spin J,

$\omega(J) \propto (2J + 1)$ leads to an isotropic angular distribution. Ericson and Strutinski, 1958-59 (ref. 43)[+44] have adopted an approach of 'evaporating molecules from a heated, rotating liquid drop'. They have shown that a level density distribution, $\omega(E,J) = \omega_0(E) e^{-\alpha J^2}$ introduces some anisotropy, but requires a symmetry about 90°. The coefficient $\alpha = \frac{\hbar^2}{2\mathcal{J}T}$ where $\mathcal{J}$ is the 'moment of inertia' of the excited nucleus and T is the nuclear temperature. In the quantal description, it has been shown, $\omega(E,J) \propto (2J+1) e^{-\alpha J(J+1)}$. In place of α nowadays another parameter σ is usually employed, called the spin cut-off parameter; the exponential $e^{-\alpha J^2}$ is written as $e^{-J^2/2\sigma^2}$; Ericson 1960 (ref. 45). When the incoming angular momentum is large compared with the most probable spin of the residual nucleus, there exists a limit on the anisotropy given by $\frac{1}{\sin\theta}$, where θ is the angle of emission (ref. 44). According to the simple picture given by Ericson and Strutinski, the compound system rotates about an axis normal to the incident beam so as to conserve angular momentum, and due to this additional velocity available for emission in the equatorial plane, the averaging of all possible directions of rotational axis gives maximum emission in the forward and backward directions, (these being contained in all equatorial planes) with a symmetry about 90°.

1.3 The Direct Interaction

The distinctive feature of the direct interaction mechanism is that the cross-sections are strongly dependent on the direction of emission of the reaction products. Various 'approximation' methods have been used to treat such reactions. Austern, Butler and McManus, 1953 (ref. 23) used the impulse approximation method of Chew for developing their 'surface direct interaction' theory to describe the angular distributions of protons going to the low lying states of the residual nucleus, in (n,p) reactions. Yntema, Zeidman, and Raz, 1960 (ref. 24) have also used the impulse approximation method for the inelastic scattering of alpha particles. The 'strong coupling approximation' is another approach, used by Chase, Wilets, and Edmonds, 1958 (ref. 25) in their rotational-optical model for the scattering of neutrons by a deformed nucleus. Adiabatic approximation methods, another approach, are regarded suitable for inelastic scattering of nucleons as a result of rotational excitation. Hayakawa, Kawai and Kikuchi, 1955 (ref. 26), and Brown and Muirhead, 1957, (ref. 27) have formulated volume direct interaction theories in a semiclassical way.

By far, the most generally adopted approach at present is that of the distorted wave Born approximation, (DWB approx.) However, calculations based on this method are

very complicated and only few have been done. In the DWB approx., optical model potential is used but an additional interaction is introduced as a perturbation to describe the non-elastic processes. This additional interaction affects some simple internal degree of freedom of one of the two nuclei involved in the collision. The simplest picture of the interaction is, when one of the nuclei is regarded as made up of two constituents (in particular, a core and a nucleon) and the other nucleus (just one constituent, say a nucleon) interacts directly with one of the ~~five~~ two sub-units of the former and produces an inelastic scattering or a rearrangement collision. A general description of even this simple picture of three constituents contributing to the interaction potential includes, inelastic scattering, knock-out and stripping types of direct reactions. A more complicated picture is of shell model. Exchange effects have to be considered, when the simple picture of three constituents in the channel is not valid. To account for the polarization effects, spin-orbit interaction terms have to be included. These direct reaction models to which we are referring, represent an oversimplification, but they have proved successful in many ways.

The theory of direct interaction is concerned with

calculating the transition (or reaction) amplitude, which is given by the matrix element with respect to the initial and final states wave functions, according to the perturbation methods. When elastic scattering, in the incident and exit channels, can be neglected, (and therefore plane waves can be used for initial and final states wave functions), simple plane wave Born approximation can be employed. Usually only the most important part of the amplitude, due to nucleon-nucleon interaction, can be conveniently calculated and the nucleon-core interactions are taken into account by some kind of estimate, or they are neglected. The calculated reaction amplitudes contain spherical Bessel functions, whose arguments contain, K , the magnitude of the difference of the ingoing and outgoing wave numbers. This quantity K , is small for forward directions because the wave number vectors are parallel for forward emission. Since the spherical Bessel functions tend to be larger for smaller arguments, the direct reactions are predicted to be peaked in the forward directions. The oscillatory nature of spherical Bessel functions is also expected to be exhibited by cross-sections for varying K . The theories of Butler, 1951 (ref. 28), and of Bhatia et al, 1952 (ref. 29) for the deuteron stripping reactions are based on the plane wave Born approximation method. Also,

many expressions of practical interest derived by employing impulse approximation method, basically lead to the same results as obtained by plane wave limit of Born approximation.

The magnitude of cross-sections for direct reactions cannot be easily estimated as that depends very sensitively on the distortion effects. ~~Usually these cross-sections are much higher in magnitude, than predictable by the application of the compound nucleus model.~~

The polarization effects normally lead to the non-random orientation of residual nuclei. When this occurs there may be a correlation between the direction of emission of the outgoing particle and the direction of radiation subsequently emitted by the residual nucleus. Some calculations have been carried out using the DWB approximation.

In the next section, we shall refer to some calculations carried out for direct reactions and shall compare them with the experimental data.

1.4 Evidence of Experiments about Reaction Mechanisms.

(a) The General Picture

Excitation functions for total cross sections are generally explained by the optical model description, though, this model cannot reproduce the sharp resonances

observed at low energies. The compound nucleus model does reproduce these resonances but fails to account for the giant resonances (ref. 10). (According to a recent study by Peterson (ref. 46), continuous families of broad maxima and minima in neutron total cross sections between 0.1 MeV and 100 MeV, all shifting smoothly to higher energy with increasing mass number, can be described in terms of a semiclassical optical model). Inelastic scattering, (p,p') (d,d') and (α,α') are now known to proceed mainly via a direct reaction mechanism, since they show very strong peaks corresponding to excitation energies less than $\sim$4 Mev, and have forward peaked angular distribtuions. It may be mentioned, however, that sometimes (α,α') and (p,p') reactions have been fruitfully analyzed with statistical model as well (e.g. refs. 47, 48). Excluding the obvious direct reactions, like stripping and pick up types, the statistical model has proved of great success as a qualitative description of nuclear reactions, but quantitatively its usefulness is still largely unknown. In the following sub-section we shall quote the experimental evidence provided by (n,α) reactions on the statistical model, and shall then proceed to give the general pattern established by some other reactions which have been well studied. The experimental facts about direct reactions

will be briefly described in another sub-section.

(b) The Statistical Model and Experiments.

(n,α) reactions, with ~ 14 MeV neutrons:- Paul & and Clarke, 1953 (ref. 49) had reported that (n,α) cross-sections (measured by activation method) for medium and heavy weight elements were generally several orders of magnitude higher than predicted by the evaporation model. According to later measurements, however, the discrepancy is generally of an order of magnitude only and in some cases even good agreement has been observed; Blosser et al 1955,58 (ref. 50) ; Coleman et al, 1959 (ref. 51) ; Weigold, 1960 (ref. 52). We now turn to the (n,α) energy and angular distributions. Results of Kumabe et al, 1957,58 (ref. 35,36,37) for ^{27}Al, ^{59}Co, ^{55}Mn, ^{51}V and ^{32}S, with 14.8 MeV neutrons, show surprisingly marked anisotropy, but symmetry about 90^{o}. They have also found that low energy alphas are emitted in excess to what can be expected from evaporation spectra; the shape of the spectrum, otherwise, is in general agreement with evaporation model, particularly for ^{27}Al, ^{51}V and ^{32}S. Cevolani et al, 1960 (ref. 38) have confirmed the excess of low energy alphas, and anisotropy (their results are only for backward angles). An earlier experiment, by Ribe and Davis, 1955 (ref, 33), on (n,α) angular distribution for Zr , also

demonstrated marked anisotropy (0° - 115°). Recently, Bormann and Langkau (ref. 53), have obtained energy spectrum of alpha particles emitted from Cs and I (in CsI crystal), for five neutron energies 12.1 to 19.6 MeV. They have analyzed their results with σ_c from continuum model (ref. 16), and also with σ_c from optical model, (Igo's tables, ref. 17). In both cases they have deduced the presence of (n,nα), (n,α) evaporation, and (n,α) direct, components. The major difference in the two analyses was, that for optical model an average nuclear temperature could be obtained independent of neutron energy when analyzed according to $\omega(E) = \text{Const.} \exp(\frac{E}{T})$, or alternatively a value of 'a' independent of neutron energy when analyzed according to $\omega(E) = C \exp(2\sqrt{aE})$; but continuum model analysis, in the similar situation, indicated a strong dependence of these parameter on incident neutron energy, while not so sensitive dependence on the excitation energy of the residual nucleus. With the optical model analysis the direct interaction component was seen enhanced. The ratio $\frac{(n,\alpha)\ \text{evaporation}}{(n,\alpha)\ \text{direct}}$ increased with neutron energy according to both analyses.

(n,p) reactions $\sim$ 14 MeV:- Results from experiments like the '4π geometry' arrangement of Storey et al 1960 (ref. 32) and the differential cross-section measurements at a

backward angle by Allan 1961 (ref. 55), have been generally in agreement with statistical model. Allan explained the fluctuations in cross-sections with mass number, from Q-value and pairing energy considerations. On the other hand there are numerous experiments, which were not designed 'to avoid' direct interaction effects, and have established the unmistakable presence of direct processes. Some of these experiments are, March and Morton, 1958 (ref. 56-58); Allan, 1957-59 (ref. 59-61); Jack and Ward, 1960 (ref. 62); Colli and collaborators 1958-61, (ref. 63-69); Kumabe and Fink, 1960 (ref. 70); and Peck (Jr.) 1961 (ref. 71). Comparisons of '4π' and 0° spectra for the same targets (ref. 32 and 62), and the angular distribution results of (ref. 56, 59, 60, 67, and 70), all show forward peaked contributions; and existence of 'gross structure' in the energy spectra showing stripping like angular distributions has also been reported (ref. 66, 69 and 71). But on the whole (n,p) reactions with medium weight nuclei, and excluding the high energy part of the spectra, are well described by the statistical model.

(p,α) reactions:- Fulmer and Cohen, 1958 (ref. 72), and Fulmer and Goodman, 1960 (ref. 73) have studied (p,α) reactions with numerous targets, with incident proton energies, 9.5 - 23 MeV. The survey showed that alphas

from heavy elements, and those in higher energy parts of spectra from lighter elements, are produced by direct interaction; and that for targets $Z \lesssim 50$, a large part of (p,α) reaction proceeds via compound nucleus. The energy spectra for $Z \lesssim 50$ (except for F and Al) were peaked at about the same energy for incident proton energies varying between 9.5 - 23 MeV; from this, those authors concluded that the coulomb barrier is lower for alpha emission from excited nuclei. Recently, Sherr and Brady (ref. 74) have also reported considerable success for describing their (p,α) results, for 17.5 MeV proton energy, in terms of statistical model.

(n,n′):- Experiments on the inelastic scattering of 14 MeV neutrons, e.g. Stelson and Goodman, 1951 (ref. 75); Whitmore and Dennis 1951 (ref. 76); Graves and Rosen, 1953 (ref. 77); and Rosen and Stewart, 1955 (ref. 78) have shown that the secondary neutrons are emitted according to the evaporation model, while higher energy neutrons are forward peaked (Rosen and Stewart).

Some other reactions:- (α,p) reactions also show the general trend of 'evaporation + direct' mechanism; e.g. Fox and Albert, 1961 (ref. 48), Swenson and Cindro, 1961 (ref. 79). Measurements of (n,^{3}He) cross-sections for medium weight elements (by activation method), with 14.8

MeV neutrons, by Kumabe et al, 1960 (ref. 80) have shown higher values than expected from evaporation model. (n,2n) cross-sections have been found to be roughly in agreement with the evaporation model; e.g. Paul and Clarke, 1953 (ref. 49), and 12.2 to 18.1 MeV excitation function for ^{64}Zn, Koehler and Alford, 1960 (ref. 81).

(c) Direct Interaction Theories and Experiments

Deuteron stripping is the reaction for which direct reaction theory has proved most successful. Simpler theories, based on plane wave approximation, e.g. Austern, Butler and McManus, 1953 (ref. 23), Butler 1957 (ref. 116), Hayakawa and Yoshida, 1955 (ref. 117) have been considerably, but not completely, successful in describing (α,α') angular distributions. A series of calculations done by Levinson and Banerjee, 1957,58 (ref. 118) using the DWB approx., have reproduced (p,p') cross-sections and angular distributions, but the optical potential giving good fits to (p,p') is different from the one used to explain elastic scattering data. The volume interaction theory of Brown and Muirhead, 1957 (ref. 27) enjoyed limited success, e.g. it explained the (n,n') results of Rosen and Stewart, 1955 (ref. 78). But Elton and Gomes, 1957 (ref. 87) have cast some doubt on the validity of this picture of reaction mechanism.

Inelastic scattering like (p,p′) show much larger cross-sections than the corresponding knock-out reaction like (p,n). The difference is explained by attributing 'anomalous' levels to (p,p′) process and 'single particle' levels to (p,n) reaction. The existence of anomalous levels was first recognized from the results of 23 MeV (p,p′) experiments [Cohen, 1957 (ref. 88); Cohen and Rubin, 1958 (ref. 89)] and their comparison with the results of 21.6 MeV (d,d′) experiment by Yntema and Zeidman, 1959 (ref. 90). Cohen, 1959 (ref. 91) pointed out the similarities between (p,p′) and (d,d′); and dissimilarities between (p,p′) and (p,n). Several (α,α′) experiments [e.g. 30 MeV, Sweetman and Wall, 1959 (ref. 92); 20 MeV, Fulbright et al 1959 (ref. 93); 41 MeV, McDaniels et al, 1960 (ref. 94); 30 MeV, Crut et al, 1960 (ref. 95); 43 MeV, Yntema et al, 1960 (ref. 24)] have also shown the existence of 'anomalous' levels. Recently Cohen and Price, 1961 (ref. 96) have surveyed 15 MeV (d,d′) scattering in heavy elements. Good correlation has been found in (p,p′) (d,d′) and (α,α′). Strongly excited states in these experiments may be classified in two groups. (1) Levels near 1 MeV, which are almost invariably excited in coulomb excitation experiments, and (2) the above mentioned 'anomalous' level generally with 2 - 4 MeV excitation energy.

First group which is known as 'quadrupole surface vibrational states', led Cohen and Rubin (ref. 89) to suggest that the anomalous level is also reached through excitation of a collective mode of nuclear motion. Many experiments have indicated that the anomalous levels are 3^-, though higher multipoles are also possible. The general theory is developed by Blair 1959 (ref. 97), as 'multipole surface vibrational states', also termed 'inelastic diffraction scattering'. However, recently Tamura and Terasawa, 1961 (ref. 98) have suggested that these collective states are not basically different from single particle states, and that the difference in (p,p') and (p,n) cross-sections can be explained just on the nucleon-nucleon interaction picture.

Note: Some of the review articles found helpful in collecting material on 'nuclear reaction mechanism' are listed as ref 115 .

CHAPTER 2. PREVIOUS (n,α) ENERGY AND ANGULAR DISTRIBUTIONS AT INTERMEDIATE ENERGIES.

2.1 Introduction

Before we discuss the experiments on (n,α) energy and angular distributions that have been performed by other workers, we shall summarize the difficulties which are normally expected and encountered in this field. We shall limit ourselves to the work with fast neutrons and targets which are not too light. Various factors decide the chances of success of any technique designed to study such (n,α) reactions. Firstly, the limit on the number of neutrons available may decide the maximum counting rate obtainable during the experiment. The most powerful and versatile neutron sources available at present are the nuclear reactions like, $^{2}H(d,n)^{3}He$ (Q = 3.27 MeV), and $^{3}H(d,n)^{4}He$ (Q = 17.6 MeV). Taking up the latter reaction; this reaction exhibits a pronounced maximum near deuteron energy of 107 KeV with a cross-section of 4.95 ± 0.14 Barns, 1952,54 (ref. 30) and 31); the angular distribution of the products is isotropic in the centre of mass system at resonance and below (ref. 30); the neutron energy at 0^{o} (lab) with ≈ 200 KeV deuterons is ≈15 MeV and at 90^{o}, ≈14 MeV. The tritium target is obtainable from Harwell

as $\sim 1/3$ c.c. of gas absorbed in a thin layer of titanium or zirconium evaporated onto a copper plate. With the deuteron beams safe from the considerations of heat dissipation, this tritium-titanium target can give a neutron flux of $\sim 5 \times 10^9$ per sec in 4π. When this figure is compared with the directed beams of $\sim 10^{12}$ particles per sec in the case of accelerated charged particle reactions, the difficulties of neutron experiments become obvious. In addition to this there is the problem of the background counts resulting from the irradiation of the detector and its immediate surroundings by neutrons. The shielding is not easy due to the extreme penetrability of the neutrons, and the obvious necessity of keeping the experimental target exposed. (This problem was tackled successfully in an experiment carried out by Storey et al, 1960 (ref. 32), at Glasgow, to study (n,p) reactions with 14 MeV neutrons.) Two other important factors are, the thickness of the experimental target, and the (n,α) cross-sections. With separated isotope targets it is desirable to use thin targets in any experiment, and for (n,α) reactions the target thickness is limited by the overriding consideration of the energy loss of the alpha particles in the target itself. This fact alone makes the (n,α) experiments of a yield lower by a factor of seven or so on the corresponding

(n,p) experiments. The (n,α) cross-sections for intermediate weight nuclei are not usually encouraging either, and thus further lower the expected yield. Lastly, there is the problem of distinguishing the alpha particles in the presence of competing (n,p), (n,d) reactions etc.

In view of the difficulties involved it is understandable that, the existing information on the energy and the angular distributions of alpha particles emitted as a result of nuclear reactions initiated by fast neutrons in targets which are not too light, is very limited. The first published work in this field is due to Ribe and Davis, 1955 (ref. 33) who reported their results on angular distributions for α zirconium target with 14 MeV neutrons. They used a counter telescope (two proportional counters and a NaI(Tl) scintillator) which Ribe and Seagrave had earlier, in 1954 (ref. 34), developed to study $^{10}B(n,d)^{9}Be$ reaction for 14 MeV neutrons. The results reported on the (n,α) reaction in Zr, were obtained with a .001" thick target, which we estimate to be greater than the range of ~ 6 MeV alpha particles. Very little information was given about the energy spectra. The results by Ribe and Davis clearly demonstrated that for any further attempt to study (n,α) reactions with counter telescopes, the detection efficiency would have to be stepped up by at

least an order of magnitude. No other experiments have been reported in this field with counter telescopes.

In 1957, Kumabe et al (ref. 35) published their results for energy and angular distributions of alpha particles from Al, with 14.8 MeV neutrons. They employed the nuclear emulsion technique. Later in 1958, Kumabe and collaborators published two more papers giving the energy and angular distributions for ^{59}Co and ^{55}Mn (ref. 36) and for ^{51}V and ^{32}S (ref. 37) using the same technique. In 1960, Cevolani, et al (ref. 38) also published information on Al target with 15.2 MeV neutrons. They also used the nuclear emulsion technique. More recently we have come to know (private communication)about the work done by Bormann and Langkau in Hamburg, on the (n,α) energy spectra in CsI employing the pulse shape discrimination technique. In the following two sections we shall review these experiments briefly.

2.2 Experiments with Nuclear Emulsion Technique

The technique of nuclear emulsion plates is extremely good from the point of view of obtaining maximum information from relatively few events. However, the time and labour consumed in the analysis of the plates offset these advantages to an appreciable extent, and in spite of so

much labour the results are expected to be of poor statistics, almost as a rule.

Kumabe and collaborators in their studies of all five targets used Ilford C-2 plates (200μ thick). They inserted the experimental target between two of these nuclear plates, and neutrons from a tritium source were incident at an angle of 45^{o}. Their experimental arrangement is shown in fig. II.1. The angle of 45^{o} for incidence was selected to reduce the errors arising from the correction of the angular distribution. The 60 mg/cm^{2} platinum foil was used to reduce the background. The neutron flux was monitored by a modified McKibben BF_{3} proportional counter, which had been calibrated by counting the associated alpha particles in the $^{3}H(d,n)^{4}He$ reaction (in an argon-filled proportional counter). Since all their results have been reproduced in this thesis in Chapters 4 and 5 for comparisons and discussion, we need not describe them here. The energy spectrum for Al is shown in fig. IV.3 page 94 b; the angular distributions with Al, in fig. IV.16 page 97 b; the energy spectra for remaining four targets, Co, Mn, V and S, are shown in fig. V.1 page 114 a; and the corresponding angular distributions for these targets in fig. V.2 page 114 b. In these results the dashed lines show the observed results and the solid lines the corrected

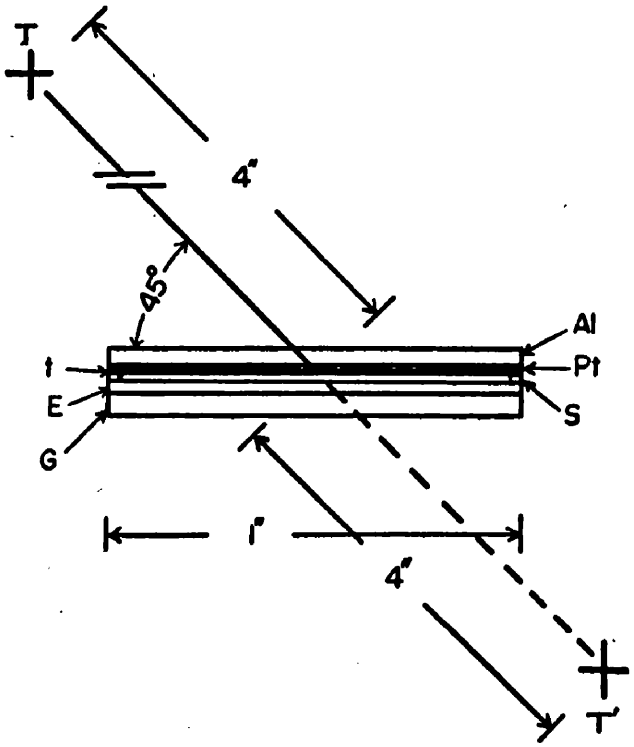

Experimental arrangement. Al: aluminum backing holder (thickness 1 mm). Pt: platinum backing (thickness 60 mg/cm²). t: target. S: celluloid spacer (thickness 0.1 mm). E: Emulsion. G: Glass. T or T': tritium target.

Fig. II.1 Experimental arrangement used by Kumabe et al.

results. The correction was due to the energy loss of alpha particles in the target material. (The thicknesses of various targets were; Al (1.8 mg/cm^2), Co (3.7 mg/cm^2), Mn (3.3 mg/cm^2), V (2.54 mg/cm^2), and S (2.43 mg/cm^2); but the importance of the energy loss correction has to be judged from the extreme closeness of the target and detector). The method that they adopted for this correction implied the uniformity of angular distributions for particles of all energies, an assumption which they based on the similarity of angular distributions of alpha particles divided in two regions, greater and less than 6 MeV, (taken from the uncorrected angular distribution). Their results indicate that they were able to distinguish alpha particles of energy as low as 1 MeV in the presence of low energy proton tracks. It may be pointed out here, that the C-2 plates which they used are not 'low ionisation' plates like K-1 and K-0. According to the manufacturers, K-0 records protons of energies < 5 MeV; K-1, records protons of energies < 7 MeV; while C-2 (now replaced by K-2) can record even 80 MeV protons. Kumabe et al, however, have pointed out that they used the temperature method for processing their plates 'to discriminate alpha particles from protons in the emulsion'. (They used low pH (6.6) amidol developer, and for hot stage they chose

values of 15 minutes and 18°C).

Cevolani et al (ref. 38) have designed a chamber of good angular definition. The results that they have published, for Al (2.7 mg/cm^2), were obtained with the arrangement shown in fig. II.2. They used 8 emulsion plates at various angles as shown; the diameter of the circle was 40 cm; the Al target was in the form of a cylindrical surface, 10 cm high, 22 cm long, but for the detected alpha particles the target was limited to 4 cm x 18 cm. The neutron flux was estimated by measuring induced activity, and during the experiment the flux was controlled by a plastic scintillator. Their results also have been reproduced in this thesis for comparisons. The energy spectrum for alpha particles which they summed over all eight plates (i.e. angles) is reproduced in fig. IV.4 page 94b; the angular distribution results are given in fig IV.17 page 97b. For these results they also used C-2 plates and adopted the temperature method. They, however, reported that alpha particles of energies < 6 MeV could not be discriminated from protons. For their results they have included alpha particles of energies ≥ 7 MeV. In addition to these results they have also published the energy spectrum at 85° obtained with a K-0 plate; with which they could discriminate alpha particles down

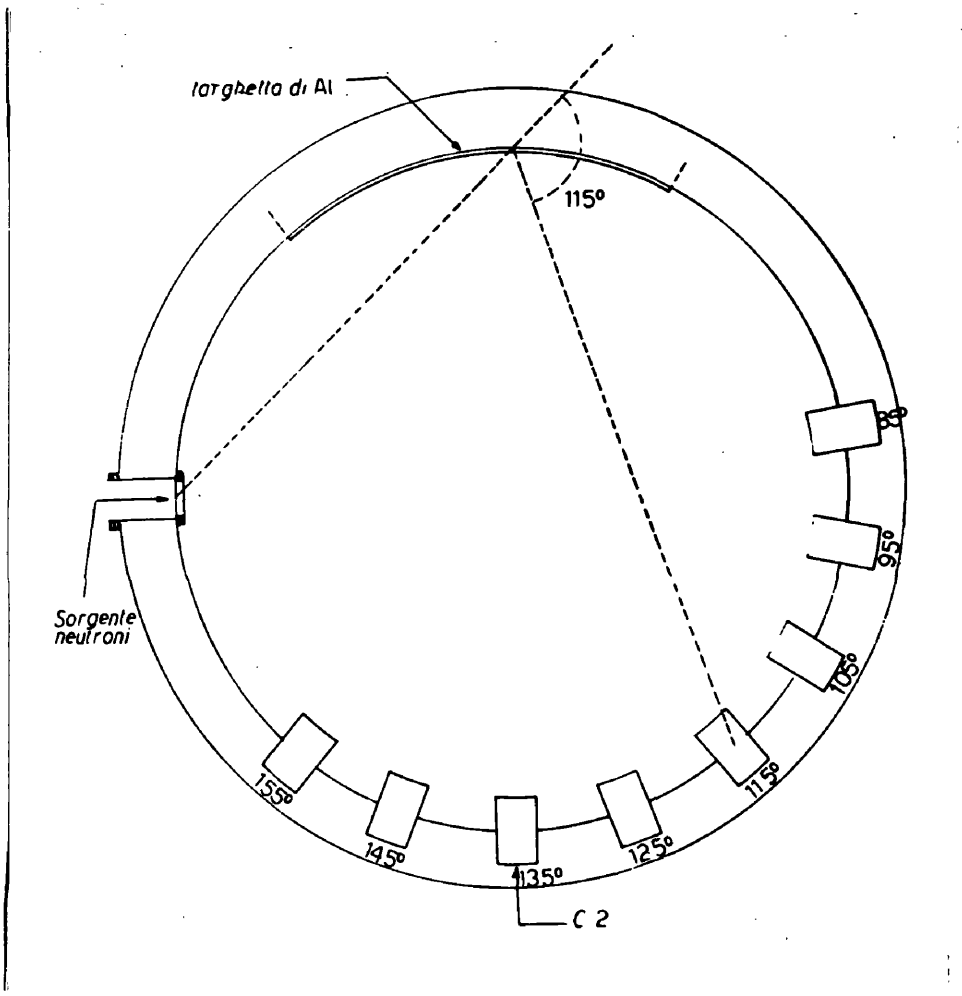

Fig. II.2 Experimental arrangement used by Cevolani et al.

to 2 MeV. This spectrum is reproduced in fig. IV.14 page 96a.

2.3 Technique of Pulse Shape Discrimination in CsI(Tl) Crystal.

During the last three years or so this new technique in scintillation spectrometry has been the subject of investigation by some workers. Robertson and Ward, 1959 (ref. 39) started on this technique, at Glasgow, after the discovery by Storey et al (ref. 32) at Glasgow, that the luminescent decay times in standard crystals of CsI(Tl), are different for particles giving rise to different ionization densities. The luminescent pulse for electrons, protons and alpha particles (i.e. in each case) can be resolved in two exponential components, long and short. The long component is same for each of these particles and is 7 ± 0.5 μs. The short component for electrons is 0.7 ± 0.025 μsec (measured with 0.66 MeV); for 8.6 MeV protons it is 0.60 ± 0.02 μsec and for 2.2 MeV protons it is 0.52 ± 0.01 μsec; and for alpha particles of 4.8 MeV it is 0.425 ± 0.1 μsec. This difference in the short component time, (longer for less ionizing particles), can be exploited to determine the nature of the particle producing a scintillation pulse by doing a 'shape analysis'.

Robertson (ref. 40) did an extensive study on the extent of usefulness of such a technique. In the final form of the technique described by him the discrimination between alpha particles and protons takes place in the following manner. The total spectrum in the scintillator is used in anticoincidence with a pulse which can be produced only by protons. To obtain this 'anticoincidence' pulse, a current pulse is obtained from the photomultiplier. (The rise time of this pulse is determined by the transit time of the photomultiplier tube; and its decay time is the actual decay time of the luminescence). This current pulse is passed on two routes; on one of them it is clipped, reversed and shaped in such a way that it looks like a pulse of decay time intermediate between the values for proton and the alpha particle. This shaped pulse is then 'mixed' with the original current pulse. The mixer output has the right polarity only for protons for 'vetoing' the signal pulse of the total spectrum. Robertson estimated that the technique could discriminate against protons of energies lower than 3.5 MeV. Noting the difference in the response of CsI(Tl) to alpha particles and protons and assuming that at a 3.5 MeV proton looks like a 5 MeV alpha particle, Robertson concluded that the technique could pick out alpha particles in the

range 5 - 16.5 MeV. Discrimination below 5 MeV alpha particles employing this technique is not possible, according to Robertson, because the luminescent decay time for protons begins to look like that of alpha particles against which it has to be distinguished.

Bormann and Langkau have used this technique with different electronics, but, basically their technique is dependent on the difference in decay times for protons and alpha particles. In their experiment, the scintillations in a CsI(Tl) crystal appear as light spots on the screen of the oscilloscope, each particle type producing a separate line of spots. The output pulses of a light sensitive device, like photomultiplier, which looks upon the screen of the oscilloscope are used in gating the total spectrum in the crystal. The desired particle type is selected by an appropriately shaped shield between the screen and the viewing photomultiplier. They irradiated the CsI(Tl) crystal with neutrons of 12.1, 14.1, 16.0, 18.0 and 19.6 MeV. (They used the 3 MeV deuteron beam from a Van de Graaff accelerator). They have reported that in all experiments it was possible to select protons or alpha particles practically without any background radiation, from a total spectrum which was composed of γ-radiation, protons and alpha particles. The crystal

used by them had a diameter of one inch and was of the same height. They have obtained the energy spectra of alpha particles jointly contributed by cesium and iodine. The Q-values for the reactions are:

^{133}Cs, [4.29 MeV for (n,α) and -2.03 MeV for (n,nα)],

^{127}I, [4.2 MeV for (n,α) and -2.27 MeV for (n,nα)],

They have also determined the values of total cross-section for the emission of alpha particles from (CsI), and give values of $\sim$ 9 mb for 19.6 MeV neutrons decreasing to $\sim$ 1 mb for 12.1 MeV neutrons.

No external targets have been studied so far using this pulse shape discrimination technique.

Present Programme.

We have seen that very limited information exists on (n,α) reactions in the intermediate energy region, and that which exists has aroused considerable urge for further investigation, e.g. the remarkable angular distribution results by Kumabe et al. Studies of (n,α) energy and angular distributions, when related to other relevant experiments, can be of great importance in deriving some sound conclusions about level density parameters, magnitude of σ_c for excited nuclei, spin cut-off parameter, etc. Any evidence of significant role of direct interaction

mechanism in (n,α) reactions may help in testing or developing 'cluster model' for nuclear structure. To decide these issues, we obviously need a systematic study covering a wide range of elements, and with different neutron energies, if possible.

Since counter-telescopes are powerful tools for such an extensive and intensive study, we decided to design a counter telescope for this purpose. Due to the multiplicity of expected difficulties we restricted ourselves, in the first phase, to concentrate on getting energy spectra with good statistics. We realized that this involved optimizing almost every geometrical factor coming into the design. Five thin isotope targets, ^{27}Al, ^{54}Fe, ^{63}Cu, ^{64}Zn and ^{107}Ag, (one light, three medium weight, and one medium heavy) were selected for measurement of spectra with the contemplated counter telescope.

Successful completion of the project of developing a counter telescope and measuring (n,α) energy spectra for the above mentioned five targets, prompted us to modify the apparatus for studying angular distributions with Al, the highest yield target.

ADDENDUM: It has come to the light of the author that recently Marcazzan et al, 1961 (ref. 104) have also studied 14 MeV (n,α) reaction in CsI by pulse shape discrimination. Their energy spectrum is consistent with the results of Bormann and Langkau.

CHAPTER 3. DEVELOPMENT AND USE OF (n,α) COUNTER TELESCOPES IN THE PRESENT WORK

3.1 Principle of the Technique.

A thin isotope target is bombarded with neutrons from a tritium target. The reaction particles emitted from the isotope target first traverse a thin proportional counter and then enter a CsI(Tl) scintillation counter. The proportional counter is employed to get a $\frac{dE}{dx}$ pulse whereas the scintillator is to detect the particle and measure its energy, with minor corrections to be applied for the energy loss before the particle entered it. To account for the background counts due to the unavoidable irradiation by neutrons of the CsI crystal, backing of the isotope target and other material in the telescope, runs are to be done for 'target in' and 'target out' positions, the difference giving the contribution from the target itself. The main object of the technique is to discriminate alpha particles due to (n,α) reaction in the target against other particles, particularly protons and deuterons from the competing (n,p) and (n,d) reactions. To do this the spectrum of the particles detected by the scintillator is gated by pulses which are required to be produced only by alpha particles. This spectrum is

measured simply by amplifying the photomultiplier output suitably and feeding it into a multichannel pulse height analyzer via a gating system. The gating pulse is obtained by the coincidence method applied to proportional counter and scintillation counter pulses in the following way. The amplified scintillation counter output is made to overcome a suitable discriminator bias and the discriminator output, which is of a standard height, supplies one input of a coincidence unit. The other input of the coincidence unit comes from the output of another discriminator which receives suitably amplified proportional counter pulses. The coincidence unit output is fed to a pulse shaping unit and the output is used for gating the properly delayed pulses going to the kicksorter. The alpha particles in a certain energy region can be picked out in the presence of protons or deuterons of any energy by virtue of the great difference in their respective $\frac{dE}{dx}$ pulse heights in the proportional counter, provided the amplifiers and discriminators have been adjusted properly. It is to be noted that for alpha particles of energy greater than 2 MeV, $\frac{dE}{dx}$ is four times greater than that for a proton of only one fourth energy and for a deuteron of only half the energy. To pick out all the alpha particles in a certain energy region and

reject all the protons and deuterons (of all energies), the $\frac{dE}{dx}$ pulse for the upper energy limit of alpha particles, (i.e. the lowest pulse height from the alpha particles in the energy region of interest), must be greater than the $\frac{dE}{dx}$ pulse for protons and deuterons which can be recorded within the alpha particle spectrum. To estimate the capability of the telescope for 'alpha particle discrimination' due consideration is to be given to (i) the fact mentioned above regarding different $\frac{dE}{dx}$ for different particles; (ii) difference in $\frac{dE}{dx}$ for the alpha particles of lowest and highest energies that are meant to be recorded; (iii) difference in the response of CsI(Tl) to different particles; and (iv) maximum pulse height in CsI crystal obtainable by protons and deuterons emitted by the isotope target.

Item (i) is the starting point for the technique and has been already considered. Under item (ii) it may be noted that for Argon, the most commonly used proportional counter gas, $\frac{dE}{dx}$ for 20 MeV alphas is approximately 3 times less than that for 4 MeV alphas and about 4.5 times less than that for 2 MeV alphas. Item (iii), the response of CsI(Tl) to different particles, goes to the disadvantage of the technique since the luminescence efficiency of protons and deuterons is more

than that of alphas. (An α MeV proton looks like roughly α+ (1.5 to 2) MeV alpha provided α is not too low). Therefore one has to make sure that protons of energy at least 2 MeV less than the low energy limit of alpha particle spectrum must not give rise to a gating pulse. In item (iv) the maximum obtainable pulse height in the crystal by protons and deuterons is limited by the thickness of the crystal which need not be more than what is required to stop the alpha particles of highest energy.

From these considerations it can be concluded that by using this technique it is perfectly feasible to pick out alpha particles over a wide energy range, in the presence of protons and deuterons of any energy, by covering the whole region in suitable steps. Three steps will be sufficient to cover a range as wide as 2 - 20 MeV. Discrimination against tritons and ^{3}He is much less satisfactory but from Q-value considerations these reactions compete very unfavourably.

In practice, difficulties arise due to low yield, signal to background ratio and statistical considerations, but, even so, the technique can be employed with great success for moderate yield isotopes provided the counter telescope is designed from maximum efficiency consideration

rather than angular resolution. To study angular distributions rather poor statistics will have to be accepted unless the technique itself is greatly modified. Still then as a first attempt it can be worthwhile to test the present technique for studying angular distributions. To do this the telescope designed with suitable geometry has to be rotated around an axis lying in the plane of the isotope target and passing through its centre but keeping the direction of the neutron beam fixed. The main point is keeping the geometry of the counters with respect to the isotope target same for all angles.

3.2 Energy Distribution Telescope. (To be abbreviated ED telescope).

(a) Essential Requirements about Geometry.

Ideally the solid angles subtended by the neutron source on the isotope target, and by the isotope target on the crystal should be so small that the direction of emission of the detected alpha particles relative to the direction of the neutrons be known within few degrees. But as mentioned above, for the ED telescope the geometry was to be decided by maximum efficiency and better signal to background ratio considerations which are discussed below.

(i) Separation between isotope target and the crystal

(This separation will be referred as S_{ic} for brevity). Obviously, higher detection efficiency can be obtained by keeping S_{ic} as small as possible but the $\frac{dE}{dx}$ proportional counter is to be accommodated in between. This counter, which has to be thin even by its nature of being an alpha particle $\frac{dE}{dx}$ counter, is to be kept to minimum thickness for keeping S_{ic} reasonably small. If the proportional counter is say 1 cm thick S_{ic} can also be kept very nearly equal to 1 cm. But we must consider another factor concerning signal to background ratio. Our experience with fast neutron work shows that CsI crystal itself is a major source of background counts. Many alpha particles due to (n,α) reaction in CsI will be emitted in the backward direction and those which cannot lose all their energy in the crystal will enter the proportional counter and will give a coincidence pulse. In addition to these alpha particles there will be many low energy protons which come out of the crystal in the backward direction with low enough energy to give a $\frac{dE}{dx}$ pulse above the bias. These protons, which originate in the crystal and then are recorded as a coincidence event, can be of much higher energy than the ones which are capable of producing a coincidence pulse

if they were travelling from the isotope target to the crystal. The important conclusion is that the solid angle for the acceptance of the particles travelling in the backward direction from the crystal should be kept as small as possible. This implies a larger separation between the crystal and the proportional counter and consequently a larger value for S_{ic}. Incidentally, this very geometry also reduces the contribution of the proportional counter (gas, wire and walls etc.) to the background counts. (Any material that lies between the active volume of the proportional counter and the crystal cannot, obviously result in a coincidence event.)
With the help of some collimation between the proportional counter and the crystal a compromise separation distance should be obtainable to get good efficiency as well as acceptable signal to background ratio. Thus the isotope target must be very close to a thin proportional counter with the crystal on the other side far enough away from background considerations but close enough from the point of view of efficiency.

(ii) <u>Separation between the tritium target and the isotope target</u>.

(This separation will be referred as S_{ti})

First point that comes in mind is that, the nonavailability of enough neutrons

for the isotope target immediately rules out very large value for S_{ti}. A still more important point, however, is brought in by signal to background ratio considerations. Since the crystal is not very far away from the isotope target, the tritium target if placed at a large distance will subtend almost equal solid angles on the isotope target and the crystal. For such distances signal to background ratio will be nearly ~~constant~~ independent of S_{ti}. On the other hand, if the tritium target is brought so much closer that the solid angle subtended on the isotope target is appreciably larger than that subtended on the crystal an improvement in the signal to background ratio is expected.

(b) Description of the Final Form of the Telescope:

The telescope is shown in figure III(1). A schematic drawing is also included. A general view of the set-up is shown in the photograph (fig. III(2). First we give a concise description of this telescope bringing out clearly all the essential features.

The telescope consisted of three main parts which were joined together by O-ring seals. (They were held together even in the absence of vacuum by six screws passing through aligned holes). These three parts were (1) a top plate, (2) a proportional counter and (3) a scintillation crystal container. The tritium

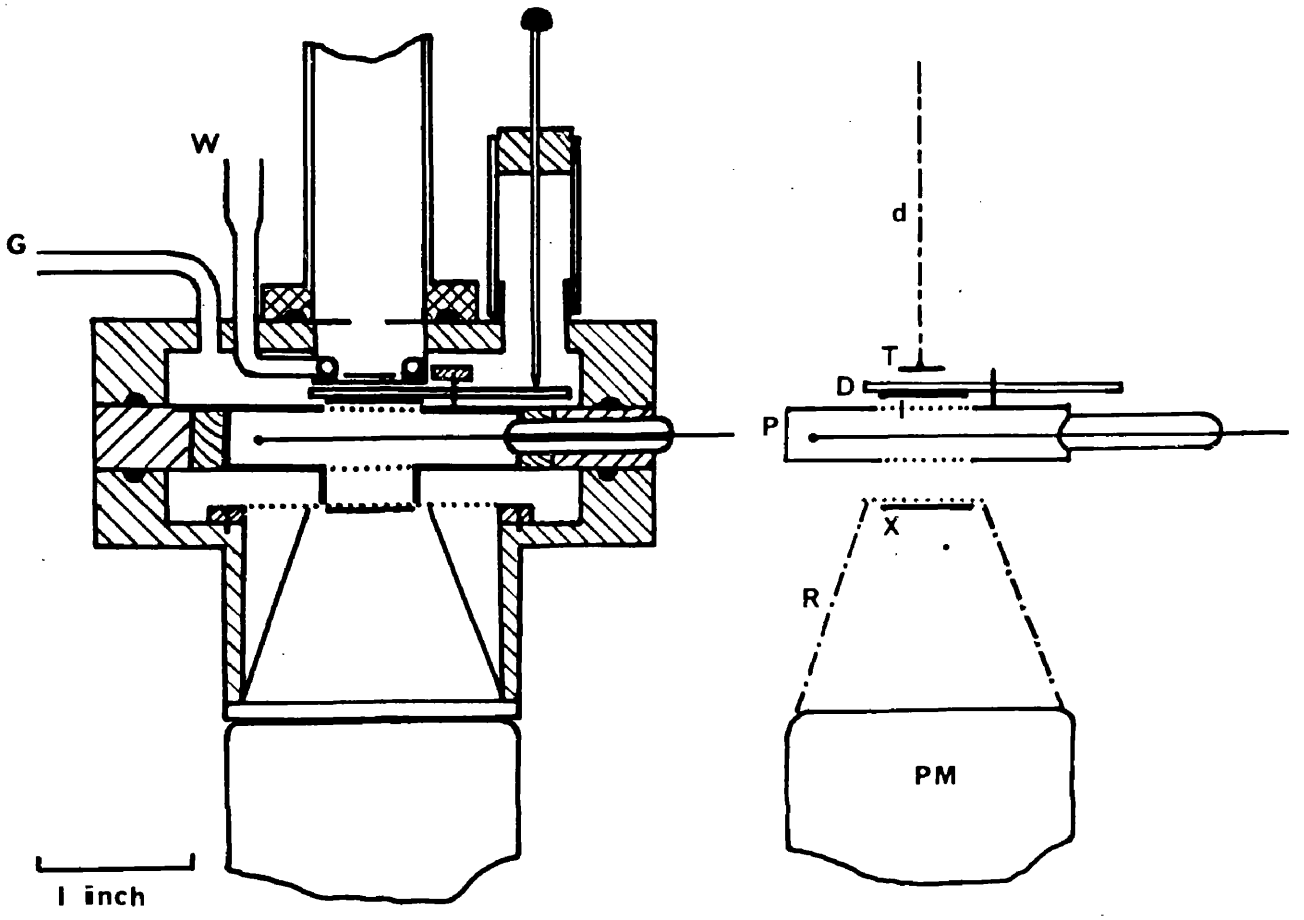

Fig. III.1 The Counter Telescope for Measuring the Energy Distribution of Alpha Particles. Drawing on the right: d, the deuteron beam; T, the tritium target; D, the disc holding isotope target; I, the isotope target in one quadrant of D; P, the proportional counter; X, the CsI(Tl) crystal; R, the reflector (for light collection); P.M., the photomultiplier tube. Drawing on the left: W, pipe carrying cooling water; G, gas inlet and outlet.

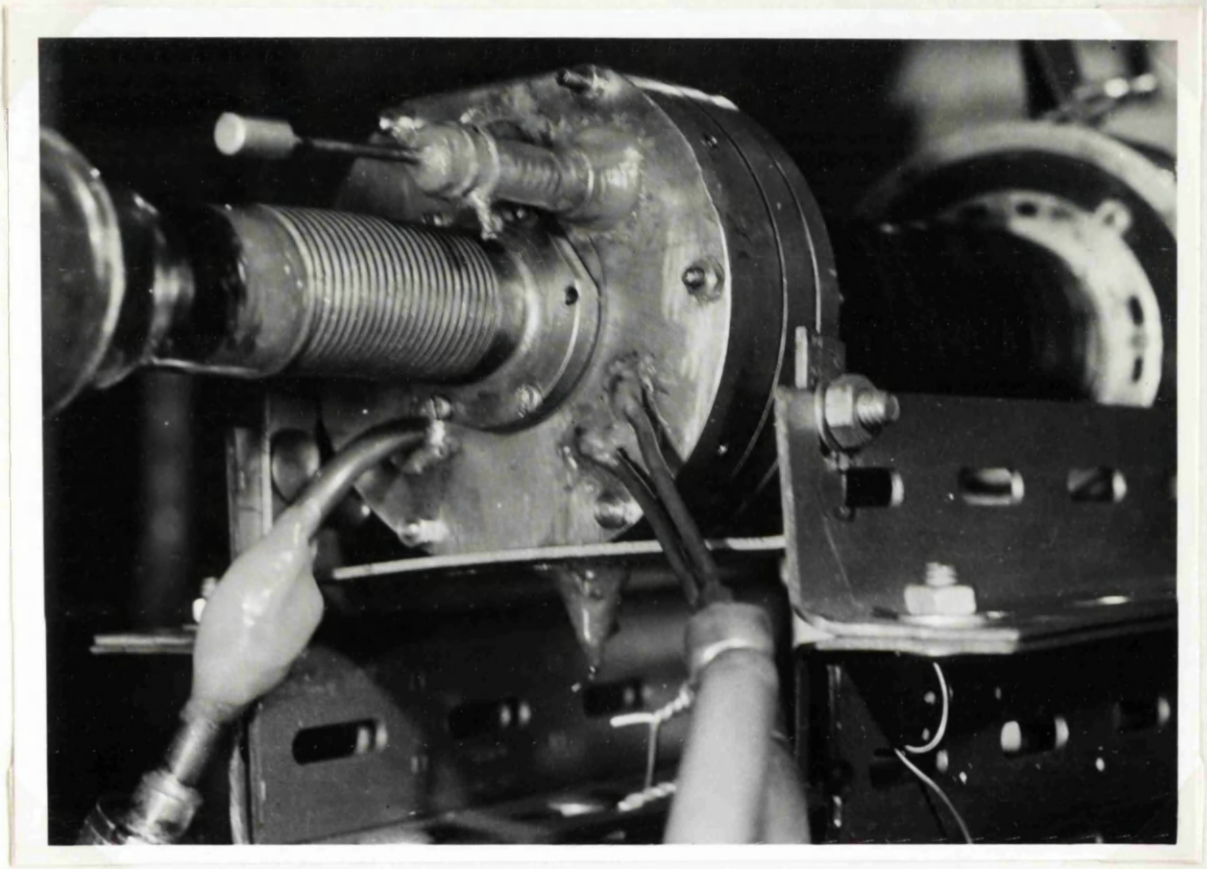

Fig. III.2 The 'Energy Distribution' Counter Telescope is shown here linked to the accelerator arm on the left.

target, with a cooling arrangement, was on the telescope itself, sitting inside a recess on the outside of the top plate. A vacuum tight link was, therefore, required to join the telescope to the 'deuteron beam end' of the accelerator, i.e. to the arm of the accelerator.

The proportional counter was 1 cm thick and was a rectangular box approximately 1.9 cm x 4.8 cm. The isotope target was placed on a disc attached to the top plate. Centrally situated on the top and bottom faces of the proportional counter were thin circular gold leaf windows, 0.95 mg/cm^2 thick and 1.7 cm in diameter. (Actually during the experiment the telescope axis was horizontal and the 'top' face of the proportional counter, in fact, means the face nearer the isotope target.) The disc carrying the target could be rotated in a plane perpendicular to the telescope axis, by manipulating externally without breaking the vacuum seal. The isotope target, 1.5 cm diameter circle, was in one quadrant of the disc. Another identical quadrant minus the isotope target only (but including an identical target backing) served as the 'target out' position for background runs. Still another quadrant contained a polonium alpha source providing a quick way of putting

alpha particles of known energy through the telescope and onto the kicksorter, to be used as reference point essential for converting the kicksorter channels into alpha particle energies from calibration curve.

The circular CsI(Tl) crystal was of 1.5 cm diameter and was supported on thin platinum wires. (Two crystals differing in thickness were used; one 37.6 mg/cm^2, the other 91 mg/cm^2.) A reflecting cavity was used for light collection from the crystal. The bottom of the crystal container was of transparent perspex and was in good optical contact with the photomultiplier tube with a thin intervening film of high vacuum silicone grease. There was a lead collimating collar on the crystal side around the window in the bottom lead plate of the proportional counter.

Some other important figures are:-

Separation between tritium target and isotope target = S_{ti} = 0.4 cm.

Separation between isotope target and first gold leaf window = 0.35 cm.

Separation between second gold leaf window and the crystal = 0.7 cm.

Therefore taking into account 1 cm thickness of the proportional counter, the separation between isotope

target and the crystal was = S_{ic} = 2.05 cm. Shape of the assembled telescope:- The outside of top plate + proportional counter + top of the crystal container formed nearly a cylindrical surface of diameter approximately 10 cm and about 3.5 cm length. (This surface was actually flattened in two opposite parts, minimum distance being $\sim$ 9 cm.) The reflecting cavity part of the crystal container and the perspex end formed a cylindrical surface (externally) of about 2" diameter chosen equal to the diameter of the photomultiplier tube.

Some of the important details of construction will now be given.

The proportional counter:- It was made by cutting away a rectangular box in one cm thick brass plate. The top and bottom faces of the counter were covered with .02" lead plates with windows. The gold foils on the windows were held in position by sandwiching them using additional thin lead foils (with windows) covering the main lead plates. The remaining four walls of the counter were lined with 0.25" thick graphite slabs which were covered by .002" lead sheet. The counter wire was of .008" diameter tungsten, one end of which came out of the counter through an insulating glass tube.

Araldite was used for vacuum sealing. The other end of the wire was about 0.5 cm from the opposite wall and had a glass bead.

The Top plate:- The disc (carrying the isotope target etc.) rotated on a tiny pivot. The supporting bar was of brass but suitably shaped so that the counter could not 'see' it. The disc, of 4 cm diameter, was made of .025" lead backed by a brass plate for rigidity. The isotope target was sandwiched between a .003" tungsten plate (with 1.5 cm diameter circles cut away in four quadrants) and the lead plate. The three pieces, brass, lead and tungsten, were practically sewn together by thin wires passing through tiny holes.

The top plate itself was made of brass and had an O-ring in a grove to provide the seal with the proportional counter. A pipe was fixed (to the top plate) for evacuating the counter and filling the counter gas. A fine 'gas flow control' valve was attached to this pipe.

The disc was rotated by a small rod passing through a hole in the top plate. The rod was contained in a semi flexible polythene tubing. Araldite was used for vacuum seal. To prevent the polythene tube from collapsing under vacuum, a coiled spring support was provided inside the tube. A double-walled glass window,

1.5 cm diameter, was incorporated in the top plate through which the rotation of the disc could be watched. There were identification marks at the back of the disc to know which quadrant was facing the proportional counter window. Straight lines were drawn on the back of the disc and on the two faces of glass window to set the disc accurately by the method of parallax.

The tritium target was inside a cylindrical cavity of 1.9 cm diameter made in the centre of the top plate. The idea was to minimise the distance between the tritium target and the isotope target. The disc was practically in contact with the thin bottom of the 'tritium target cavity'. The tritium target was fixed by soft solder (Wood's metal) and was cooled (under deuteron bombardment) by a water carrying copper tubing hard soldered along the periphery of the target. A little above the tritium target was a collimator to restrict the diameter of the deuteron beam to 4 mm only. The crystal container:- It was also made of brass with the perspex end araldited. The top part had the O-ring in a grove to provide vacuum seal with the proportional counter. The crystal was supported on two platinum wires (.005" diameter) which were soldered onto a bismuth ring which was in turn screwed to the

container. The crystal was held in position by four tiny pieces of platinum wire spot welded to the two supporting wires. The reflector was moulded out of lead to form a truncated cone reflecting cavity with the inside aluminized (very thin coating put on by evaporation). The depth of the cavity was about 1.5 cm

The telescope-accelerator link:- It consisted mainly of copper bellows about 2 cm in diameter and approx. 10 cm long with a glass cone at one end (the counter part of the accelerator arm end). The other end of the bellows had a brass fitment with O-ring for vacuum seal with the top plate. There were screws to fasten the 'link' to the top plate.

(C) Considerations and Earlier Attempts leading to the Final Form of the Telescope

Choice of material for construction:- Brass was chosen mainly because of machining and availability considerations. However lead (a heavy element) was used for lining, wherever necessary, to absorb all the charged particles (mainly protons) produced in brass (due to neutron bombardment) before they could reach either counter. It may be noted that heavier elements have much lower yield for charged particle emission. Choice of gold leaf for counter windows, and for bismuth and platinum for crystal mounting was also because of their being heavy. Graphite lining was preferred to lead lining

in the proportional counter since in the experience of Madame Colli and co-workers in Italy graphite is a lesser evil from β-particle background considerations. This graphite had to be covered with thin lead sheet to stop about 9 MeV alpha particles and low energy protons due to (n,α) and (n,p) reactions in carbon. (Q values -5.7 MeV and -12.6 MeV respectively) Choice of S_{ti} (Separation between isotope and tritium targets):-
In the first version of the telescope the tritium target was not on the telescope itself but was in the accelerator arm. This had obvious advantages from the point of view of access to the target. Also the actual process of putting on a new tritium target was much easier than that in the final form of the apparatus. But S_{ti} could not be as small as 4 mm in the final case. Preliminary runs were carried out with an aluminium target keeping S_{ti} = 2.5 cm. The runs, though not very unsatisfactory, made it strongly desirable to improve signal to background ratio. From the experience gained at that stage it was considered worthwhile to design the final telescope with minimum S_{ti}. In the final telescope this quantity has been brought down to almost its limit from practical consideration. Another advantage gained by putting the tritium target on the telescope was in ensuring a rigid

geometry - very important factor when S_{ti} is so small.

Isotope target 'disc':- In some of the earlier attempts the disc was attached to the proportional counter and not to the top plate. That meant smaller separation between the target and the proportional counter, which was a desirable thing. However, it was found that rotation of the disc from outside needed a very critical adjustment of the length of the manipulating rod. This was extremely inconvenient especially because the telescope had to be dismantled and reassembled very frequently during the thorough study of its performance. This led us to the decision of attaching the disc to the top plate. Before adopting the new system we had tried the manipulation of the disc by a magnet. Due to the compactness of the telescope and its link with the accelerator this method did not work satisfactorily. In passing it may be mentioned that before trying the polythene tube to contain the manipulating rod we used a small metallic bellows but because of its colapsibility under vacuum the adjustments were somewhat tedious. We accepted the polythene tube only after ascertaining that this did not affect the performance of the proportional counter unfavourably.

The proportional counter:- A relatively thick

counter wire was used to ensure better uniformity of electrical field over the region traversed by alpha particles. The wire was sealed on one side only (the other being left free) just to keep vacuum seals to minimum, particularly in the counter itself. The glass bead at the free end was to minimise the chances of sparking. The counter worked very well from the beginning and was retained in the final telescope.

The crystal container:- Basically the shape of the crystal container was kept same from the first attempts, but for light collection an alternative method of 'perspex light guide' with aluminium reflector was also tried. There was no improvement over the present system which was preferable due to the non-necessity of so much material used in light guide.

3.3 Angular Distribution Telescope (AD Telescope)

(a) Essential Requirements about Geometry

To define the directions reasonably, one immediately sees the case for increased separations between tritium-isotope targets ($=S_{ti}$) as well as between isotope target and the crystal ($=S_{ic}$). In this connection another point also deserves consideration. The orientation of the isotope target relative to the neutron beam will be

different for different angles. (But the geometry of the counters relative to the isotope target will remain same). To compare the observations at various angles account has to be taken of different orientations with respect to the neutron beam. If the neutron source is far enough to justify, $\frac{\text{effective area of isotope target}}{(\text{distance})^2}$ as the value of solid angle involved, then a change in the solid angle is completely offset by the corresponding change in the effective thickness and thus the product of the two will be same for all angles. This approximation greatly simplifies the calculations on yields at different angles and, therefore, S_{ti} must be large enough to justify this approximation. As to S_{ic}, it should be as large as tolerable from efficiency considerations. Here again we have to consider another point as well. Increased S_{ic} means greater energy loss of alpha particles in the gas because the gas fills the whole telescope and not the proportional counter alone. (Confinement of gas to the proportional counter will be much more involved problem). Hence one can aim only at moderately large value for S_{ic}.

It has already been mentioned that the contribution to background counts (in coincidence) from either counter

is less for larger separations between them. Now when we want to increase the path between the isotope target and the crystal it is obviously desirable to achieve this by increasing the separation between the two counters.

(b) The Telescope (Modified Version of ED Telescope)

The AD telescope differed from the ED telescope mainly in that the tritium target was not on the top plate of the telescope but on a platform in a specially designed 'extension' of the accelerator arm and that the crystal to isotope target distance ($= S_{ic}$) was 4 cm. instead of 2.05 cm. The tritium target being separate from the telescope S_{ti} was variable, limited only by the size of the telescope and position of the tritium target in the accelerator arm.

To rotate the telescope the following arrangement was adopted. An attachment was made to fit part of the outermost surface of the top plate. (Fig. III(3) gives the drawing of the telescope and fig. III(4) shows the photograph). This attachment had a small rod projecting out and very accurately aligned to provide the axis of rotation of the telescope. This rod had a matching cylindrical cavity in a stand and the telescope could be easily rotated by turning the rod in that cavity.

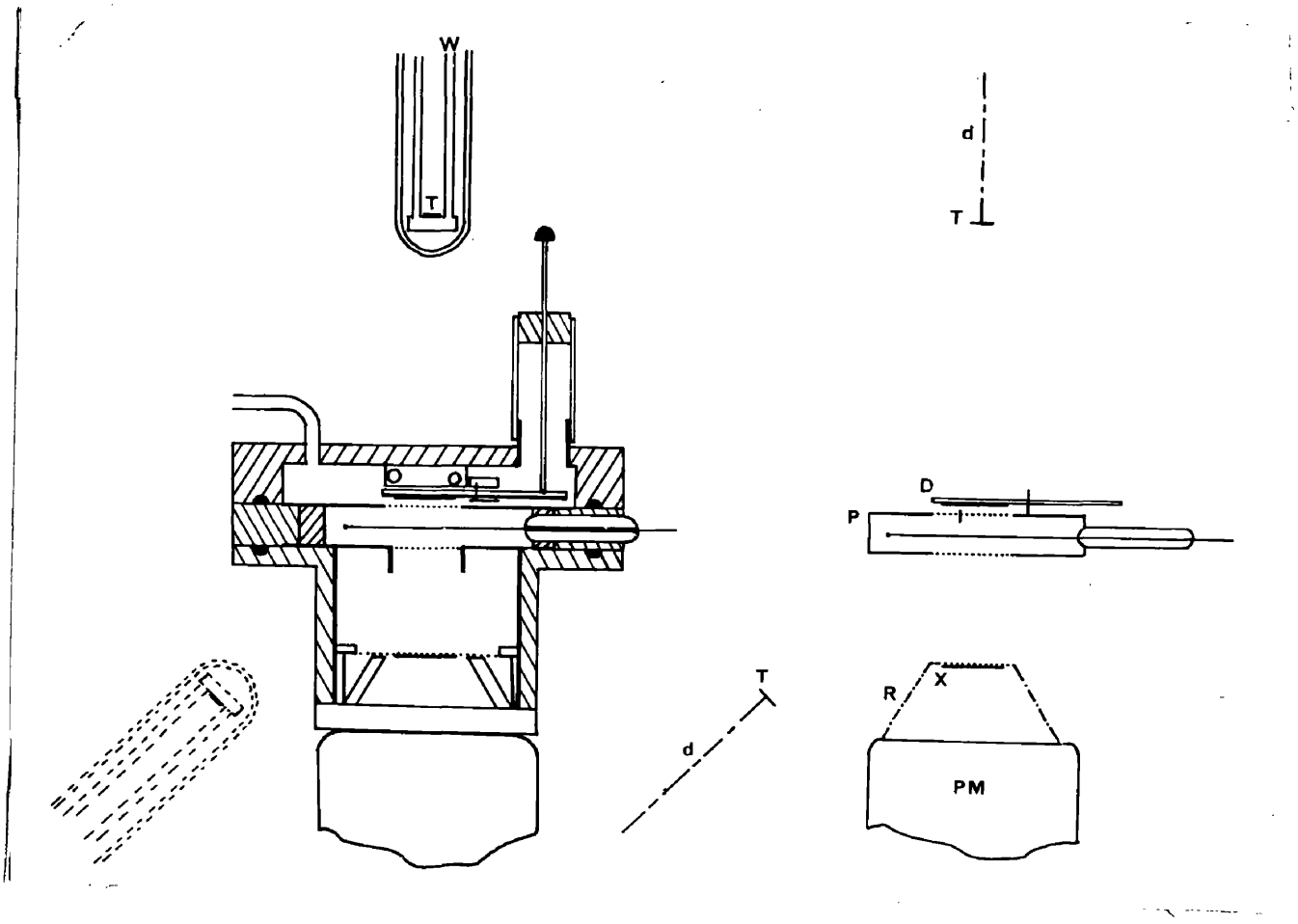

Fig. III.3 The Counter Telescope for Measuring the Angular Distributions of Alpha Particles. Here the tritium target 'T' is in the accelerator arm, on a water cooled platform. Excluding the crystal container, the main body of this telescope is same as for the 'Energy Distribution' telescope of fig. III.1. The cavity in the top plate is filled in by a brass plug. Relative positions of telescope and tritium target are shown for 0^{o} and 135^{o} (lab. angles).

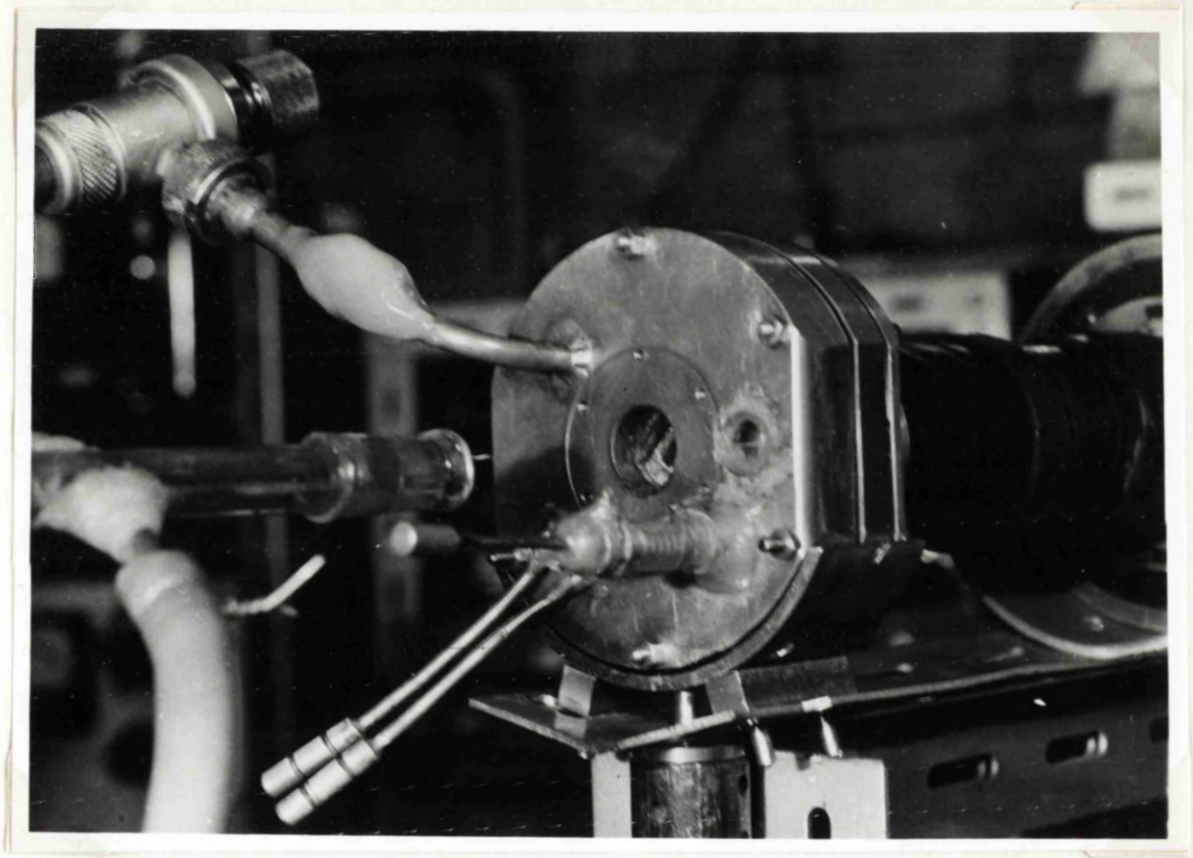

Fig. III.4 Set-up of the Angular Distribution Telescope. The attachment to the top plate was firmly screwed onto it during the experiment, and the cavity was filled in with a brass plug.

A suitable bracket was used for seating the telescope. The bracket with its supporting bars formed a rigid system with the telescope and it was 'the whole system' which was rotated. The angular position of the telescope could be easily determined with the help of some pointers attached to the rotating part.

Since it was decided that the original top plate and the proportional counter should be retained, (and S_{ic} was chosen mainly from geometry considerations already discussed) the design of the new crystal container and of the 'extension' of the accelerator arm (including the target platform) was dictated by the requirement that the telescope would be positioned at various angles while being only at moderately large distance from the target. The crystal mounting had to be put on a narrow seat rather deep inside the cylindrical part of the container. The crystal was mounted on the bismuth ring as described for ED telescope, and the bismuth ring was held in position by a tightly fitting 'opened' hollow cylinder of brass (with inside lead lined). One consideration was also given to the necessity of having roughly the same neutron attenuation for different angles, so that only minor corrections were needed. Though the shape of the telescope was far from ideal on this count, the only

large angular region that had to be avoided due to this difficulty was approximately 90^{o} - 120^{o}. Angles above 150^{o} were not obtainable due to the size of the telescope and its support.

The telescope could be used for studying angular distributions with $S_{ti} \approx 5.5$ cm. In our experiment we set $S_{ti} = 7$ cm.

3.4 Experimental Set-up

Voltage pulses were obtained from both counters (proportional and scintillation) and, therefore, the rise time was determined by the 'collection time' in the case of the proportional counter pulse and by the luminescence decay time of CsI(Tl) in the case of scintillation counter pulse. The decay time of the output pulse was determined by the external electronics. By the time the pulses were out of their respective cathode followers and were ready to be fed into their respective amplifiers their rise time was about 0.6 μsec and decay time about 10μsec. (There was not much difference in the shape of the pulses due to proportional and scintillation counters). Wide-band I.D.L. amplifiers (Type 652) were used and they had the facility of built in discriminator unit following two 'ring' of three amplifier stages. The inherent

integration time of the amplifiers was adjustable, with .03 μsec as minimum. The differentiation time could be adjusted as high as 100 μsec. Minimum gain with these settings was about 100 and a further gain of 100 in steps of 2db was obtainable. The outputs from the discriminator units fed a coincidence unit with resolving time ~~of~~ 2τ of approximately ~~1.25~~ 2.5 μsec. The coincidence unit could be adjusted to give an output even with single input, if so desired. The adjustability covered a fairly wide range and was very helpful in checking the performance very quickly. The coincidence unit output fed a flip-flop circuit to obtain a gating pulse of suitable shape and size. There was an adjustable bias at the flip-flop input to give useful flexibility in operation to meet conditions varying up to some extent. To study the coincidence spectrum, in either counter, its amplified output was delayed by about 1 μsec and then fed to a 'proportional-gate' unit which gave a proportional output. (This output pulse was available only when a gating pulse was produced by the coincidence unit). The 'signal' pulse had to be delayed to give sufficient time for the corresponding gating pulse to arrive and open the gate; the delay time was chosen 1 μsec by trial and error. The output of the 'proportional-gate' unit was obtained

via a white cathode follower and was fed to a 60 channel Hutchinson-Scarrot kicksorter. (For part of the work Marshall's (Model H,S.100) 100 channel kicksorter was also used.) Some pulse shaping was needed to suit the kicksorter. Monitoring of neutrons will be discussed in the next section.

3.5 Neutron Monitoring

A proton-recoil type neutron monitor was used to measure the neutron flux. The monitor had been designed in this department a few years ago by Dr. Storey.

The monitor consists of a circular polythene radiator and a circular CsI(Tl) crystal which detects the protons knocked out of the radiator in the forward direction. If the crystal does not subtend a large solid angle at the radiator a monoenergetic neutron beam gives a peaked spectrum of detected protons. For high enough neutron energies the background (i.e. radiator out) counts can be kept at very low level just by proper shielding. (We used lead lined container.) This simplifies the set up greatly and no coincidence arrangement is required.

The radii of the radiator and crystal, and the separation between them were so chosen that the tables of

Bame et al (ref. 97) given for the exact calculation of telescope efficiency (within 3 percent) could be used. In our monitor the radiator and the crystal were of equal radius (= 0.375") and the separation was 2.25" (exactly six times the radius of the radiator). The radiator and the crystal were 40.4 mg/cm^2 and 0.05" thick respectively. The efficiency was of the order of 10^{-6}.

The crystal was supported and mounted in the same way as described for (n,d) ED telescope. The light collection system was also of the same type i.e. a reflecting cavity. To eliminate the background counts due to (n,p) and (n,d) in air, the telescope was evacuated.

The amplified pulses were fed to a scaler biased to record only above a point somewhere midway in the flat region of the spectrum of the knocked out protons. The bias was set by first seeing the spectrum on the kicksorter. The flatness of the spectrum near the scaler bias made small drifts in the discriminator bias, and gain tolerable. A correction was applied for the background counts coming above the bias. Figures III(5) and (III(6) show the monitor and the spectrum respectively.

In addition to the above mentioned 'peaked spectrum' monitor a big plastic scintillator (cylinder 4 cm long,

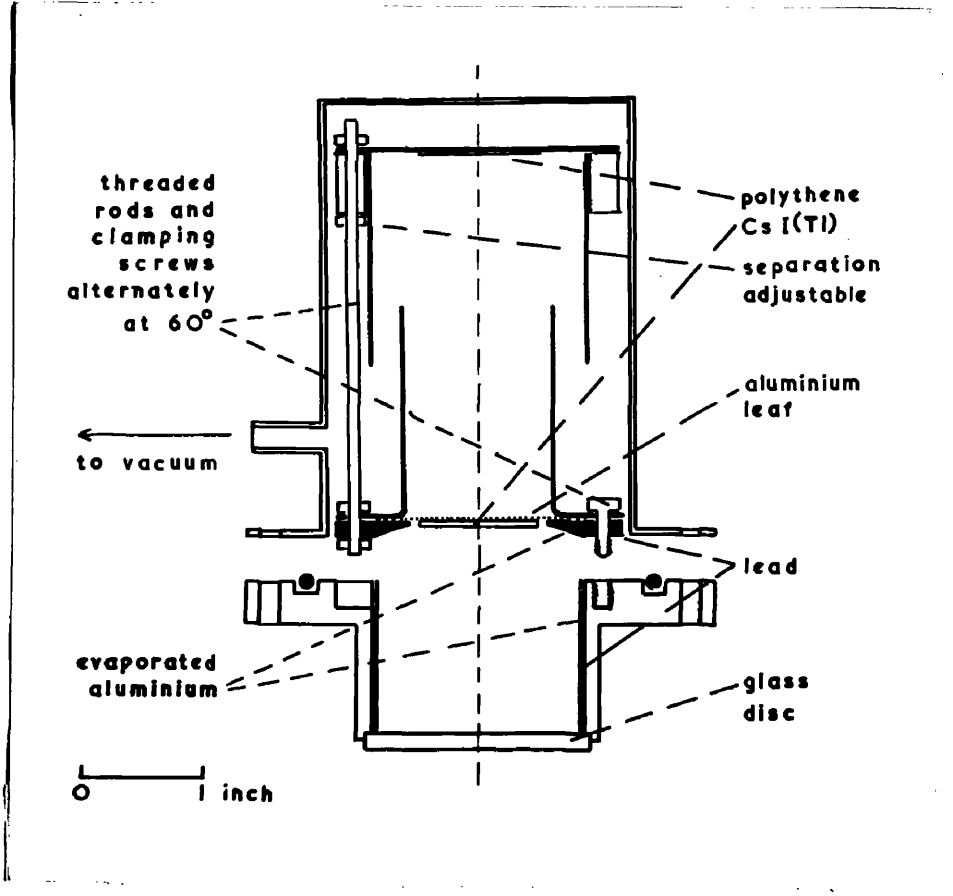

Fig. III.5 Neutron monitor

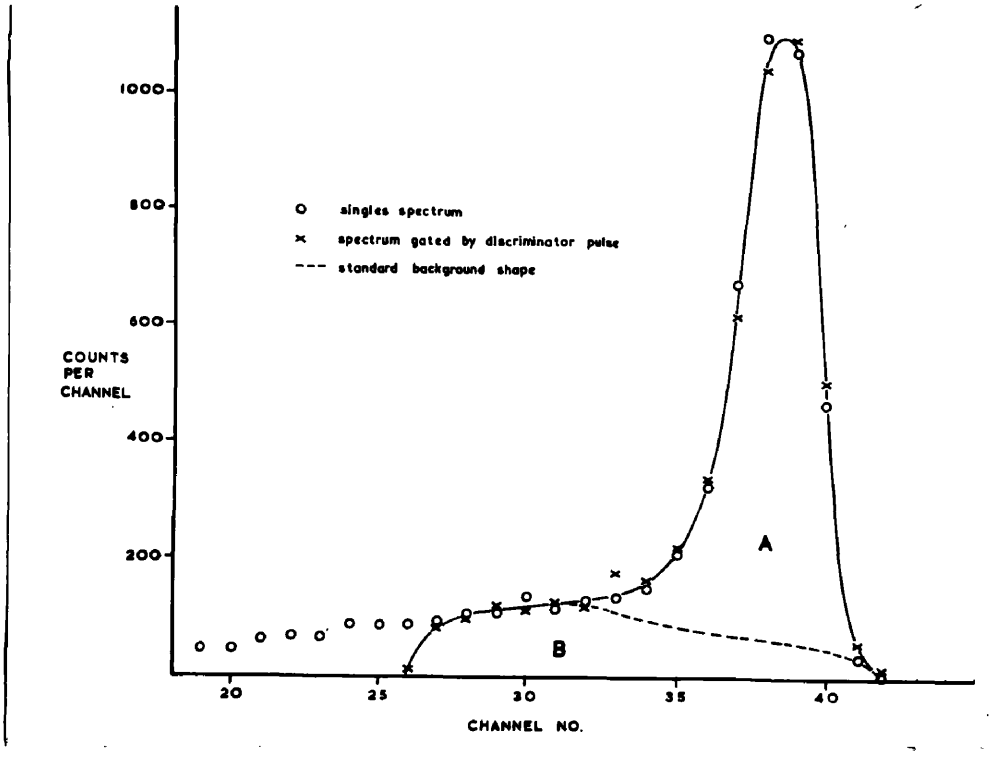

Fig. III.6 Spectrum of recoiling protons, in neutron monitor.

4 cm diameter) was used with suitable bias to cut off most of the γ-rays background. This monitor being of high efficiency was coupled to a rate meter which ensured a constant check of the neutron beam stability.

3.6 Performance of the Telescopes

Three groups of alpha particles from natural radioactive sources found much use in the study of the performance of the counter telescopes. They are ^{210}Po (half life ~138 days, energy ≈ 5.3 MeV); ThC (i.e. ^{212}Bi, half life 60.5 minutes, energy 6 MeV); and ThC′ (i.e. ^{212}Po, half life ~3×10^{-7} sec, energy ~ 8.8 MeV). ThC′ is a daughter product of ThC by its alternative decay with β emission. Both, ThC and ThC′, are usable while in equilibrium with ThB (i.e. ^{212}Pb, half life 10.5 hours) the parent of ThC. As mentioned earlier the disc holding the isotope target also had a ^{210}Po source in one quadrant and was more frequently relied upon mainly because of its longer life.

Energy resolution of the scintillation counter:- A Du Mont 6292 photomultiplier tube was used. The energy resolution obtained for ^{210}Po alpha source fixed on the disc, (a source placed almost in the same conditions as pertaining to the alpha particles emitted from the

experimental targets), was less than 9% for the ED telescope. The energy spent in the crystal itself was about 4.1 MeV. By energy resolution we imply $\frac{\text{full width at half height} \times 100}{\text{position of the peak}}$. Figure III(7a) shows this spectrum. Single and coincidence spectra do not differ in and around the peak region. For the AD telescope energy resolution seen by the same alpha source was about 10%. It was poorer because of more absorption in the gas.

The energy resolution was slightly better for higher energy alpha groups and quite naturally so.

The proportional counter:- Two gas mixtures, Argon-Methane and Argon-Propane were investigated, and two partial pressures of the quenching gas, 10% and 20%. Argon-propane was preferred to argon-methane because of better $\frac{dE}{dx}$ peak with the former. At 8 cm. of mixture pressure, with 10% quenching gas, ^{210}Po alphas with an average energy of 4.7 MeV in the counter gave a $\frac{dE}{dx}$ spectrum of resolution 19-24% when measured in coincidence. The estimated energy loss in the counter for those alphas was about 140 KeV. Figure III(7b) shows the $\frac{dE}{dx}$ spectrum. The 'Single' spectrum naturally had much wider spread due to the presence of alpha particles which did not pass through the second window.

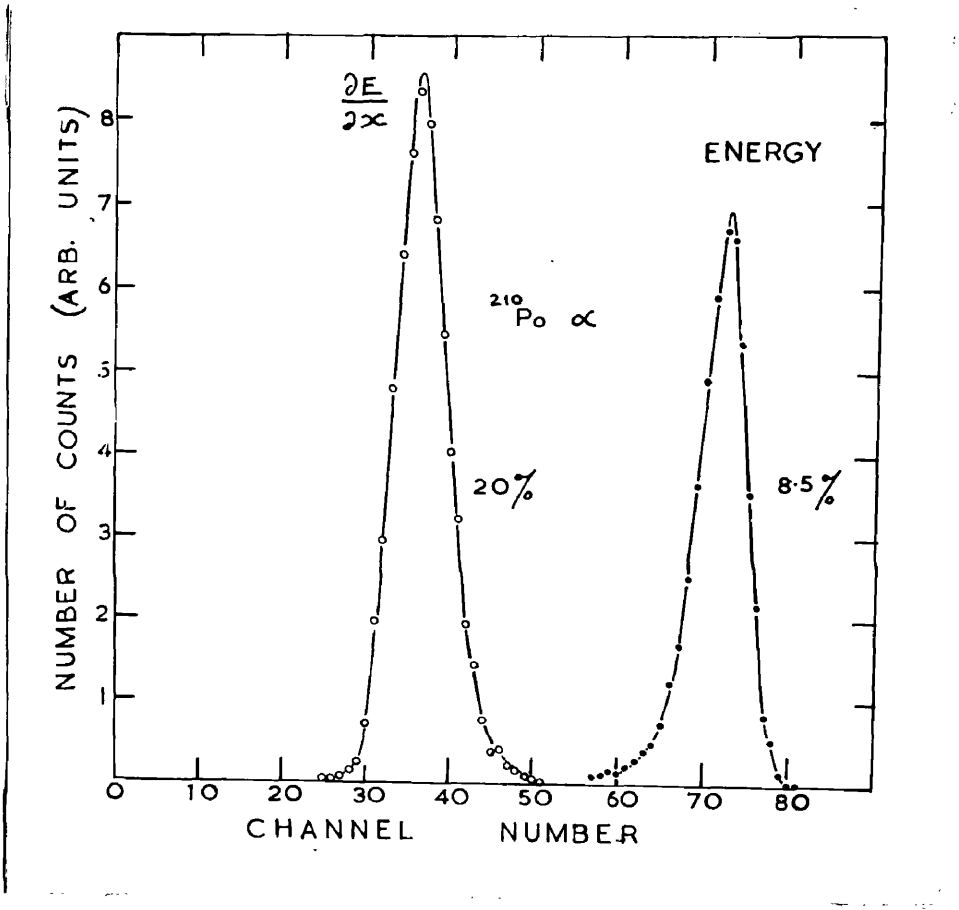

Fig. III.7 (a & b) On the right, the scintillation counter spectrum of ^{210}Po alphas. On the left, proportional counter, $\frac{dE}{dx}$ spectrum, of ^{210}Po alphas.

The choice of 8 cm for pressure was due to the following reasons. To minimise the energy loss of emitted alpha particles low pressure is preferable. Signal to background ratio considerations also lead to the same conclusion. But resolution of the $\frac{dE}{dx}$ peak is expected to improve with increase in pressure. In our case it was found that pressures as high as 20 cm did not improve $\frac{dE}{dx}$ resolution significantly over 8 cm value, and pressures as low as 4 cm did not improve signal to background ratio, studied with an aluminium target. As to the considerations of energy loss it may be stated as an illustration that an 8 MeV alpha particle emitted at the half depth of ~ 1.8 mg/cm^2 thick target of mass number 60 would lose approximately 1 MeV before it enters the crystal, in the case of ED telescope. Out of 1 MeV less than 0.18 MeV is lost in the gas, considering the whole path. For the AD telescope the absorption in the gas was approximately twice of this. These considerations show that 8 cm pressure chosen by us, though by no means a critical one, was a justified compromise.

To give an idea of operating conditions it may be mentioned that with 900 volts on the counter wire (+ve) and an external gain of 100, an 8 MeV alpha would give

about 35 volts high $\frac{dE}{dx}$ pulse. (With 8 cm, 90-10%, argon-propane mixture.)

For the experiment we chose 90-10% mixture rather arbitrarily because higher percentage of the quenching gas did not show any advantage.

The counter needed refilling after about a week or so. Minor drifts during this period could be taken into account by the setting procedure before every run.

Test of proportionality of the proportional counter:- Over and above some indirect evidence for proportionality a direct test was made with Polonium and Thorium (C & C′) alpha groups. Good agreement was found with the expected variation in $\frac{dE}{dx}$.

Capability of the telescope for picking out alpha particles:- One direct test was made to be sure of discrimination against protons. The top plate of the telescope was replaced by another with a 0.00025" thick Mylar window in the centre so that protons and alpha particles from external sources could be allowed in. The ED telescope with thicker of the two CsI crystal (ie, 91 mg/cm^2) was then set on the big 1 MeV Cockroft-Walton accelerator. An old tritium target, containing sufficient quantity of ^{3}He due to decay of ^{3}H, was irradiated by a deuteron beam of 500 KeV energy. Protons

of about 14 MeV were obtained due to $^{3}He(d,p)^{4}He$ reaction. (Q value $\approx$ 18.3 MeV, broad resonance in cross section at deuteron energy $\sim$ 400 KeV). The intense flux of protons was accompanied by a very weak flux of D-T neutrons due to the tritium. The reason for low neutron intensity was the 'off resonance' energy of deuterons for this reaction. The telescope was set to record Polonium and ThC, ThC' alpha particles. Then it was exposed to the proton flux of various energies. Different proton energies were obtained by using absorbers. The performance of the telescope was found extremely satisfactory.

It was concluded that at the most three different proportional counter gains (or equivalently, three different biases) were certain to detect and discriminate alpha particles in a range probably wider than 3-20 MeV in the presence of protons of any energy.

Another direct test of the telescope was made with the aluminium target actually used for final observations. When the proportional counter discriminator bias was just set to cut-off the entire $\frac{dE}{dx}$ spectrum for Po alphas and, therefore, none of the alpha particles $\gtrsim$ 4.5 MeV emitted from aluminium were expected to be recorded, nothing was actually recorded above that energy in the

subtracted spectrum ('target in' and 'target out' positions). This observation strongly supports the contention that the telescope faithfully observed the $\frac{dE}{dx}$ requirements.

Signal to background ratio:- Since this quantity depends on factors other than the telescope itself we shall point out here, only its general character relevant to any estimate of the successful use of the telescopes. To put very broadly, with targets of medium weight elements, about 2 mg/cm^2 thick, an overall signal to background ratio (target in' to 'target out' ratio) of (2-3) to 1 is estimated for the major part of the spectrum with the ED telescope. For the AD telescope the ratio will be smaller and very much so for the backward angles. However, even this performance of the telescopes is very satisfactory considering the difficulties inherent in the nature of such experiments. More will be said about the shape of the background spectrum later.

Limitations due to random coincidence rate:- This rate was estimated from the singles count rates in the two counters and the resolving time of the coincidence unit. It was realized that for the ED telescope rather low neutron flux ($\sim 3 \times 10^7$ per sec in 4π) would be admissible for keeping the random rate about 2% of the

background, on the average. Fluctuations in the neutron flux up to a factor of 2 would keep the uncertainties due to random rate well within 8% of the background spectrum.

For the AD telescope, with S_{ti} = 7 cm, forward angles would permit $\sim 5 \times 10^8$ neutrons per sec in 4π whereas for backward angles one would be limited to $\sim 10^8$ per sec in 4π.

3.7 The Isotope Targets

It has been mentioned earlier that the targets were of 1.5 cm diameter. The aluminium target was in the form of a thin foil of thickness 1.562 mg/cm^2. The other four targets, ^{54}Fe, ^{63}Cu, ^{64}Zn and ^{107}Ag were prepared for us by the Electromagnetic Separation Group of A.E.R.E., Harwell. The targets were in the form of thin layer of electroplated deposit on a backing of .002" thick platinum foil. The targets were of following specifications.

^{54}Fe:- Thickness 1.782 mg/cm^2; isotopic enrichment 95.3%; other isotopes present, Fe-56,57 and 58 (4.68%,0.045% and 0.011% respectively)

^{63}Cu:- Thickness 1.85 mg/cm^2; enrichment 99.76%; the only other isotope present ^{65}Cu (0.24%).

^{64}Zn:- Thickness 1.776 mg/cm^2; enrichment 96.4%; other isotopes present; Zn-66,67 and 68 (2.60%, 0.06% and 0.7% respectively; other elements present Bi(0.2%); Cu(0.05%); Ca(0.03%) and Ag (0.01%).

^{107}Ag:- Thickness uncertain but within the limits 2-2.5 mg/cm^2; enrichment 97.8%.

We had specifically pointed out in our request to Harwell for these targets that they must not contain oxygen, which has a high (n,α) cross section. (310 mb for 14.1 MeV neutrons, ref. 106)

3.8 Experimental Procedure for Obtaining the Data

Energy Spectra:- The essential features of the procedure adopted are as follows. (i) To cover the entire energy range of the emitted alpha particles, each target had to be studied thoroughly with three different settings of bias level of the proportional counter. Short confirmation and check runs were done with some other settings as well. (ii) Investigations for each of the three settings consisted of several runs to obtain reasonable statistics on the energy spectra. Each run was of about 80-90 minutes duration and corresponded to the same number of neutrons incident on the target.

(iii) Each run was checked for the stability of telescope settings (gain for the counters etc.) by putting a reference alpha source in the position of the experimental target before and after the run. (iv) Signal and background runs, and runs with different settings, were interspersed. The repeatibility of runs separated by intervening adjustments and readjustments ensured very satisfactory operation of the system. (v) The reference alpha source was also used to normalize the spectrum (in terms of the kicksorter channels) to be converted to the absolute energy scale with the help of the calibration curve.

The reference source was ^{210}Po, fixed in one quadrant of the disc holding the isotope target. A monoenergetic source of alpha particles of higher energy would have been preferable, if it were available with reasonably long half life. The reference peak in the scintillation counter was displayed on the kicksorter with gain on the counter about 10-12 db higher than was intended for the run. This enabled us to define the reference point more accurately.

The proportional counter settings were also carried out with the help of the $\frac{dE}{dx}$ spectrum of the reference alpha source. The extremes of the bias level on the

proportional counter, for various settings, were required to accommodate a factor of ~ 2.5 in the $\frac{dE}{dx}$ for the low and high energy limits of alpha particles encountered in the present work.

Aluminium was the first target to be investigated, and variations of telescope settings which were used and the number of runs taken were more than needed. This attitude was adopted mainly to understand the telescope thoroughly. To obtain good statistics, on the average seven to nine runs on the target were needed for each setting. The set of background spectra for aluminium had to be taken separately, but for Fe, Cu and Zn, all having the same backing material and run with the same settings, background spectra were accumulated over the complete set of runs with those targets. Runs on Ag were done with different settings, since a wider channel width had to be accepted because of extra low yield of this target.

A run was acceptable only if the positions of the reference peak before and after the run were within 1% of the average in the case of scintillation counter and within 3% of the average in the case of the proportional counter.

The counting rates were of the order of 2-3 per sec

for coincidence (with target in); 125 per sec for the proportional counter singles above the bias; and 25 per sec for the scintillation counter singles above the bias.

Performance of the coincidence unit and gating unit was checked frequently.

For aluminium observations were taken with two different crystals, 91 mg/cm^2 and 37.6 mg/cm^2. For all other targets only the thicker crystal was used.

The output pulses of both discriminators were constantly monitored by coupled scalers. This check on the singles counting rate ensured the detection of any violent fluctuations during the run which would necessitate the rejection of the run from random coincidence rate considerations.

Angular distributions for the aluminium target:- The general procedure was the same as adopted for energy spectra except that the runs were taken mainly with one setting of the proportional counter to pick out alpha particles $\geqslant$ 6 MeV (centre of mass system). Five angles (5°, 38°, 90°, 130° and 139°, all in centre of mass system) were studied. The runs for different angles were interspersed.

CHAPTER 4. PRESENTATION OF RESULTS

4.1 General Considerations

In this chapter we present only the basic results. These include, the energy spectra of alpha particles from ^{27}Al, ^{54}Fe, ^{63}Cu, ^{64}Zn and ^{107}Ag, (c. of m. system); the statistical plots; cross-sections for the total emission of alpha particles in the reactions studied; the energy spectra for ^{27}Al at 5° and 90°; and the differential cross-sections for (n,α) in ^{27}Al, for alpha particles of energy $\geqslant 6$ MeV (c. of m. system) and measured at 5°, 38°, 90°, 130° and 139° (c. of m. system). For Al, we have also given the results obtained by other workers. For Fe, Cu, Zn and Ag no other results have been published so far. We also include the background spectrum in the results, and to give an idea of a typical signal to background comparison, a signal spectrum is also displayed. (In the case of runs for angular distributions in Al, figures ~~are given~~ for signal to background ratio for different angles were; $\frac{2}{1}$ (5°), $\frac{3}{2}$ (38°), $\frac{7}{5}$ (90°), and $\frac{7}{6}$ (130°, 139°).)

Before presenting these results towards the end of this chapter, we discuss the corrections, calculations and approximations connected with obtaining the final data.

The analysis and interpretation of these spectra

and the statistical plots will be deferred till next chapter, in which, also will be presented the results derived from the analysis.

4.2 Corrections Applied

(a) Non-linearity of Response of CsI(Tl) Crystals to Alpha Particles

It has been mentioned earlier that the energy spectrum of alpha particles from aluminium was studied with two crystals, 91 mg/cm^2 and 37.6 mg/cm^2. The runs for angular distribution (on Al target), were taken only with 37.6 mg/cm^2 crystal. The energy spectra for all the remaining four targets were taken with 91 mg/cm^2 crystal. (The choice of thinner crystal for Al, was from considerations of background, coupled with the fact that we could use a thinner crystal due to negative 3.14 MeV, Q value for (n,α) in Al. The background consideration was particularly important for runs on angular distribution.) The 91 mg/cm^2 crystal was experimentally calibrated for pulse height against alpha particle energy, in the range, 3.25 to 10.7 MeV. The method and results are described in Appendix I, attached to this thesis. The linearity of response above $\sim$8 MeV, made it possible to extrapolate to higher energies. The results for Al, with the thinner crystal were in

complete agreement, as we had expected, with those obtained with the thicker one. Hence, the experimentally measured response curve for the thick crystal was used for the other one as well.

If the linear part of the curve at higher energies is extrapolated backwards, then for 4 MeV alphas departure from the extrapolated line is $\sim 40\%$, and for 6 MeV $\sim$ 7% only.

(b) Non-linearity of Electronics

Not much correction was needed due to this factor. Most of the non-linearity that was there, came from the 'proportional gate unit' which had a constant step of ~ 1.5 volts in the output. (For our settings a 10 MeV alpha usually corresponded to $\sim$ 30 volts). The entire electronics, beginning from the amplifier input to the kicksorter channels, was calibrated with the help of a pulse generator. Some checks and cross checks were made to be sure of accuracy.

(c) Energy Losses between Emission and Detection of Alpha Particles

The following corrections were taken into account, (1) half thickness of the isotope target, (2) the counter gas (over the entire path), (3) gold leaf windows, and (4) the aluminium reflector on the crystal. The energy

losses were, either determined from the known experimental results, or were calculated. For calculations we used the equation given in (ref. 86 p. 213), for the atomic stopping power, $\varepsilon_\alpha(E_\alpha)$,

$$\varepsilon_\alpha(E_\alpha) = \frac{4 \times 0.96\, Z}{E_\alpha}\left[\log_e \frac{E_\alpha}{Z} + a - 1.38\right] 10^{-15} \frac{\text{ev-cm}^2}{\text{atom}} \quad (4.1)$$

'a' has values between 5.05 to 5.25 for medium Z elements. The approximate values for 'a' were read off the curve given in the reference quoted. About the equation, it may be pointed out, that as written in there, (ie, in the reference) it is out by a factor of 4, which we have indicated by writing separately. To determine the energy loss in propane (C_3H_8) we used the additive rule for molecular stopping power.

After determining the energy losses for several energies we drew a smooth calibration curve from them. These curves were so obtained for all the targets separately

(d) <u>The Centre of Mass Effect</u>

This correction was most important in the case of aluminium, and could not be neglected even in the case of Fe, Cu or Zn. To convert from lab energy to centre of mass energy, we proceeded to determine the average angle of emission of alpha particles (relative to the incident neutron direction). From the geometry of ED telescope it

is clear that this angle varied over a wide range (0°-100°). To find a justifiable value for this average angle we did some simple graphical calculations, for which we treated the neutron source as a point source (this approximation will be examined later). We divided the isotope target into ten concentric circular zones, each subtending same solid angle at the point neutron source (situated on the axis). Due to a reasonable assumption of the isotropic nature of the neutron flux, each zone received equal number of neutrons. We, then, proceeded to determine the mean direction of the alpha particles, which were detected by the crystal. We assumed that the detection efficiency of the crystal for all the zones on the target was same, and we also assumed that equal area zones drawn concentrically on the crystal, divide it into equal solid angle parts for any area element on the target. We drew mean directions for neutrons incident on each zone of the target. We found that for nine out of ten zones, the detected alpha particle emitted from a point in a particular zone could have travelled anywhere within a cone, with the incident neutron direction lying outside the cone. For the central zone on the target, the neutron direction was contained within the cone. For the former nine zones, the direction determined by the point of emission and the

centre of the cone base was a very good 'mean direction' for the alpha particles emitted from that point. The angle contained between the mean neutron direction and mean alpha direction was same for all the subdivisions around a zone. To determine the average angle over all zones we needed the weightage that should be given to each zone. Geometrically (for the crystal) we assumed them to be at par. They also had equal number of neutrons. The most important factor was that of effective thickness of the isotope target for each zone; this varied by a factor of 2 for the outermost to the innermost zone. We took the effective thickness for each zone as the weight for that zone. This consideration led us to conclude that on the average outer zones were more effective and important from the point of view of the number of events recorded. It should be, however, pointed out that we did not take ~~inot~~ into account any effects of a possible non-isotropic angular distribution. This approximation will be discussed later. Thus, ignoring the central zone, we calculated a weighted average over nine zones, and got the value for the average angle as 55°.

For the calculation of centre of mass effects, we also needed the energy of the neutrons, for which we needed an acceptable average value for the direction of

neutrons relative to the deuteron beam. This was evaluated by taking the average of the mean angles for various zones on the isotope target, already referred to. This angle came out to be 41^{o}.

For converting from lab energy to centre of mass energy, nomographs were drawn for several energies, for Al; Fe; and for (Cu and Zn); and conversion curves were plotted. For Ag, the correction was estimated and was found to be negligible.

4.3 Calculation of Cross-Sections

(a) Efficiency of the Neutron Monitor

This was calculated with the help of the tables given by Barme et al (ref. 97). For a given flux of $\frac{N_n}{4\pi}$ neutrons per steradian, per sec, and for the observed counting rate 'C_m' in the monitor, the efficiency ϵ is given by

$$\epsilon = \frac{C_m}{(N_n/4\pi)} = M.P.\,\sigma_{n,p}(E_n) \qquad (4.2)$$

where M is taken from the tables (it depends mainly on the geometry, with very slow variation due to neutron energy); P is the number of hydrogen atoms per cm^2 of the radiator, and $\sigma_{n,p}(E_n)$ is the n-p scattering cross section for the neutron energy E_n.

$\sigma_{n,p}$ being different for different energies, will be different for different E_n; being higher for lower energies. Thus if the monitor is placed in a direction different from the isotope target, (as is usually necessary), the efficiency calculations will be affected. There is another effect; though the emission of neutrons in the centre of mass system is almost isotropic, there is some anisotropy in the lab system; there is slight forward peaking. It can be calculated, and has been experimentally verified by the research group at Glasgow, that the counting rate in the neutron monitor of this type does not change perceptibly with the direction; the reason being that the anisotropy and change in $\sigma_{n,p}$ compensate each other. Thus the neutron monitor would have given the same number of counts, if it were in the direction of the isotope target. However, for calculating the efficiency we are required to put the value of $\sigma_{n,p}$ appropriate to the neutron energy in the direction of the isotope target itself.

(b) <u>Calculation of Cross-section from the Energy Distribution Telescope</u>

We assume the neutron source to be a point ~~concentrated~~ of the tritium target. at the centre. Let ϕ be the angle of incidence of neutron on the target. Then dN_n, number of neutrons

incident on a circular strip of the target contained within angle $d\phi$ will be given by,

$$dN_n = \frac{N_n}{4\pi} \times \text{Solid angle} = \frac{N_n}{4\pi} \times 2\pi \sin\phi \, d\phi \qquad (4.3)$$

Let the average solid angle subtended by the isotope target, on the crystal be Ω_o; and the number of alpha particles emitted from circular strip on the isotope target (mentioned above) and accepted by the crystal, be $dN_{\alpha\Omega_o}$ then

$$dN_{\alpha\Omega_o} = dN_n \cdot \frac{n}{\cos\phi} \cdot \frac{d\sigma}{d\Omega} \cdot \Omega_o \qquad (4.4)$$

where 'n' is the number of target nuclei per cm^2 for $\phi = o$; and $\frac{d\sigma}{d\Omega}$ is the (n,α) cross-section per unit solid angle.

The integration of the expression over the range of ϕ , known from the geometry, leads to

$$\frac{d\sigma}{d\Omega} = \frac{N_{\alpha\Omega_o}}{0.377 \cdot N_n \cdot n \cdot \Omega_o} \qquad (4.5)$$

where $N_{\alpha\Omega_o}$ is the total number of alpha particles recorded corresponding to total number of neutrons N_n (in 4π).

The average value for Ω_o was determined graphically for the points lying on a circle in the isotope target surface, dividing the target area in two equal parts. Value of Ω_o thus determined, was $\propto 0.35$ steradians.

For the final calculation account was taken for the

neutron attenuation, between the tritium target and the monitor. The estimated correction was about $\sim$ 15%.

(c) Calculation of Cross Sections from the Angular Distribution Telescope.

The geometry being much simpler, the calculations were straightforward. $\frac{\text{Effective area}}{(\text{Distance})^2}$ was a very good approximation for the values of solid angles involved. Hence, the change in effective area of the isotope target as seen by the neutron source (with different orientations of the telescope) was compensated by the change in the effective thickness of the isotope target.

Account was taken for slightly different attenuation of neutrons between the neutron source and the target, for measurements at different angles. It may be pointed out here that, during the experiment, the cavity in the top plate was ~~plugged~~ filled in with a brass ~~cork~~ plug to minimise the difference in attenuation.

4.4 Implications of Approximations.

Tritium target as a point source:- The neutron source, in fact, extended to about 2 mm radius. The peripheral part subtended somewhat less solid angle on the isotope target; therefore, our calculated cross-sections will be a little underestimated on this count.

However, the effective thickness of the isotope target will be, on the average, more for peripheral points, and that makes the calculated cross-sections a little overestimated. Thus the two effects go in opposite directions. As to the implications regarding the 'average angle' estimated for the detected alpha particles, it can be argued that this average angle will still have to be taken with respect to the mean position of the neutron source, and that will be its centre. The effect on the weights of the zones will also go in both directions from different points of the neutron source. It is fair to assume that as long as the neutron source is not too much extended, and is symmetrically situated, our calculations will represent the average situation.

Estimates about solid angles:- For calculating the 'average angle' of emission, we assumed that equal areas of the crystal have equal detection efficiency for any point on the isotope target. In reality, for very oblique directions the solid angle may differ by as much as 20%. In any case, for the cross-section calculation we estimated an average solid angle Ω_o. The overall uncertainty introduced by the geometry, in the calculation of cross-sections, is estimated to be within $\pm$10%.

Ignoring the possible angular distribution effects:-

At the first sight it appears that the angle of emission of the detected alpha particles (when measured relative to the direction of neutron) can be anywhere between 0^{o} and 100^{o}. But looking at the average situation and in view of the greater effective thickness towards the periphery of the isotope target it seems reasonable to assume that relatively large contribution falls around the estimated average angle of 55^{o}. The intention is not to minimise the significance of the inevitable angular divergence but to point out the fact that any possible strong forward peaking does not materially change the value of this average cross-section, since most of the contribution comes from the region which is, in all probability, not showing violent fluctuations. As a matter of fact, this poor geometrical definition is an advantage for comparisons with the statistical model predictions.

Some other factors:- The calculation for neutron attenuation effect could not be very accurate. This can lead to a systematic error of $\pm 5\%$ in the cross-sections calculated by us.

The deuteron beam might have at times, drifted across the tritium target making it an assymetrical neutron source for the telescope. However, this effect is expected to be random.

The reference alpha source, ^{210}Po being of inconveniently low energy, might have introduced some systematic error in energy calibration of the spectra. Extreme precautions were taken to avoid this error, and we estimate ±5% as the very utmost upper limit on this error.

4.5 Results

(a) Background Spectrum

Fig. IV.1 shows a background spectrum along with a signal spectrum (for ^{64}Zn), both for the same bias, and normalized to same number of neutrons. For different biases, the background showed comparatively bigger change in the low energy part. A1, was run without the platinum backing but the corresponding background spectrum had similar shape. Spectra for two crystals showed more variation for the low energy part. The most striking feature of the background spectrum is the distinct peak at $\sim$8 MeV alpha particle energy spent in the crystal. This peak obtained by subtracting the 'smoothed' spectrum from the actual spectrum is also separately shown (enlarged in height by a factor of two).

(b) The Average Angle (55^{o}) Energy Spectra for Alpha Particles Emitted in Forward Directions.

These spectra were composed from the partly overlapping

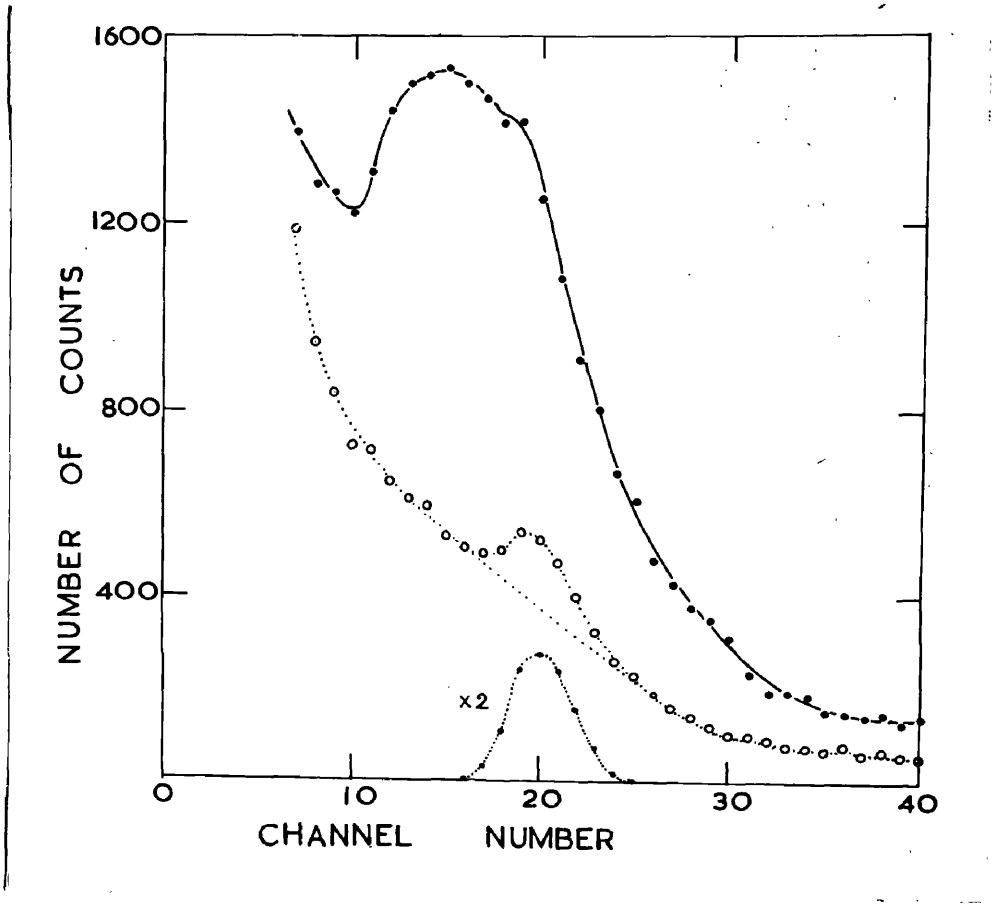

Fig. IV.1 Background and signal (^{64}Zn) spectra, for an intermediate bias.

—•—•—•— Signal ^{64}Zn), (i.e. target in)
o---o---o---o Background (target out)
The hump in the background spectrum shown as a peak obtained by subtracting the dotted 'smoothed' curve.

spectra obtained with different bias settings. The true spectrum for 'alpha particles only' could be picked out without any ambiguity.

Fig. IV.2 shows ^{27}Al spectrum while spectra for ^{54}Fe, ^{63}Cu, ^{64}Zn and ^{107}Ag are given in figs. IV.5 to 8, in that order. All spectra are in the c. of m. system. The arrow in the high energy part of each spectrum indicates the transitions to the ground state of the residual nucleus; the Q-values were calculated from the mass values taken from (ref. 82). The arrow at the low energy part in Fe, Cu, Zn and Ag denotes the energy below which (n,nα) can contribute to the observed spectrum. The dotted lines in these spectra are to explain the analysis and will be discussed in the next chapter. The error shown on each experimental point is the 'statistics' on the target and background counts. Figs. IV.3 and 4, reproduce respectively the corresponding spectra for Al obtained by Kumabe et al (ref. 35) 14.8 MeV neutrons, alphas summed over all angles 0° - 170°; and by Cevolani et al (ref. 38), 15.2 MeV neutrons, alphas of energy $\geqslant$ 7 MeV and summed over eight angles between 85° - 155°.

We have determined the total cross-sections, (n,α) + possible (n,nα) , by integrating the energy spectra. (Some extrapolation at the low energy end of

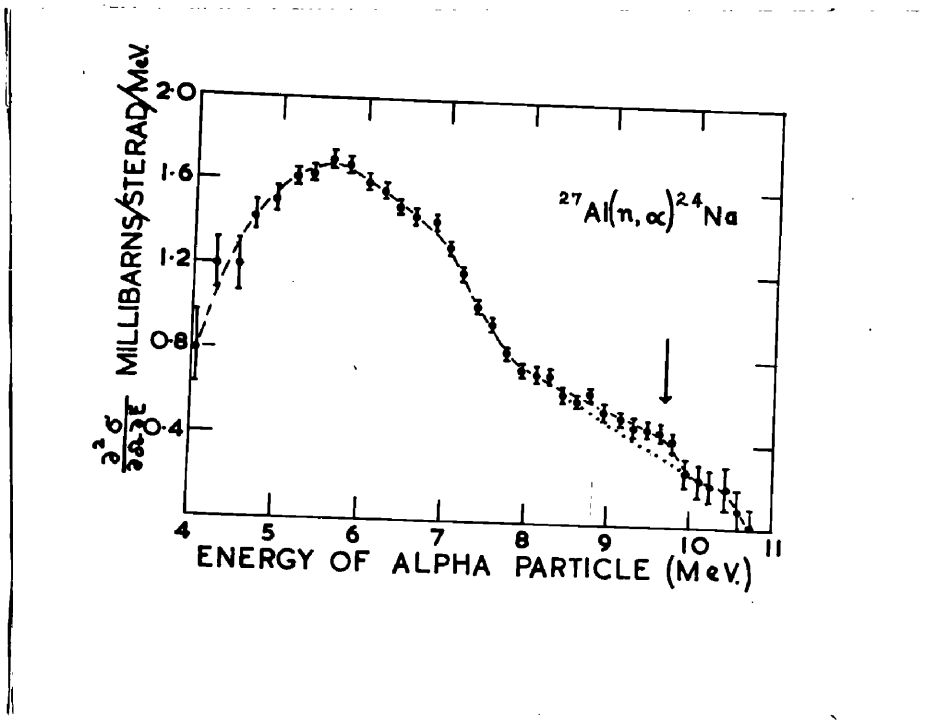

Fig. IV.2 The energy spectrum of alpha particles produced in $^{27}Al(n,\alpha)^{24}Na$ reaction on bombardment with 14.8 MeV neutrons. The spectrum has been plotted in the c. of m. system. The arrow indicates the ground state (n,α) transition. The dotted line is the extrapolation of straight line fit to the statistical plot (Ch. 5).

The spectrum was measured with the 'Energy Distribution' Counter-Telescope, and as explained in the text, the emission of alpha particles was in forward directions with an average angle of 55°. This also applies to Fe, Cu, Zn and Ag spectra presented in figs. IV.5-8. (For comparisons the results of Kumabe et al. and Cevolani et al. are presented on the next page, figs. IV.3 & 4).

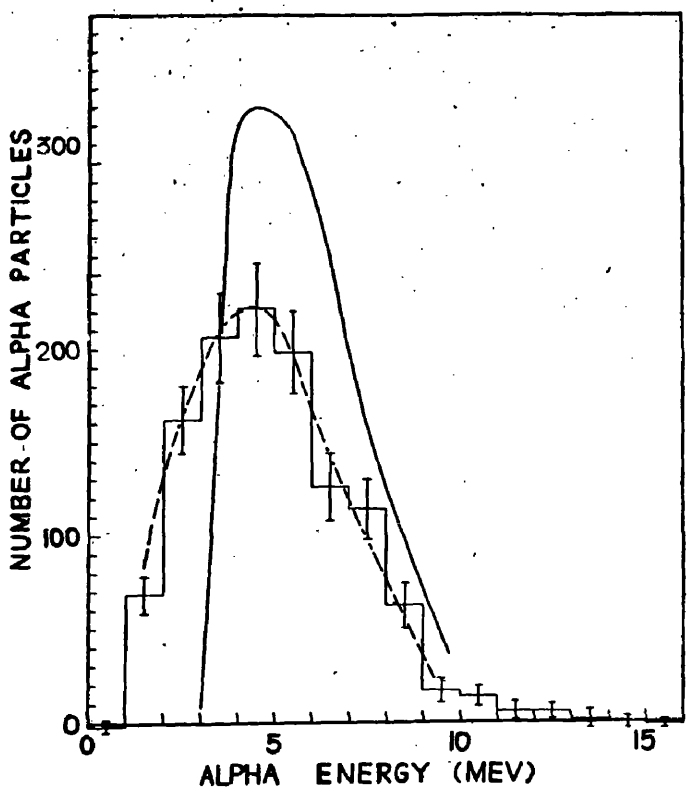

Energy distribution of alpha particles from the $Al^{27}(n,\alpha)Na^{24}$ reaction. The histogram and dashed curve show the observed energy distribution, while the solid curve shows the corrected energy distribution.

Fig. IV.3 Results of Kumabe et al. (ref. 35).

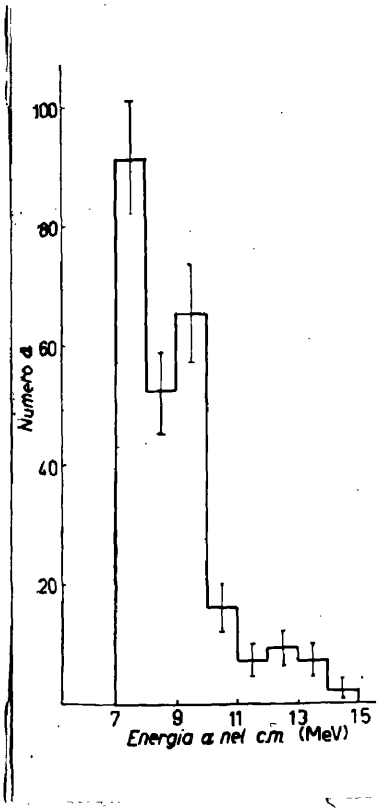

Fig. IV.4 Results of Cevolani et al (ref. 38) $^{27}Al(n,\alpha)^{24}Na$, for alphas $\geqslant$ 7 MeV.

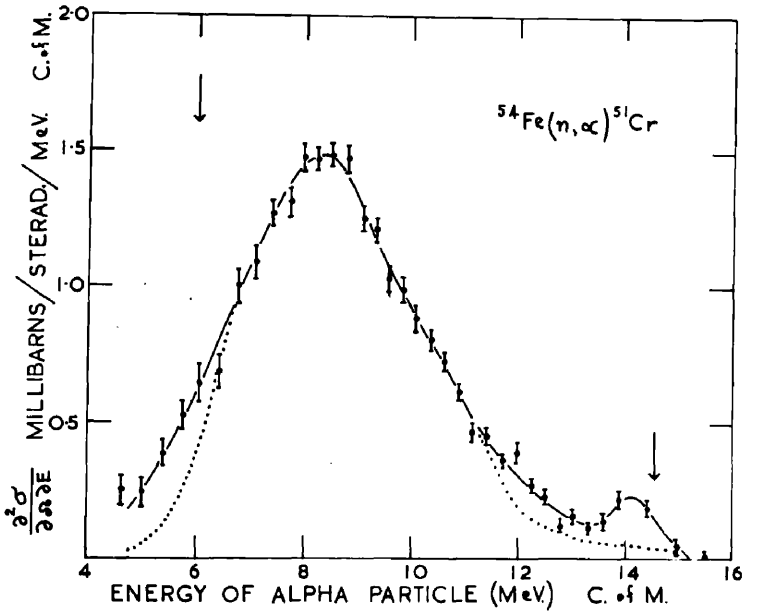

Fig. IV.5

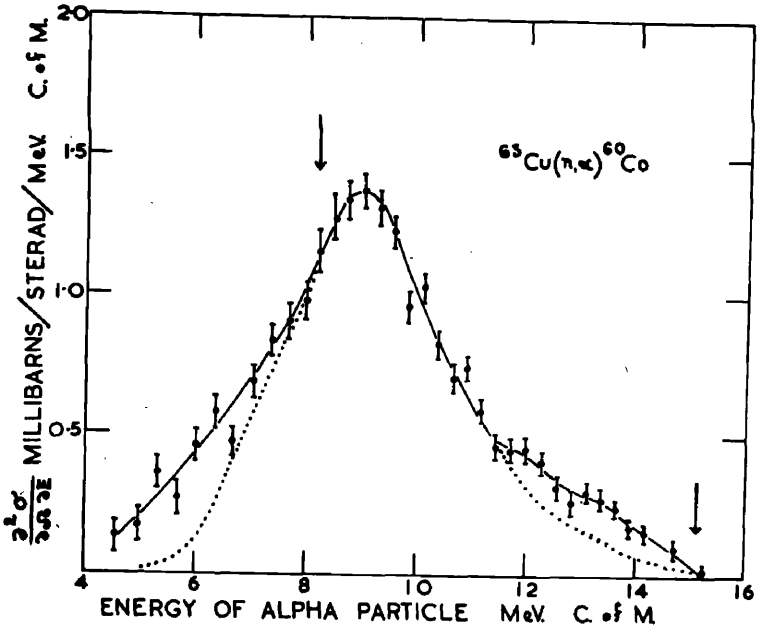

Fig. IV.6

The energy spectra of alpha particles emitted from ^{54}Fe (above), and ^{63}Cu (below). Measurements in forward directions, with the Energy Distribution Telescope. Dotted lines are extrapolations of straight line fits to statistical plots. Arrow, at lower energy, indicates the onset of (n,n α); and that at higher energy is the ground state (n,α) transition.

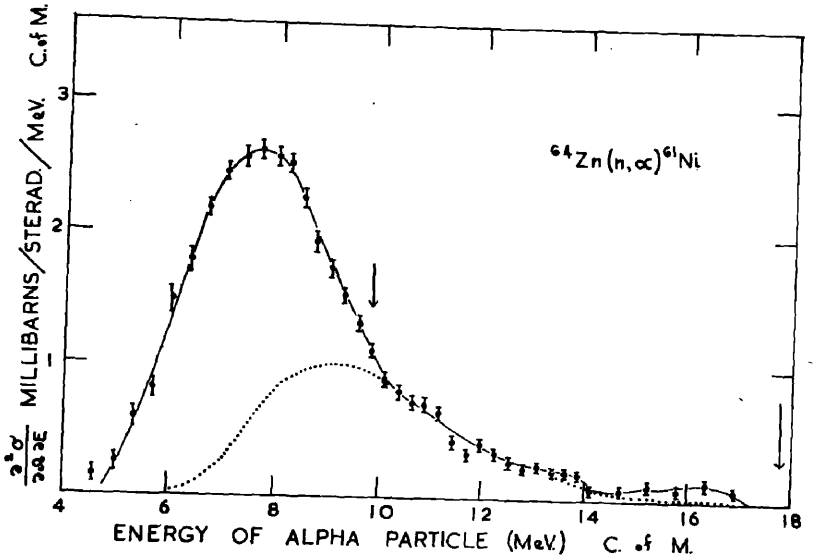

Fig. IV.7

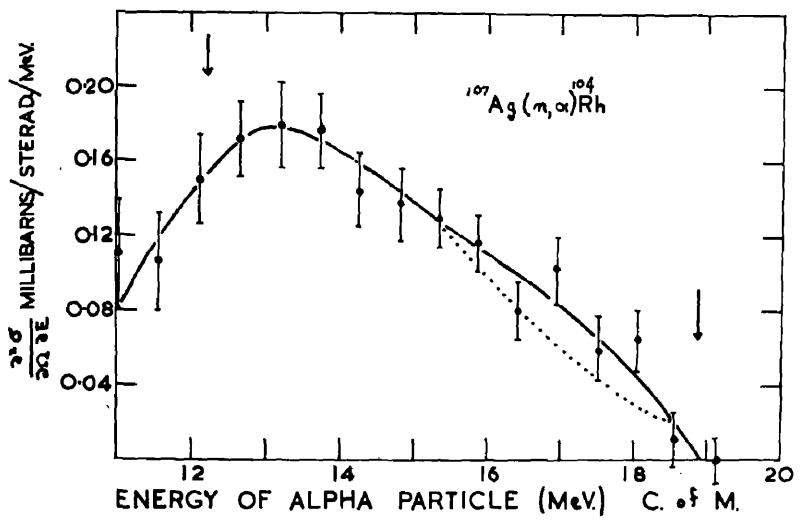

Fig. IV.8

Results for ^{64}Zn (above) and ^{107}Ag (below) corresponding to the preceding figs. IV.5 and 6, for Fe and Cu.

the spectra was necessary; the extrapolations which did not introduce much uncertainty in the values of cross-sections, were done in accordance with the evaporation model). The total error of all kinds is estimated to be ±15%. Table IV.1, page 95a, gives the values of the cross-sections.

(c) <u>The Statistical Plots</u>

For each energy spectrum, two statistical plots were obtained, corresponding to two values of σ_c , taken from Blatt & Weisskopf tables (ref. 16) and Igo's tables (ref.17). The former are based on the continuum model and the latter, on the optical model. Values of σ_c for the experimental points were determined by interpolation. Blatt & Weisskopf have given tables for two values of the radius parameter,

r_0 = 1.3 and 1.5 fermis. (Effective channel radius $R = r_0 A^{1/3} + 1.2 \times 10^{-13}$ cm). We chose the value

r_0 = 1.5 fermis. Figs. IV.9 and 10 show these plots for continuum model and optical model, respectively. E and $\frac{dN}{dE}$ refer to the alpha particles. Black dots are the experimental points and the open circles are obtained by analysis, to be discussed later. The dotted curve below the plot for each target gives the variation of $\log_{10} \frac{1}{E\sigma_c}$ against E. (The plots are designated by target nuclides, but they refer to the residual nuclei). The

Table IV.1

Cross-sections calculated by integrating the energy spectra of alpha particles emitted in forward directions (average angle 55°; average neutron energy 14.8 MeV (Estimated error ± 15%)

Target	Reaction	Cross-section
^{27}Al	(n,α)	6.45 mb/steradian
^{54}Fe	(n,α) + (n,n α)	6.9 "
^{63}Cu	(n,α) + (n,n α)	6.3 "
^{64}Zn	(n,α) + (n,n α)	10.9 "
^{107}Ag	(n,α)	0.96 "

Table IV.2

Differential cross-sections for the emission of alpha particles from ^{27}Al on bombardment with 15 MeV neutrons. (Values in c. of m. system)

Angle	for alphas of energy 6 MeV.	Estimated for alphas of all energies
5°	8.6 ± 0.7 mb/ster	15.9 ± 1.3 mb/ster
38°	3.18± 0.8 mb/ster	5.9 ± 1.4 mb/ster
90°	4.25± 0.75 mb/ster	7.85± 1.4 mb/ster
130°	3.14± 1.6 mb/ster	5.8 ± 2.96 mb/ster
139°	4.1 ± 1.5 mb/ster	7.6 ± 2.77 mb/ster

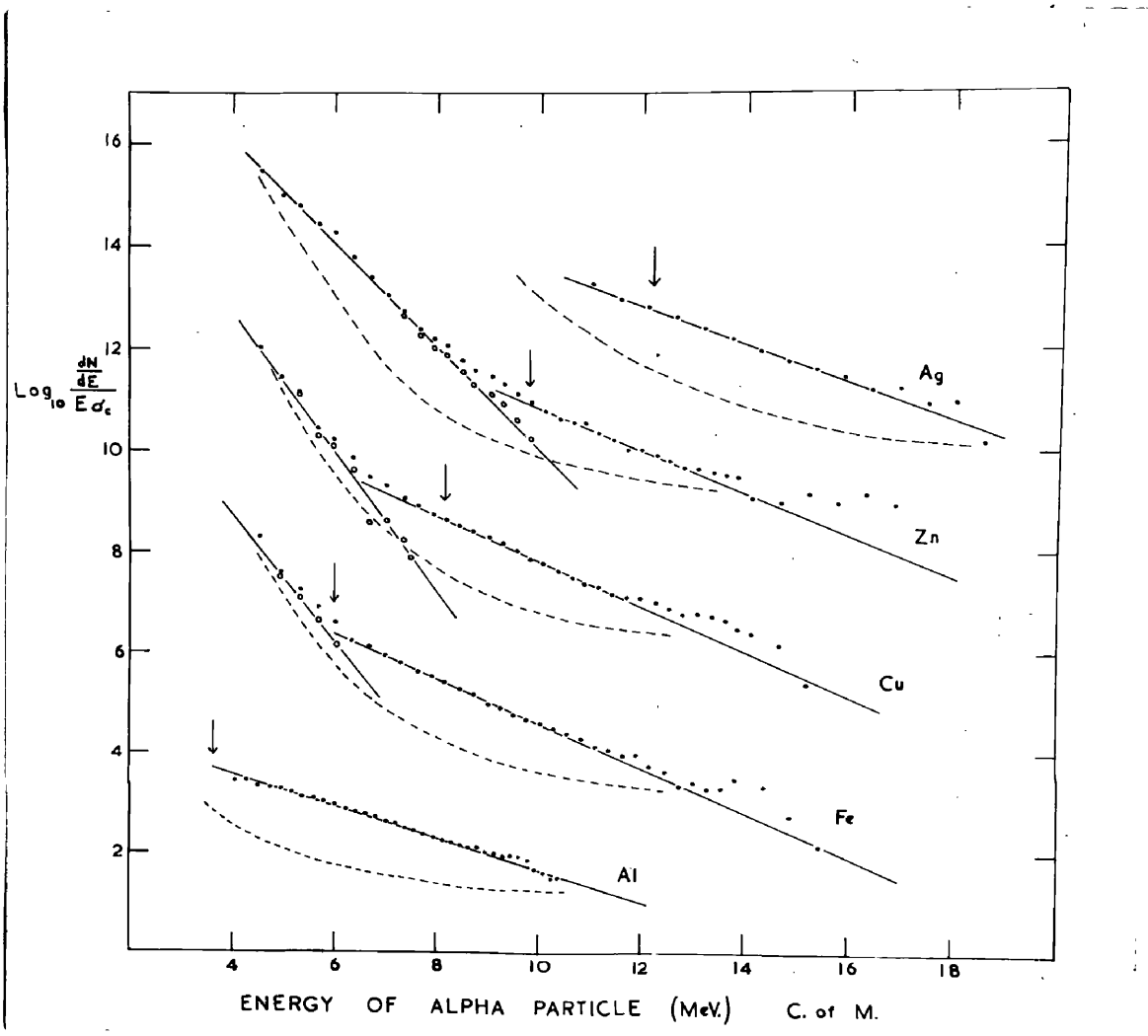

Fig. IV.9

The statistical plots from all five energy spectra σ_c according to the continuum model. Plots are designated by target nuclei for convenience. The dotted curves give $\log_{10} \frac{1}{E\sigma_c}$ vs E. The arrows indicate the onset of (n,n α). The statistical plots (and log $\frac{1}{E\sigma_c}$ curves) are arbitrarily displaced with respect to the ordinate scale for convenience.

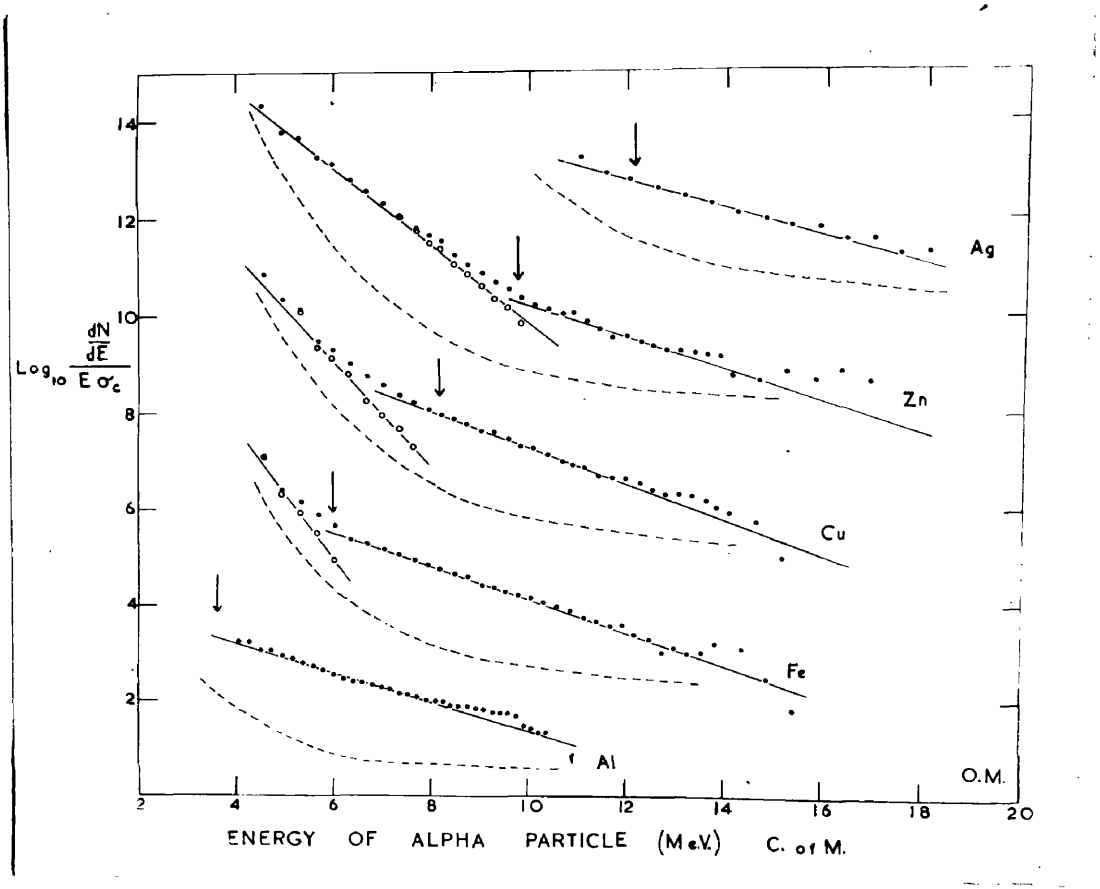

Fig. IV.10

Statistical plots for all five targets; σ_c according to the optical model.

Fig. IV.11

Results of Kumabe et al. (ref. 35) Plot for $^{27}Al(n,\alpha)^{24}Na$ energy spectrum shown in fig(IV.3)
σ_c: continuum model

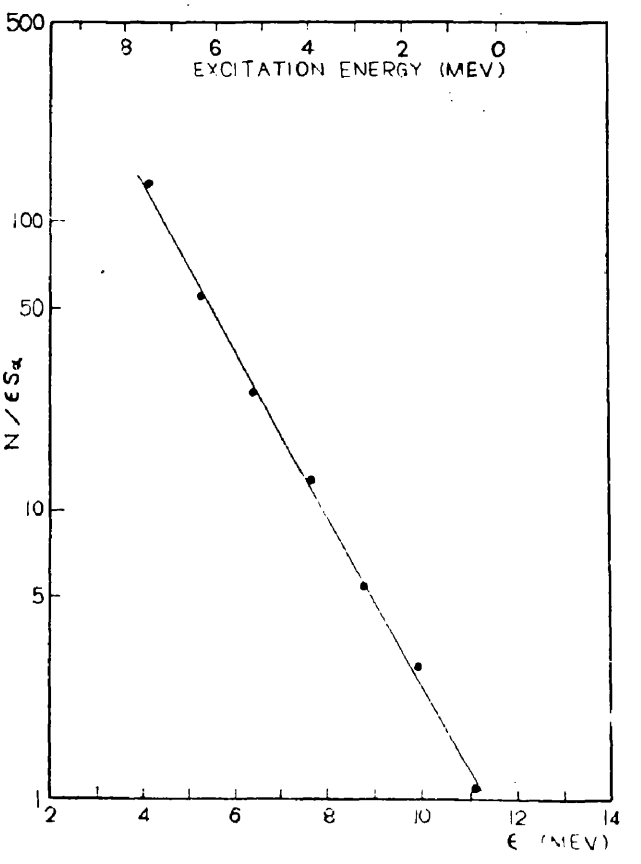

Fig. IV.12

Results of Cevolani et al (ref. 38) C2, plot for $Al(n,\alpha)^{24}Na$ spectrum shown in fig. (IV.4); K-0 plot for only 85° spectrum fig. (IV.14)
σ_c : continuum model.

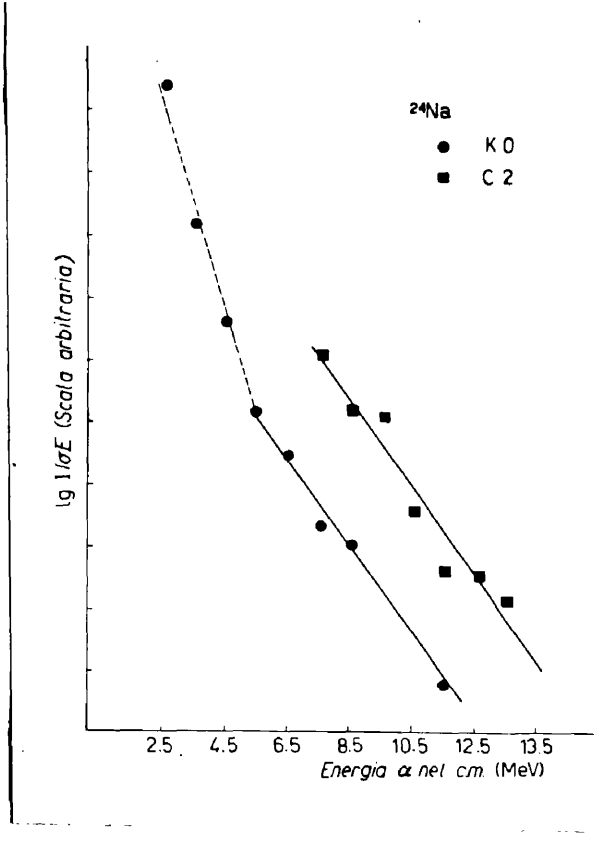

arrow in each case indicates the energy below which (n,nα) can contribute. The plots and $\log_{10}\frac{1}{E\sigma_c}$ curves are all arbitrarily placed as far as the ordinate is concerned. Statistical plots given by Kumabe et al and Cevolani et al for the Al spectra shown in figs. IV.3 and 4 are reproduced in figs. IV.11 & 12 respectively. The K-O, plot in IV.12 refers to an 85° spectrum to be mentioned in the next sub-section.

(d) <u>The Angular Distributions of the Alpha Particles Emitted in the Reaction $^{27}Al(n,\alpha)^{24}Na$, with 15 MeV Neutrons</u>.

Fig. IV.13 presents the energy spectra of alpha particles emitted at 5° and 90°. Due to poor yield, the points shown are averaged over one MeV interval. The results for other angles; 38°, 130° and 139°, were statistically too poor to be given as energy spectra. The 5° and 90° spectra are reliable for alphas $\geqslant$ 6 MeV, from the point of view of the bias settings. The 90° spectrum appears to be about half the height of 5° spectrum, but the shapes are same within the statistical errors. Uncertainty in the angles is estimated to be ±10°. One 85° spectrum obtained by Cevolani et al is shown in fig. IV.14.

Differential cross-sections for alphas of energies $\geqslant$ 6 MeV have been measured at all five angles. The

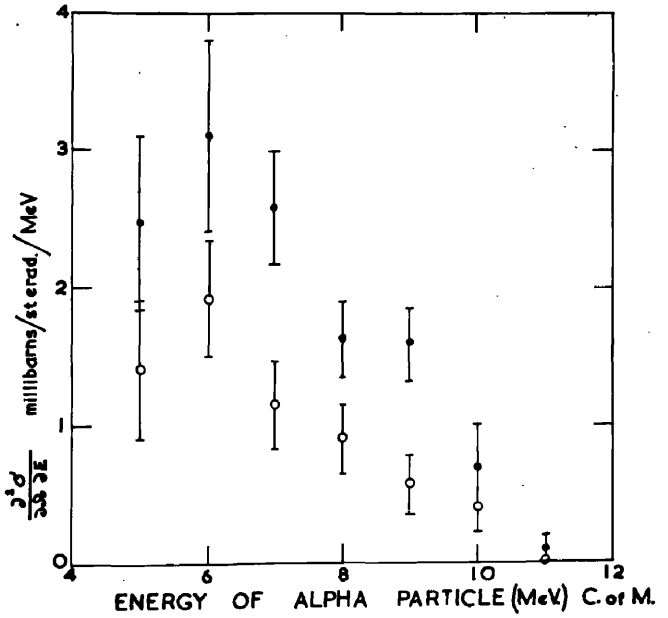

Fig. IV.13 5° and 90° energy spectra of alpha particles emitted in $^{27}Al(n,\alpha)^{24}Na$ reaction with 15 MeV neutrons; measurements with the Angular Distribution Counter Telescope

5° ●

90° ○

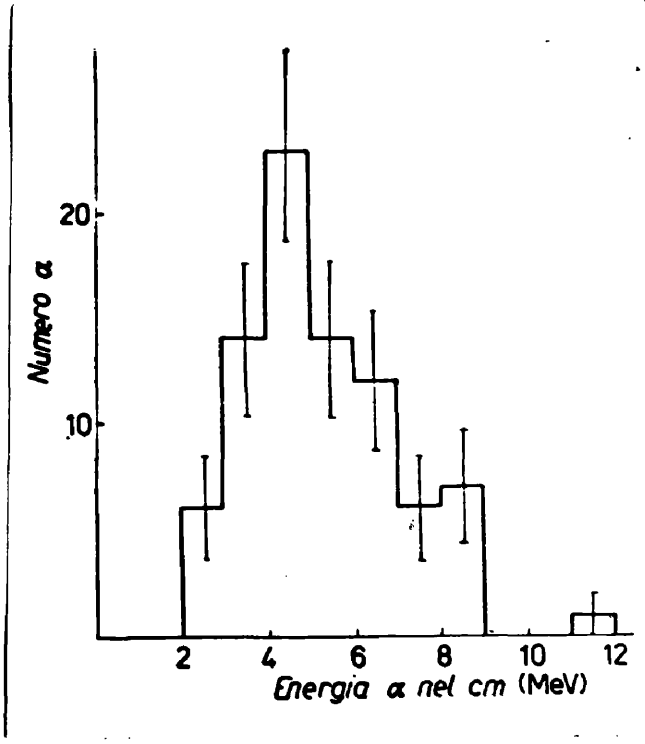

Fig. IV.14

85°, spectrum for $^{27}Al(n,\alpha)^{24}Na$ with 15.2 MeV neutrons, by Cevolani et al (ref. 38)

results are shown in fig. IV.15, in which the values for energies $\geqslant$ 6 MeV, have been stepped up by a constant factor 1.85, which is the ratio $\left(\frac{\text{number of alphas in entire energy region}}{\text{number of alphas of energies} \geqslant 6 \text{ MeV}}\right)$, as determined by the "average angle" spectrum obtained with ^{27}Al, in ED telescope measurements. Hence, provided that the shape of the spectrum does not change with the angle, the ordinate in fig. IV.12 gives the values of the differential cross-sections for all energies. The same figure also contains the results of Kumabe et al, for that angular region. The cross at 55° gives the 'average angle' cross-section, measured with ED telescope. The complete angular distribution curve obtained by Kumabe et al is shown in fig. IV.16; and fig. IV.17 gives the angular distribution results of Cevolani et al. Table IV.2, on page 95a, gives the values of differential cross-section obtained by us.

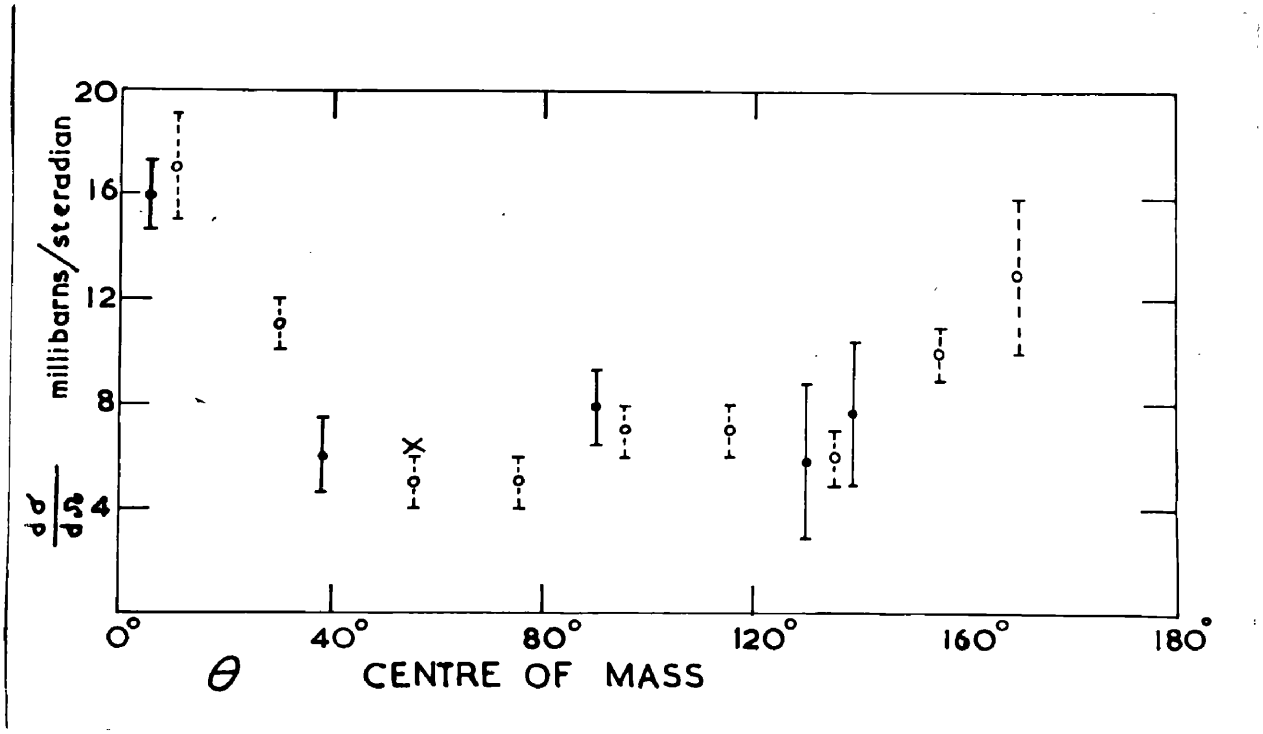

Fig. IV.15 Angular distribution of alpha particles from the $^{27}Al(n,\alpha)^{24}Na$ reaction.

I Present work; measured for alphas of energy $\geq$6 MeV, the ordinate scale stepped up by a factor of 1.85 to give $\frac{d\sigma}{d\Omega}$ for alphas of all energies.

Results of Kumabe et al (ref. 35), their drawing reproduced in fig. IV.16.

× at 55°, denotes the value of $\frac{d\sigma}{d\Omega}$ obtained from the 'wide angle' measurements with the Energy Distribution Counter Telescope.

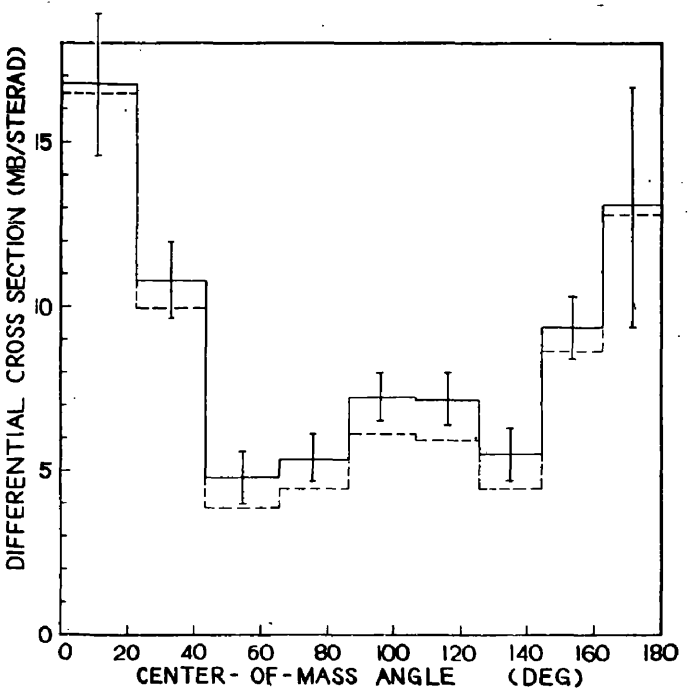

Angular distribution of alpha particles from the $Al^{27}(n,\alpha)Na^{24}$ reaction. The dashed line shows the observed angular distribution, while the solid line shows the corrected angular distribution.

Fig. IV.16 Kumabe et al (ref. 35) points plotted on fig. IV.15 as well. (Alphas of all energies).

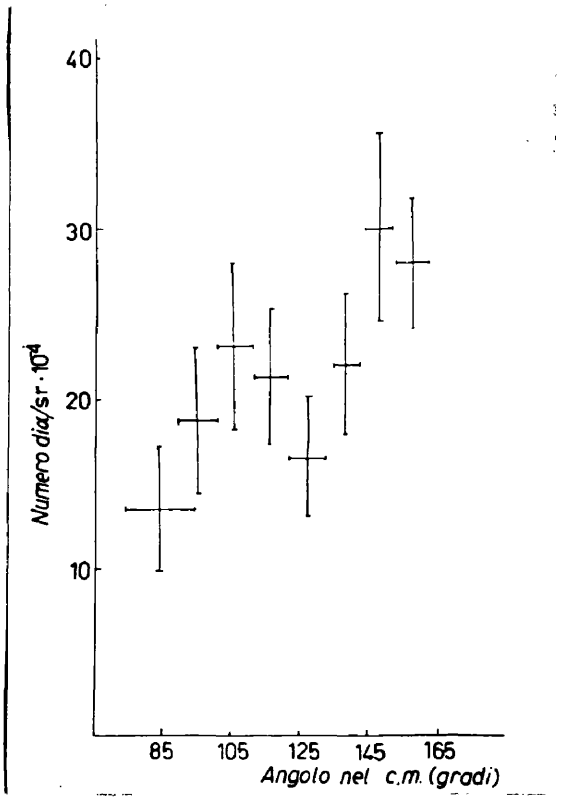

Fig. IV.17

Angular distribution results of Cevolani et al (ref. 38) Alphas of energy $\geq$ 7 MeV, from $^{27}Al(n,\alpha)^{24}Na$ reaction with 15.2 MeV neutrons.

CHAPTER 5. INTERPRETATION AND DISCUSSION OF RESULTS

5.1 The Background Spectrum (shown in fig. IV.1, page93a)

It appears that fairly large proportion of the background counts originate in the crystal itself. Counter gas is probably the other major contributor, though we did not see much difference on increasing the amount of the gas by a factor of two. Protons, deuterons, and alphas are produced in neutron induced reactions in all parts of the crystal, and those travelling backwards, and producing pulse in the proportional counter above the bias level (if the particles have right magnitude of energy), traverse different path lengths in the crystal, depending upon the place of origin. Q values for these reactions in ^{133}Cs are as follows: (in MeV), 0.35, for (n,p); -6.47, for (n,np); -4.15, for (n,d); +4.2, for (n,α); and -2.27 for (n,nα). Values for ^{127}I are roughly the same (Q-values have been quoted from (ref. 53)). Protons and deuterons must have sufficiently low energy to produce a gating pulse. The low energy part of the background spectrum seems to contain many such protons and deuterons; the almost exponential rise, and bigger variation at low energy end with different biases or different crystals, are consistent with this picture. The counts in the peak and after it must be due to alphas, since (1) peak is at about $\sim$8 MeV,

whereas the crystal thickness is equivalent to the range of only $\sim$5 and 2.5 MeV protons for 91 mg/cm^2 and 37.6 mg/cm^2 crystals, respectively, and (2) Peak remains at the same position for considerable variation in proportional counter bias, and for two crystals.

These alphas are unlikely to come from argon; Ribe, 1956 (ref. 99), has reported seeing two peaks in argon-gas counter fillings (with 14 MeV neutrons), the higher peak at 5 MeV only, was attributed to (n,α) in argon. We think that the peak in our background spectrum is due to (n,α) reaction in CsI. According to Bormann and Langkau, (ref. 53) the alpha particle peak in a CsI spectrum should be at $\sim$ 15 MeV, for 15 MeV incident neutron, but realizing that the alphas from CsI recorded in coincidence are only those which have not spent all the energy in the crystal, a superposition of spectra from various layers could have given the final shape. It may be mentioned that the thickness of various layers in the crystal shifting the spectrum to the same extent will be greater for the top part of the crystal, due to $\frac{dE}{dx}$ difference for various alpha energies. The contribution from top layers corresponds to less energy spent in the crystal itself, and this fact may be one of the important factors in giving a peak at a lower energy instead of a more probable 'flat'

spectrum due to superposition of spectra from various layers.

5.2 Average Angle Energy Spectra from Isotope Targets

(a) Break-up of Spectra in Various Components by the Use of Statistical Plots.

Continuum model plots are shown in fig. IV.9 page 95b and the optical model plots in fig. IV.10 page 95c. These plots in the case of Al, and Ag give quite good fits to single straight lines, if slight departure at the high energy end is ignored. Plots for Fe, Cu and Zn indicate 'two lines' fit, the steeper one corresponding to the excess of alpha particles (in that part of the spectrum) over what would have fitted the extrapolated single line.

Making use of the continuum model plots, we have shown with dotted lines on each spectrum, the shape corresponding to the 'single line' fit in the region where the observed spectrum has shown departure from it. [Al (fig. IV.2, page 94a), Fe, Cu, Zn and Ag, (figs. IV.5-8, page 94c,d) Assuming that the evaporated part of (n,α) spectrum is faithfully represented by the single line fits, we shall attribute the excess of low energy alphas to $(n,{}^{n'\alpha}_{\alpha\ n'})$ reaction, later to be referred only (n,nα), and excess of high energy alphas to direct interaction. We shall discuss the validity of this break-up later. The

application of optical model plots gave approximately the same break-up, hence we have not shown it separately.

(b) Nuclear Temperatures

The nuclear temperatures derived from the slopes of the straight lines drawn on the statistical plots are given in table (V.1), page 101a.

First we shall compare the values of T obtained from two models. Confining to (n,α) temperatures only, it is seen that optical model always gives higher values for T. This is due to the fact that the optical model calculations of Igo give relatively higher values of σ_c for alpha particles of lower energy. As an illustration we present the following figures for Z = 30.

Alpha energy	σ_c (Optical)	σ_c (Continuum) (by interpolation)
7.52 MeV	16.56 mb	3.2 mb
18.8 MeV	1230.8 mb	540 mb

To examine the difference between the sets of values of σ_c from two models, we drew an ideal straight line plot for continuum model (choosing T, arbitrarily equal to 1.3 MeV); from this we constructed the energy spectrum, and then derived the 'optical model' statistical plot from this constructed spectrum. We found that optical model plot was somewhat wavy in shape and could not be fitted to

Table V.1 (Nuclear Temperatures, T)

Target	(n,α) Residual nucleus	Value of T (MeV) (Continuum model)		Value of T (MeV) (Optical model)	
		(n,α)	(n,n α)	(n,α)	(n,n α)
^{27}Al	^{24}Na	1.35	-	1.41	-
^{54}Fe	^{51}Cr	0.97	0.35	1.24	0.32
^{63}Cu	^{60}Co	0.97	0.32	1.16	0.4
^{64}Zn	^{61}Ni	1.05	0.41	1.34	0.55
^{107}Ag	^{104}Rh	1.18	-	1.51	-

a single line, though a 'mean' line could be drawn reasonably. Making this comparative study for Z = 10,20, 30 and 50, we concluded that in the energy region of concern, the optical model analysis would give higher temperatures. Since our experimental results give nearly same degree of straight line fits to both analyses, it is not possible to favour one of them on this basis. One point we did notice that an ideal 'continuum model' evaporation spectrum can easily be analyzed as 'evaporation + direct' spectrum on optical model. This tendency is not visible from our results, but Bormann and Langkau (ref. 53) reported it from their results on (n,α) reaction in CsI.

The (n,n α) temperatures, determined from the steeper lines, have larger values, in case of Cu and Zn, for the optical model; but in case of Fe, the value for the continuum model is slightly bigger. Not much importance can be attached to this discrepancy, since a little adjustment of lines drawn for Fe can give the values of (n,n α) temperatures in reverse order. It may be pointed out that for drawing the lines the judgment was based entirely 'on the average best fit' to the experimental points. However, values of temperatures determined by these plots, are estimated to have uncertainty of not more than $\pm$ .1 MeV.

(c) Level Density Parameter 'a'

We have derived the values of 'a' by carrying out the analysis of our spectra, for the level density expression $\omega_y(E_y) = C \exp(2\sqrt{aE_y})$ and also from the relationship between E_y and T implied in this expression of $\omega_y(E_y)$ i.e. the relation, $E_y = aT^2$, (E_y is the excitation energy of the residual nucleus). We have ignored the difference between the true nuclear temperature Θ and T. As we have mentioned earlier, T is determined from the statistical plots, through the relation $\frac{d}{dE_y}\left(\log_e \omega_y(E_y)\right) = \frac{1}{T}$ where $\omega_y(E_y)$ is proportional to $\left[\frac{dN(E_\alpha)}{dE_\alpha} / E_\alpha \cdot \sigma_c(E_\alpha)\right]$. The fact that we are able to draw straight lines on this log plot of the relative level density (which we have drawn against E_a) implies that 'T' is constant while E_y is varying in the region of the straight line fit; this, furthermore, yields a different expression for the level density, $\omega_y(E_y) \propto \exp\left(\frac{E_y}{T}\right)$. This situation is clearly contrary to the prescription $E_y = aT^2$ (or equivalently, $\omega_y(E_y) = C \exp(2\sqrt{aE_y})$ However, when we plotted $\log\left[\frac{dN(E_\alpha)}{dE_\alpha} / E_\alpha \cdot \sigma_c(E_\alpha)\right]$ vs $\sqrt{E_y}$, we again found 'straight line fits' more or less to the same extent as for the log plots vs E_y (equivalently, vs E_a); the high and low energy ends showed departures from straight lines. This partial applicability of both expressions for $\omega_y(E_y)$ is not

uncommon, and like the results of numerous other experiments, our results also do not decide which form for $\omega_\gamma(E_\gamma)$ is more suitable.

We have determined the values of a, called by us a_1, from the log plot vs $\sqrt{E_\gamma}$ for both the continuum and the optical, models. We have also determined a, called by us a_2, from $(E_\gamma)_{av.} = \alpha T^2$, with $(E_\gamma)_{av.}$ as the average value of E_γ over the region of constant temperature straight line. In addition, we have also adopted the approach $(E_\gamma)_{max} = a\, T^2_{max}$ and have determined $a = a_3$. The values of a_3 are meaningful when the T_{max}, can be ascribed to the $(E_\gamma)_{max}$, but due to the presence of (n,n α) this is not practicable in the case of Fe, Cu and Zn. We have put $T = T_{max}$ for the determination of a_3. In the case of Al, it is interesting to note, that the continuum model analysis gives few such points at the high E_γ end (i.e. low E_α end) which can be ascribed to a higher temperature $\approx$ 2.1 MeV compared with the value 1.35 MeV deduced from the straight line. We have derived the value of 'a_3' for this temperature as well; a_3 for T = 2.1 MeV is 2.2 MeV^{-1} whereas for T = 1.35 MeV, a_3 = 5.3 MeV^{-1}. In principle the value corresponding to T = 2.1 MeV should be more reliable, but due to paucity of experimental points we should regard this value with some caution. A slight

tendency for higher temperature at the low E_α end in Al, is also visible in the optical model analysis. For Ag, it appears that $T_{max} = T$ is much more reasonable approximation than in the case of Fe, Cu or Zn. All three sets of values, a_1, a_2 and a_3 are given in table V.2 page 105a.

In view of the approach adopted for determining a_1, a_2 and a_3, it may be remarked that a_1 and a_2 were expected to agree with each other, and they are found to be nearly so. Noticing the increasing value for 'a' with increasing mass from Al to Zn, the value for Ag seems to be anomalously low. As far as the values of a_3 are concerned, perhaps they have some meaning in the case of Al and Ag, whose spectra were not contaminated with (n,n α).

In the following sub-section, we shall discuss the values of 'T' and 'a' obtained in the present work, by comparing them with other known results.

(d) Discussion on the Values of 'a' and 'T'

Before making any direct comparisons with other results we shall point out the experimental evidence on the behaviour of 'T' and 'a' with different masses and energies. We shall first make some general statements and shall quote some specific examples later.

Reasonable applicability of constant temperature form

Table V.2 (Values of the level density parameter 'a')

Target nucleus	(n,α) residual nucleus	$a = a_1$, MeV^{-1}		$a = a_2$, MeV^{-1}		$a = a_3$, MeV^{-1}	
		Continuum model	Optical model	Continuum model	Optical model	Continuum model	Optical model
^{27}Al	^{24}Na	1.7	1.5	1.4	1.6	5.3 (2.2?)	4.8
^{54}Fe	^{51}Cr	3.7	3.5	6.1	3.5	15.4	9.4
^{63}Cu	^{60}Co	4.9	4.4	5.6	4.7	16.1	11.2
^{64}Zn	^{61}Ni	5.4	4.2	5.7	3.3	16.1	10.4
^{107}Ag	^{104}Rh	3.9	2.9	3.5	2.2	13.5	8.3

a_1, from the analysis $\log_e \left[\frac{dN(E_\alpha)}{dE_\alpha} \Big/ E_\alpha \cdot \sigma_c(E_\alpha) \right]$ vs $\sqrt{E_y}$

where E_y is the excitation energy of the residual nucleus

a_2, $(E)_{average}/T^2$; a_3, $(E)_{max}/T^2$

of the level density (i.e. $\omega_y(E_y) \propto exp \frac{E_y}{T}$) is quite frequently found; but at the same time it is usually observed that when comparisons are made between different reactions, like (p,p′) and (n,p), correlation is found when comparison is made with different spectra related to the energy of the emitted particle, rather than to the energy of the residual nucleus. This trend is more explicitly demonstrated when comparisons are made between different spectra of the same reaction but with different incident energies. Another thing quite frequently reported is the simultaneous applicability of the commonly adopted forms of level density, $\omega_y \propto exp \frac{E_y}{T}$ and $\omega_y = C\ exp(2\sqrt{aE_y})$

Colli et al, 1957 (ref. 63) compared 14 MeV (n,p) spectra at forward angles, with 18 MeV (p,p′) spectra obtained at 150° by Gugelot, 1954 (ref. 100), who had already compared (p,p′) spectra in Ag with 16 and 18 MeV. Both comparisons suggested that the shape of the spectrum is determined by the energy of the emitted particle. Storey et al, 1960 (ref. 32), who studied 14 MeV (n,p) reactions in several elements and also examined the results of other workers, suggested an empirical relation, that barring few exceptions the average value of $E_c^*/A T_m^2$ is constant and is equal to 0.158 ± 0.003 MeV^{-1}, where E_c^*

and A are the excitation energy and mass number for the compound nucleus, and Tm is equivalent to 'T' of present work. This empirical relation is also contrary to the final form of the evaporation spectrum. Lassen and Sidorov, 1960 (ref. 101), in their (α,p) spectra with elements of A $\sim$ 60 and alpha particle energy between 11.9 and 19.3 MeV reported a correspondence with the constant temperature form of the level density, but the temperature showed strong dependence on the incident energy, (decreasing with the decrease in the energy). We could quote several other papers, but we shall refer to the comparative study made by Swenson and Cindro, 1961 (ref. 80), in connection with their results on 30.5 MeV (α,p) reactions on eight elements from Al to Ta. They have analyzed their 150° spectra in terms of the statistical model, and compared their results with those of others. They have shown that for the same E_γ ($\sim$10 MeV), the temperature T varied from $\sim$.6 to 2.6 Mev, for different incident energies, 11.9 to 40 MeV, used in different experiments, (mass number around 60); correspondingly the value of 'a' changed from 25 to 1.5 MeV^{-1}. The parameters a and T, however, showed a mass variation qualitatively in agreement with the predictions of any nuclear model, but quantitatively with none. (T is smaller for heavier elements).

We must, however, point out that recently, Bormann and Langkau (ref. 53) were able to resolve the discrepancy of this dependence of a and T on incident energy (while insensitive to E_y) by using σ_c from optical model. (This feature of their analysis was described in Chapter 1). Recently Sherr and Brady, (ref. 74) have also reported a consistent behaviour of constant T form of level density with (p,α) reactions on Ni and Co, for three different proton energies, 15, 17.5 and 19 MeV. It is not known whether both continuum and optical models lead to the same conclusion. In another recent work by Houck and Miller, 1961 (ref. 102), on the excitation functions of reactions induced by alpha particles (from low energies to $\sim$ 40 MeV), it is reported that the experimental values for total reaction cross section agreed with the continuum model (with $r_0 = 1.7$ fermis) but disagreed with the predictions of the optical model calculations (by Igo, ref. 17).

From comparisons of values of 'a' obtained from different experiments and surveys, it is interesting to note the 'bewildering' varieties of this parameter as summarized by Dostrovsky et al 1959 (ref. 103).

We shall now make a comparative study of the values of 'T' and 'a' obtained by us. Our value of T for $^{27}Al(n,\alpha)^{24}Na$ reaction is smaller than reported for the

same reaction by Kumabe et al, 1.45 MeV, and by Cevolani et al, 1.41 MeV (back angles). Comparing $^{63}Cu(n,\alpha)^{60}Co$ with $^{60}Ni(n,p)^{60}Co$, our temperature, 0.97 MeV, is again smaller than 1.4 MeV, by Storey et al, 1960 (ref. 32) but in fair agreement with 1.0 MeV reported by March and Morton 1958 (ref. 57). It may be pointed out that Kumabe et al, have reported low values for T in 14.8 MeV (n,α) reactions on ^{51}V, ^{55}Mn and ^{59}Co, (0.9, 0.85 and 0.7 MeV respectively).

For ^{60}Co as a residual nucleus our value of a_3 is much higher than the corresponding value 5.5 MeV^{-1} reported by Jack and Ward, 1960 (ref. 62) based on the 14 MeV (n,p) results of Storey et al. (Our values in table V.2). In other cases direct comparison is not possible but it appears that our values of a_3 for Al and Ag are consistent with their results, but for Cu and Zn (like Fe) are high by a factor of 2.5 to 3. On comparing our a_1 and a_2 with the values of 'a' determined by Swenson and Cindro, 1961 (ref. 79), in 30 MeV (α,p) reactions, better agreement is observed; for the residual nuclei ^{30}Si, ^{54}Cr, ^{62}Ni, ^{78}Se, ^{96}Mo and ^{106}Pd, they find a = 1.8, 2.8, 2.8, 3.9, 2.8 and 3.2 MeV^{-1} respectively. (As remarked earlier for ^{107}Ag target we get anomalously low value). Swenson and Cindro found their values of 'a' to be about 2.5 times smaller than those predicted by the Fermigas model treatment of Lang and

Le Couteur 1954 (ref. 21), or of Newton 1956 (ref. 22). We shall extend the comparison to another empirical relation for odd A values, $a = 0.035\ (A - 12)\ MeV^{-1}$, for $15 < A < 70$, deduced by Heidmann and Bethe, 1951 (ref. 107) from the study of the photocapture process. According to this relation, for ^{51}Cr and ^{61}Ni (residual nuclei for (n,α) on ^{54}Fe and ^{63}Cu), 'a' should be 1.37 and 1.72 MeV^{-1}; our values of a_1 and a_2 are larger than these. Blatt and Weisskopf (ref. 16) give for A = 63, somewhat higher value than $a = 0.035\ (A - 12)\ MeV^{-1}$. Values of a from 11.9 MeV (α,p) reactions studied by Lassen and Sidorov, 1960 (ref.101) are much higher than ours (from, Swenson and Cindro, ref. 79).

One point of interest in the values of 'a' determined by us is, that ^{60}Co and ^{61}Ni do not show any striking difference due to even and odd A values.

(e) Cross-Sections

We have listed the values of cross-sections (expressed in mb/ster) determined by our spectra, in table IV.1, page 95a. As shown in the table, values for ^{54}Fe, ^{63}Cu and ^{64}Zn contain (n,n α) contribution, which cannot be determined from activation measurements as the end products are stable. (This is true for a majority of stable isotope targets). In case of ^{64}Zn, even $\sigma(n,\alpha)$ cannot be determined by that method, since ^{61}Ni, the residual nucleus, is stable. For

^{54}Fe, ^{63}Cu and ^{107}Ag no previous measurements exist, and ^{27}Al is the only case for which a direct comparison is possible. $\sigma(n,\alpha)$ for ^{27}Al, with 14 - 15 MeV neutrons has been determined by several workers, and some of these results are as follows; Paul and Clarke, 1953 (ref. 49), 79.8 mb; Yasumi, 1957 (ref. 108), 120 ± 15 mb; Grundl et al, 1958 (ref. 109), 116 ± 8.1 mb; and Poularikas and Fink, 1959 (ref. 110), 114 ± 7 mb. The commonly accepted value is ≃115 mb. $\sigma(n,\alpha)$ for Al, from our measurements is 81 ± 12 mb, which seems in good agreement with the accepted value, when due consideration is given to the angular distribution effects. According to Paul and Clarke, the theoretical value of $\sigma(n,\alpha)$ in Al, for the evaporation model, is 273 mb; but the Q value used by them is + 2.3 MeV, whereas from mass values (ref. 82) we find Q = -3.14 MeV. This discrepancy may account for the predicted value being higher. For a ready reference we have tabulated all the Q values for reactions studied by us (Table V.3, page 111a). Our $\sigma(n,\alpha)$ for Al, is in good agreement with the value obtained by Kumabe et al from their (n,α) energy spectrum; they observed the value 92 ± 15 mb, out of which they attributed 82 ± 17 mb to (n,α). Our $\sigma(n,\alpha)$ for ^{107}Ag, ≈ 12 mb, is about a factor of 5 - 10 higher than would be estimated from the results of Blosser et al, 1955-58 (ref. 50) and of

Table V.3 Q-values

Target nucleus	(n,α) Residual nucleus	(n,α) Q-value	(n,n α) Residual nucleus	(n,n α) Q-value
$^{27}_{13}Al$	$^{24}_{11}Na$	-3.14 MeV	$^{23}_{11}Na$	-10.1 MeV
$^{54}_{26}Fe$	$^{51}_{24}Cr$	+0.85 MeV	$^{50}_{24}Cr$	-8.26 MeV
$^{63}_{29}Cu$	$^{60}_{27}Co$	+1.50 MeV	$^{59}_{27}Co$	-5.92 MeV
$^{64}_{30}Zn$	$^{61}_{28}Ni$	+4.38 MeV	$^{60}_{28}Ni$	-4.16 MeV
$^{107}_{47}Ag$	$^{104}_{45}Rh$	+4.1 MeV	$^{103}_{45}Rh$	-2.57 MeV

Coleman et al, 1959 (ref. 51); and it is certainly higher by at least a factor of 10 than would be expected from evaporation model. The statistics on our $^{107}Ag(n,\alpha)$ spectrum are far from satisfactory, but it is interesting to note that recently Mukherjee et al, 1961 (ref. 111) have measured $\sigma(n,\alpha)$ in ^{109}Ag (Q value + 3.9 MeV), and found it to be $\lesssim$ 12 mb. Our cross-sections for ^{54}Fe, ^{63}Cu and ^{64}Zn are also estimated to be about 5 - 10 times higher than expected from theory. Kumabe et al also observed high cross-sections in their results; we are reproducing the contents of their tables in, table V.4 page 112a. Very recently, Strohal et al 1961 (ref. 112) have reported $\frac{\sigma_{exp.}(n,\alpha)}{\sigma_{theoret}(n,\alpha)}$ between 12 ~ 200, for 14 MeV neutrons on six elements, A $\lesssim$ 80 to 100. Some other measurements of interest are; (n,α) for ^{68}Zn (Q, + 0.94 MeV), (7.5 mb; and for ^{59}Co (Q, 0.37 MeV) 31 ± 3 mb by Blosser et al (ref. 50), and again for ^{59}Co, 29 ± 6 mb by Weigold, 1960 (ref. 52).

(f) <u>(n,n α) and Direct Interactions</u>.

We have already mentioned about the break-up of energy spectra by using statistical plots (figs IV.2, 5 - 10). One fact is easily noticed that the slope in the log plots, at the low energy end, changes with the possible onset of (n,n α) reaction. We have plotted log $\frac{1}{E\sigma_c}$ curves to see

Table V.4 Comparison of Cross Sections (mb)

(Contents reproduced from Kumabe et al).

Target	Kumabe et al.		Activation Methods (n,αγ)			Theoretical
	(n,αγ) + (n,αn) +(n,nα)	(n,αγ)	Paul and Clarke	Hughes*	Yasumi	
^{27}Al	92 ± 15	82.0 ± 17	78.9 ± 16	110 ± 20	120 ± 14.4	273
^{32}S	109 16	38.2 7.6	-	-	-	-
^{51}V	126 19	43.2 8.6	28.6 12	30 10	-	4.6
^{55}Mn	96 14	39.4 8.0	52.5 7.9	30 12	-	4.5
^{59}Co	84 13	25.0 5.0	39.1 7.8	52 8	-	3.7

* These data are summarized by D.J. Hughes and J.A. Harvey (Neutron Cross Sections McGraw Hill Book Co, Inc., New York, 1955).

Theoretical cross sections were derived from the calculation by Paul and Clarke (our ref. 49).

Yasumi; (our ref. 108).

how far the interpretation is influenced by σ_c, which obviously affects the analysis. Comparison of log plots for various targets, particularly Al and Ag against others, suggests that the break up is strongly influenced by the shape of the measured spectra themselves. Attributing the excess of low energy alphas to (n,n α) and of high energy alphas to direct interaction, we have determined the contribution from each mode, and have tabulated the details on page 113a, table V.5. Except ^{64}Zn, all other targets show a reasonable relative contribution. In ^{64}Zn, 57% of the total yield is accounted by (n,n α), a very unusual situation. According to Q-values (table V.3), (n,n α) in Fe, Cu and Zn is in the right order but the huge contribution in ^{64}Zn is hard to explain just by Q-values. We have considered the possibility of oxygen being present as an impurity, but the known $^{16}O(n,\alpha)^{13}C$ spectrum, Lillie, 1952 (ref. 113), is not consistent with the ^{64}Zn spectrum measured by us. It is suggestive that ^{64}Zn contains two protons in excess of 28, the magic number, and perhaps it is likely that when a neutron is inelastically scattered, the excited ^{64}Zn nucleus finds it easier to get rid of the excess energy by the emission of an alpha particle.

(g) <u>Some Other Features of the Observed Spectra</u>

^{27}Al, spectrum is seen extending by about 1 MeV beyond

Table V.5 Analysis of Observed Cross Sections

Estimated values for various contributions, and their approximate percentage of the observed cross section.

ALL VALUES IN MILLIBARNS PER STERADIAN.

Target	Observed cross section	(n,n α)	(n,α) Evaporation	(n,α) Direct
^{27}Al	* 6.45	-	6.45(100%)	negligible
^{54}Fe	6.9	0.43(6%)	6.06(88%)	0.41 (6%)
^{63}Cu	6.3	0.65(10%)	5.3(84.5%)	0.35(5.5%)
^{64}Zn	10.9	6.28(57.5%)	4.35(40%)	0.27(2.5%)
^{107}Ag	0.96	negligible	0.96(100%)	negligible

the ground state transition. Though the ground state transition was calculated for average geometry we think it is somewhat curious to get relatively so many alphas in Al, above that mark. This Q-value 'violation' is also apparent in the results of Kumabe et al and Cevolani et al (page 946). The peak in our Al spectrum is slightly higher than deduced by Kumabe et al and Cevolani et al. ^{54}Fe spectrum shows a small peak at the tail end at $\sim$14 MeV; the peak is not due to any statistical fluctuations. Not much can be inferred about the origin of this peak, unless its angular distribution is known.

The peaks due to (n,α) evaporation components, are seen consistently moving upward with atomic number.

The cross-sections and temperatures are influenced by Q values and coulomb barriers, at least qualitatively, in the right sense; but T for ^{107}Ag seems to be unusually high compared with 'T' for ^{64}Zn.

Due to lack of other experimental results for comparisons, we are also reproducing the results of Kumabe et al on pages 114 a, b, c.

5.3 The Angular Distributions of Alpha Particles from $^{27}Al(n,\alpha)^{24}Na$ Reaction

Our results on differential cross-sections agree

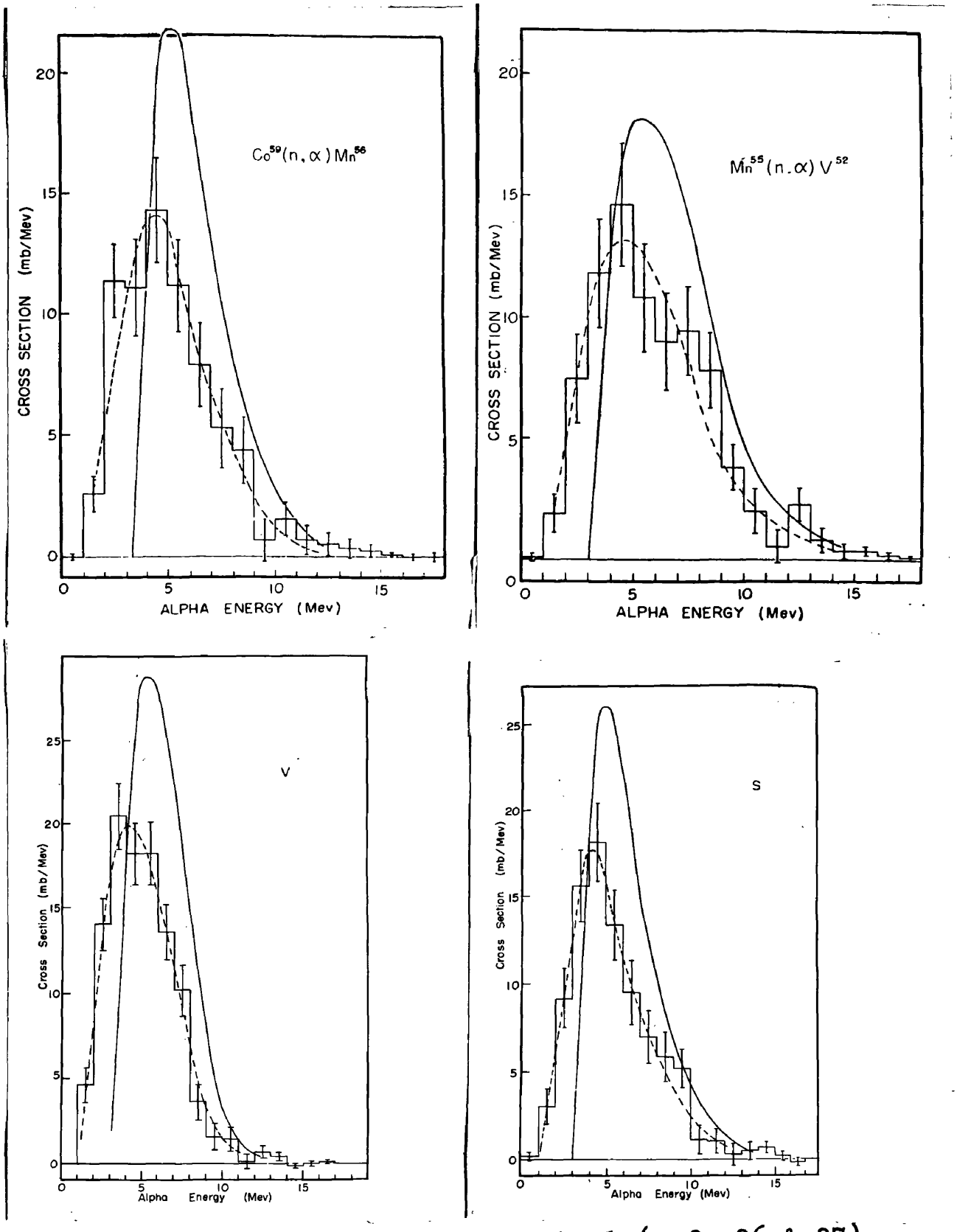

Fig. V.1 Energy spectra by Kumabe et al (ref. 36 & 37) from the (n,α) reaction in ^{55}Mn, ^{59}Co, ^{32}S & ^{51}V.

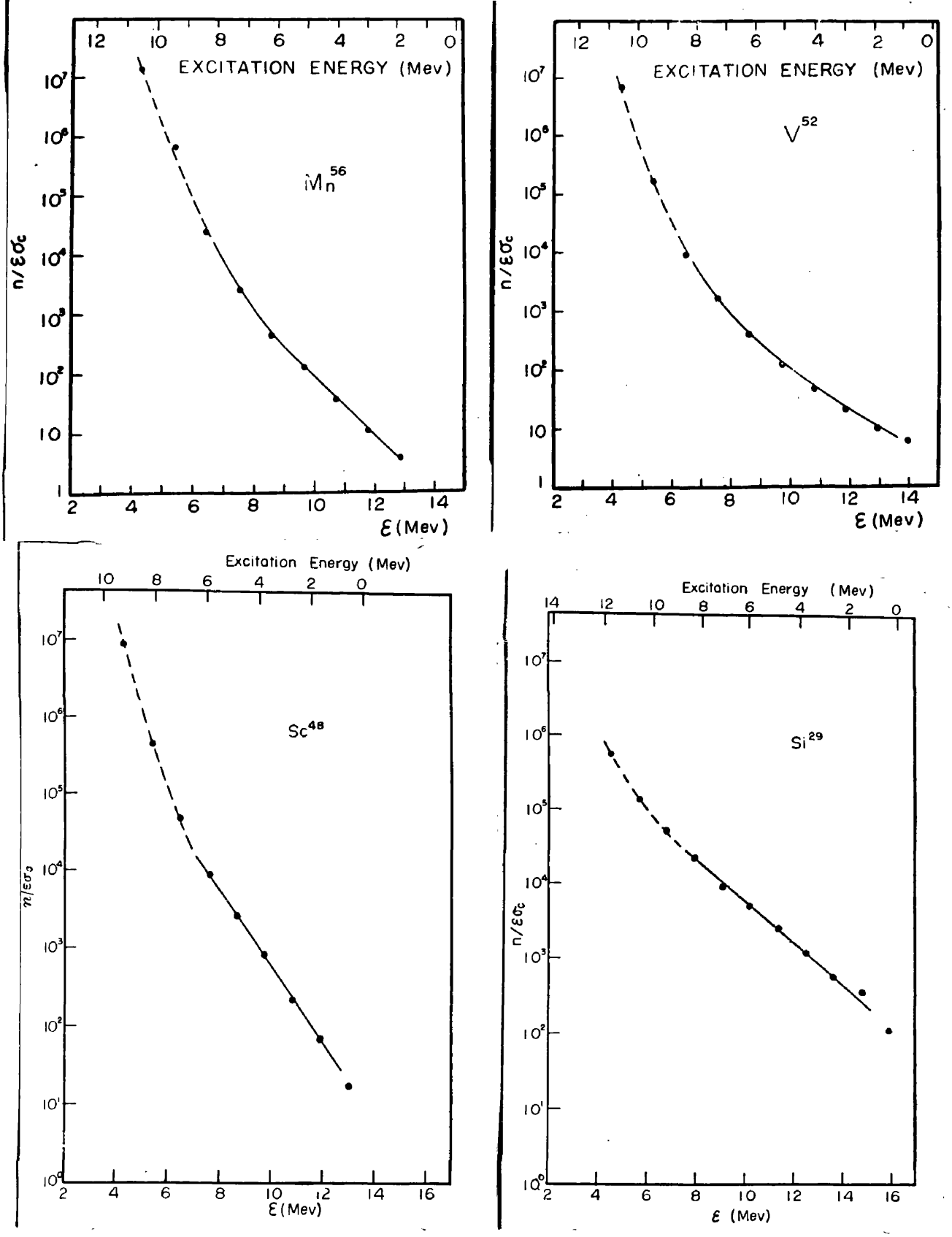

Fig. V.2 Statistical plots corresponding to the energy spectra in V.1. (Designations by residual nuclei). Kumabe et al. (ref. 36 & 37); Continuum model.

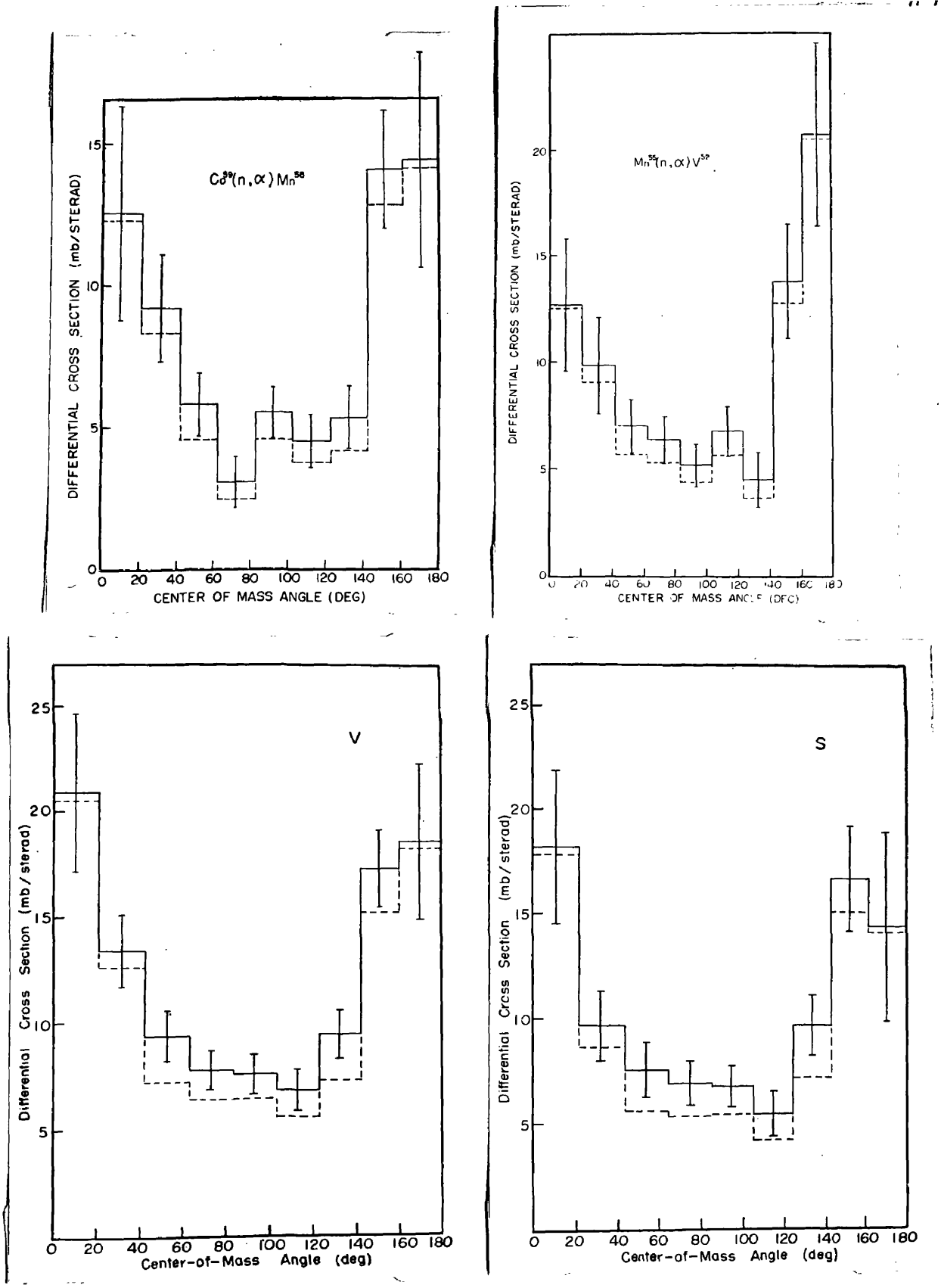

Fig. V.3 Angular distributions of alpha particles of all energies produced by 14.8 MeV (n,α) reactions in ^{55}Mn, ^{59}Co, ^{32}S and ^{51}V. Kumabe et al (ref. 36 & 37).

extremely well with those of Kumabe et al, as shown in fig. IV.15, page 97a. Also the 5^{o} and 90^{o} spectra shown in fig. IV.13, page 96a, are not contrary to the view that the shape of the spectrum does not change with angle. This approximately 90^{o} symmetry but marked anisotropy is difficult to understand on the basis of simple evaporation picture. Accerding to Kumabe et al, this (n,α) angular distribution is typical of even medium weight elements.

5.4 Conclusions

We have seen that with targets of medium weight elements, the low energy alpha particles find it easier to come out than would be expected from coulomb barrier restrictions. This suggests that the barrier to the emission of an alpha particle from an excited nucleus is lower than the values indicated by total reaction cross section measurements with nuclei in the ground state. This view is supported by the conclusions of Fulmer and Goodman, 1960 (ref. 73), based on their (p,α) experiments. If the barrier penetrabilities are very much larger than those assumed for σ_c values used by us, then a good part of the component shown as (n,n α) may belong to (n,α). It is unfortunate that for ^{64}Zn, where this component is dominating, activation measurements for (n,α) cannot be done.

The high cross-sections for (n,α) as a whole may also be explained on the basis of lowered coulomb barrier.

The small peak at the tail end of ^{54}Fe spectrum brings in mind the so called 'cluster model' and recent suggestions of Wilkinson (ref. 11) about the texture of nuclear surface, i.e. the presence of alpha particle groups in the surface (in a kind of dynamic equilibrium). However, we have very little data for any hypothesis of this nature.

Another picture of the (n,α) reaction mechanism can be taken as, the emission of the particle before the compound system has reached a proper thermodynamical equilibrium; but again the question may arise whether alpha particles exist in the nuclear surface.

The angular distribution is even harder to explain. It is quite important to do an extensive systematic study of angular distribtuions. If this 90^{o} symmetry ~~but~~ with marked anisotropy is a common feature of the (n,α) reaction, then probably the explanation will be found in angular momentum effects coupled with modified partial transmission coefficients for the barrier penetration.

Future Programme

In view of the successful runs on medium weight elements it is tempting to study as many isotope targets as possible. There is, however, greater urgency for studying the angular distributions. The counter telescopes designed in the present work have shown their limitations regarding any extensive study of the angular distributions and of the low yield targets. Remembering that the random coincidence considerations forced us to use rather low neutron flux, only $\sim 3 \times 10^7$ for energy spectra and $\sim 10^8$ for back angles, while we could conveniently obtain a flux of 2×10^9 (all figures for 4π), it is extremely desirable to remove this limitation.

If a second proportional counter is introduced, it is possible that with a triple coincidence arrangement, we may use so high a neutron flux, that on the balance it will be a gain against the loss in efficiency due to the increased target-crystal distance. Use of a differential discriminator on the $\frac{dE}{dx}$ counter, to limit the operation to a useful region, can be another improvement. If we are successful in improving the technique, we hope to undertake a series of angular distribution measurements.

Appendix I

The Luminescent Response of CsI(Tl) to Alpha Particles

Several workers have found that the response of crystals like CsI(Tl), NaI(Tl), KI(Tl), is apparently linear for protons but distinctly non linear for alpha particles of few MeV energy, and also that the light output due to alphas is less than that due to protons of the same energy. Amongst others, Halbert, 1957 (ref. 83) and Bashkin et al, 1958 (ref. 84) have studied the response of CsI(Tl) to alphas of low energies (up to $\sim$ 5 MeV). According to Fulmer and Cohen 1958 (ref. 72) the response of CsI(Tl) to alphas, is linear above $\sim$ 5 MeV and is displaced by about 1.5 MeV relative to the proton curve. However, Quinton et al, 1959 (ref. 85) have studied this response over a wide energy range of 2 - 40 MeV. (They also studied response to protons, ^{12}C, ^{14}N and ^{16}O). According to them non-linearity for alphas exists up to about 8 MeV, and the proton curve is displaced by about 2 MeV. For the region 2 - 8.8 MeV, Quinton et al used natural alphas from ThC-C', and for higher energies He^{++} ions were obtained from an accelerator.

To calibrate the crystals used by us in (n,α) experiments we have studied their response to alpha particles. We did this in the range 3.25 to 10.7 MeV. For 3.25 to 8.2

MeV we used ^{210}Po (5.3 MeV) and ThC-C′ (6.1 and 8.8 MeV) alpha particle groups. Aluminium absorbers in an evacuated chamber were used to vary the energy. (Range energy table of ref. 86 was used.) Above 8.2 MeV, points were obtained from $^{7}Li(d,\alpha)^{5}He$ and $^{6}Li(d,\alpha)^{4}He$, (Q, 14.2 and 22.24 MeV). A natural thin Li target was prepared by evaporation. Again, the alphas were detected in vacuum, and only those points were finally accepted which were unambiguously identified, by using Al absorbers, to be alphas.

Our results shown in fig. I are in general agreement with those of Quinton et al, shown in fig. II. The response is practically linear after about 8 MeV. If the curve by Quinton et al is normalized to ours at 8 MeV, very good agreement is found in the region 5 - 8 MeV. Below 5 MeV our curve is slightly higher; at 4 MeV the departure is about 11%. From D-D protons we have estimated that above 8 MeV for alphas, the proton curve is displaced by about 2.2 MeV, in the direction expected.

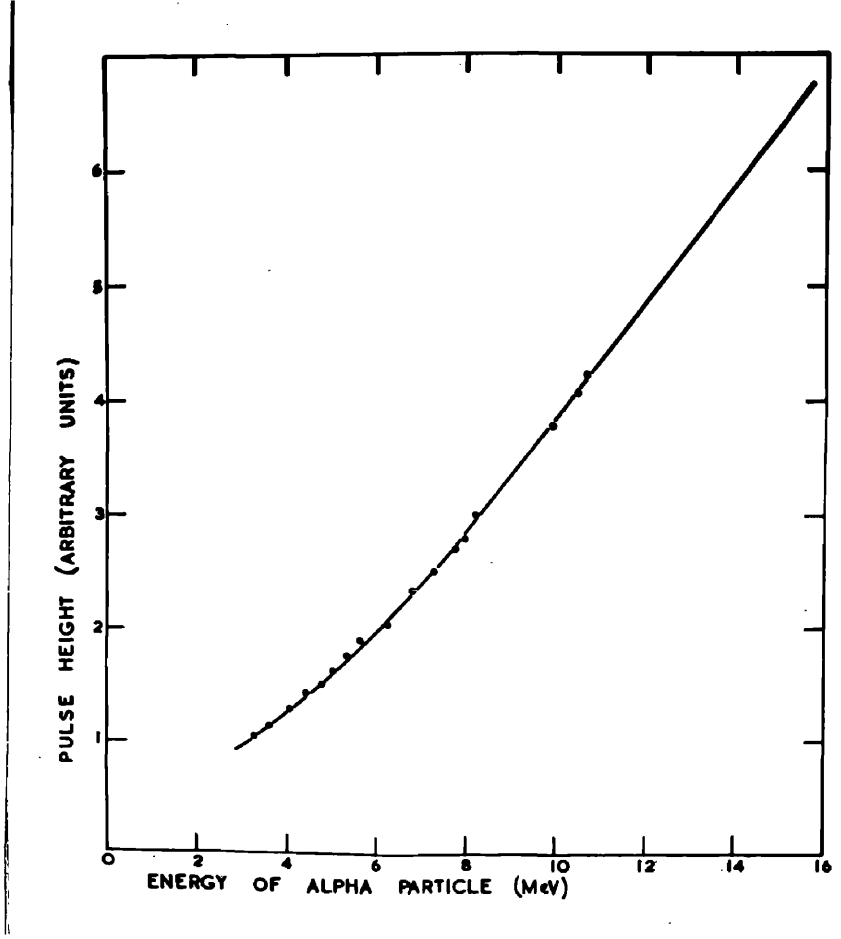

Fig. I

Response of CsI(Tl) to alpha particles (present work).

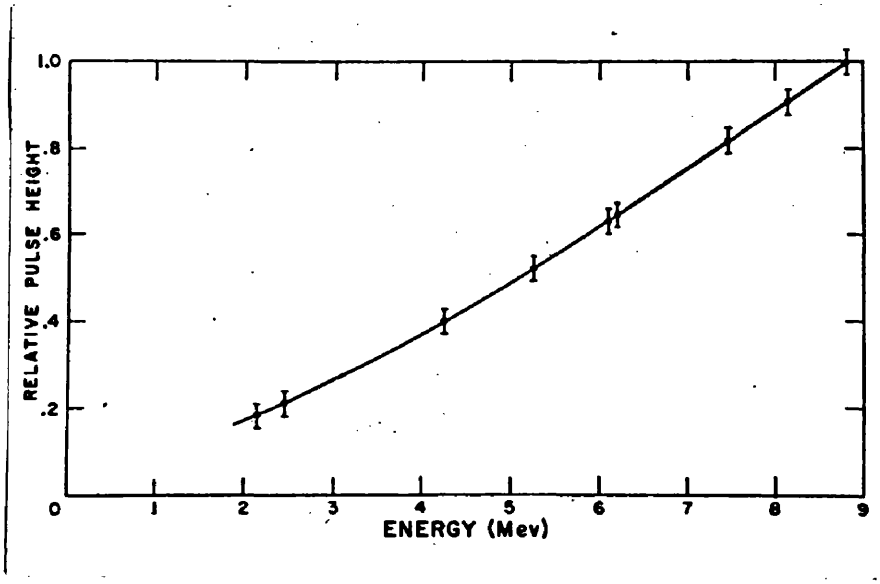

Fig. II.

Response of CsI(Tl) to alpha particles measured by Quinton (ref. 85).

Appendix II

Equation 1.19: Squaring both sides of equation 1.13, we get

$$\omega^2 = \frac{e^{2S}}{\theta^2 2\pi \frac{dE}{d\theta}}$$

Taking natural logarithm on both sides gives,

$$2 \log_e \omega = 2S - \log_e 2\pi - \log_e\left(\theta^2 \frac{dE}{d\theta}\right)$$

or

$$2 \frac{d}{dE}\left(\log_e \omega\right) = 2 \frac{dS}{dE} - \frac{d}{dE}\left(\log_e \left[\theta^2 \frac{dE}{d\theta}\right]\right)$$

Since $\frac{dS}{dE} = \frac{1}{\theta}$, we get

$$\frac{d}{dE}\left(\log_e \omega\right) = \frac{1}{\theta} - \frac{1}{2}\frac{d}{dE}\left(\log_e \left[\theta^2 \frac{dE}{d\theta}\right]\right)$$ which is eq.1.19

Equation 1.21: From the expression for $G_c(\beta)$ which describes the decay by particle 'b' into the single channel β only, we write down the corresponding expression for the branching ratio for decay by particle 'b' when several channels are open. We multiply by the density ω_y of the levels of Y, available for decay by the particle 'b', and integrate over the energy range of the emitted particle. Same procedure is adopted for the competing reactions X(a,i)W, and we get

$$G_c(b) = \frac{\int_0^{E_{bm}} k_b^2 \cdot \sigma_c(b) \cdot \omega_y(E_{bm} - E_b) \cdot dE_b}{\sum_i \int_0^{E_{im}} k_i^2 \, \sigma_c(i) \cdot \omega_W(E_{im} - E_i) \cdot dE_i}$$

where E_{bm} is the maximum energy with which the particle 'b'

can be emitted. Now $E_{bm} = E_a + Q_{ab}$ and $k^2 = \frac{2ME}{\hbar^2}$

By writing $G_c(b) = \frac{F_b}{\sum_i F_i}$ we get the form as given in 1.21.

There we put σ_c in more appropriate form, ie $\sigma_c(E_b)$

Equation 1.26: Now $\frac{dS}{dE} = \frac{1}{\theta}$; and if we use the approximation $T \simeq \theta$, we get $S = \log_e \omega$ (by using eq. 1.20)

Writing for the residual nucleus,

$$S_y(E_y) = \log_e \omega_y(E_y)$$

or $$\omega_y(E_y) = \exp S_y(E_y)$$

Substituting this value of $\omega_y(E_y)$ in the equation 1.23, we get, $$\frac{dN(E_b)}{dE_b} \propto E_b \cdot \sigma_c(E_b) \cdot \exp S_y(E_y) \quad \text{..... A}$$

But $S_y(E_y) = S_y(E_c - B_{bc} - E_b)$ and if $E_b \ll E_c - B_{bc}$,

by Taylor's expansion we get,

$$S_y(E_y) \cong S_y(E_c - B_{bc}) - E_b \left(\frac{dS_y}{dE_y}\right)_{E_y = E_c - B_{bc}} \quad \text{.....B}$$

Noting that $(E_c - B_{bc})$ is the maximum excitation energy for Y, and hence $\left(\frac{dS_y}{dE_y}\right)_{E_y = E_c - B_{bc}} = \frac{1}{T_m}$, we get from A and B,

$$\frac{dN(E_b)}{dE_b} \propto E_b \cdot \sigma_c(E_b) \exp\left[S_y(E_c - B_{bc}) - \frac{E_b}{T_m}\right]$$

or $$\frac{dN(E_b)}{dE_b} \propto E_b \cdot \sigma_c(E_b) \cdot \exp\left(-\frac{E_b}{T_m}\right)$$ which is eq. 1.26.

References

1. E. Fermi and E. Amaldi, Ric. Sci., A6 (1935) 544.
P.B. Moon and J.R. Tillman, Nature, 135 (1935) 904.
L.R. Hafstad and M.A. Tuve, Phys. Rev., 48 (1935) 306.
R. Frisch and G. Placzek, Nature, 137 (1936) 357.
Frisch, Hevesy and McKay, Nature, 137 (1936) 149.
2. N. Bohr, Nature 137 (1936) 344; Science 86 (1937) 161.
3. G. Breit and E.P. Wigner, Phys. Rev. 49 (1936) 519, and 642.
4. H.A. Bethe, Revs. Mod. Phys. 9 (1937) 69.
5. V.F. Weisskopf, Phys. Rev. 52 (1937) 295.
6. H.A. Bethe and G. Placzek, Phys. Rev. 51 (1937) 450.
7. V.F. Weisskopf and D.H. Ewing, Phys. Rev. 57 (1940) 472.
8. P.L. Kapur and R.E. Peierls, Proc. Roy. Soc. (London), A166 (1938) 277.
9. E.P. Wigner and L. Eisenbud; Phys. Rev. 72 (1947) 29.
10. H.H. Barschall, Phys. Rev., 86 (1952) 431; Am. Jour Phys. 22 (1954) 517.
N. Nereson and S. Darden, Phys. Rev. 89 (1953) 775; ibid, 94 (1954) 1678.
11. H. Feshbach, C.E. Porter and V.F. Weisskopf, Phys. Rev. 90 (1953) 166; ibid, 96 (1954) 448.
12. A.M. Lane, R.G. Thomas and E.P. Wigner, Phys. Rev. 98 (1955) 693.

13. H. Feshbach, D.C. Peaslee and V.F. Weisskopf, Phys. Rev. 71 (1947) 145.

14. H. Feshbach and V.F. Weisskopf, Phys. Rev. 76 (1949) 1550.

15. V.F. Weisskopf, Helv. Phys. Acta, 23 (1950) 187.

16. J.M. Blatt and V.F. Weisskopf, Theoretical Nuclear Physics (John Wiley & Sons) 1952 p.353 and 372.

17. G. Igo, Phys. Rev. 115 (1959) 1665.

18. H.A. Bethe, Phys. Rev. 50 (1936) 332.

19. H.A. Bethe, Revs. Mod. Phys. 9 (1937) 79.

20. E. Fermi, (notes compiled by Orear, Rosenfeld and Schluter) "Nuclear Physics", University of Chicago Press, 1950.
T.P. Kohman, Phys. Rev. 85 (1952) 350.

21. J.M.B. Lang and K.J. Le Couteur, Proc Phys. Soc. A67 (1954) 585.

22. T.D. Newton, Canad. Jour. Phys. 34 (1956) 804.

23. N. Austern, S. Butler and H. McManus, Phys. Rev. 92 (1953) 350.

24. J.L. Yntema, B. Zeidman and B.J. Raz, Phys. Rev. 117 (1960) 801.

25. D.M. Chase, L. Wilets and A.R. Edmonds, Phys. Rev. 110 (1958) 1080.

26. S. Hayakawa, M. Kawai and K. Kikuchi, Progr. Theoret. Phys. Japan, 13 (1955) 415.

27. G. Brown and H. Muirhead, Phil Mag. 2 (1957) 473.

28. S.T. Butler, Proc. Roy. Soc. A208 (1951) 559.

29. A.B. Bhatia, K. Huang, R. Huby and H.C. Newns, Phil Mag. 43 (1952) 485.

30. Ajzenberg and Lauritsen, Revs. Mod. Phys. 24 (1952) 321.

31. Arnold, Phillips, Sawyer, Stovall and Tuck, Phys. Rev. 93 (1954)483.

32. R.S. Storey, W. Jack and A. Ward Proc. Phys. Soc. 75 (1960) 526.

33. F.L. Ribe and W. Davis, Phys. Rev. 99 (1955) 331.

34. F.L. Ribe and J.D. Seagrave, Phys. Rev. 94 (1954) 934.

35 & 36 I.Kumabe, E. Takekoshi, H. Ogata, Y. Tzuneoka and S. Oki, Phys. Rev. 106 (1957) 155, Jour. Phys. Soc. Japan, 13 (1958) 129).

37. I. Kumabe, Jour, Phys. Soc. Japan 13(1958) 325.

38. M. Cevolani, S. Petralia, B. Righini, U. Valdre and G. Venturini, Nuovo Cim. 16 (1960) 950.

39. J.C. Robertson and A. Ward, Proc. Phys. Soc. 73 (1959) 523.

40. J.C. Robertson, Ph.D. Thesis, Glasgow University, 1961.

41. L. Wolfenstein, Phys. Rev. 82 (1951) 690.

42. W. Hauser and H. Feshbach, Phys. Rev. 87 (1952) 366.

43. T. Ericson and V. Strutinski, Nuc. Phys. 8 (1958) 284.

44. T. Ericson and V. Strutinski, Nuc. Phys. 9(1958/59)689. (addendum to ref. 43).

45. T.Ericson, Advances in Physics, 9 (1960) 425.

46. J.M. Peterson, Phys. Rev. (to be published).

47. N.O. Lassen and N.O. Roy Poulsen, Proc. of the Inter Conf. on Nuc, Phys., Paris July 1958 (Compiled by Gugenberger) p.477.

48. R. Fox and R.D. Albert, Phys. Rev. 121 (1961) 587.

49. E.B. Paul and R.L. Clarke, Canad. Jour Phys. 31(1953) 267.

50. H.G. Blosser, C.D. Goodman, T.H. Handley and M.L. Randolph, Phys. Rev. 100 (1955) 429. Phys. Rev. 110 (1958) 531.

51. R.F. Coleman, B.E. Hawker, L.P. O'Conner and J.L. Perkin, Proc. Phys. Soc. 73 (1959) 315.

52. E. Weigold, Austr. Jour Phys. 13 (1960) 186.

53. M. Bormann and R. Langkau (Private Communication).

54. M.M. Shapiro, Phys. Rev. 90 (1953) 171.

55. D.L. Allan, Nuc. Phys. 24 (1961) 274.

56,57 and 58 P.V. March, and W.T. Morton, Phil Mag. 3 (1958) 143, 577, 1256.

59, 60 and 61. D.L. Allan, Proc Phys. Soc. A70 (1957)195, Nuc. Phys. 6 (1958) 464, ibid, 10 (1959) 348.

62. W. Jack and A. Ward, Proc. Phys. Soc. 75 (1960) 833.

63. L. Colli, M. Pignanelli, A. Rytz and R. Zurmuhle, Nuovo Cim. 9 (1958) 280.

64. L. Colli, U. Facchini, I. Iori, M.G. Marcazzan and A.M. Sona, Nuovo Cim. 13 (1959) 730.

65. L. Colli, F. Cvelbar, S. Micheletti and M. Pignanelli, Nuovo Cim. 13 (1959) 868.

66. L. Colli, F. Cvelbar, S. Micheletti and M. Pignanelli, Nuovo Cim., 14 (1959) 81.

67. L. Colli, I. Iori, M.G. Marcazzan, F. Merzari, A.M. Sona and P.G. Sona, Nuovo Cim. 17 (1960) 634.

68. L. Colli, S. Micheletti, M. Pignanelli and I. Iori, Nuovo Cim. 20 (1961) 94.

69. L. Colli, I. Iori, S. Micheletti and M. Pignanelli, Nuovo Cim. 21 (1961) 966.

70. I. Kumabe and R.W. Fink, Nuc. Phys. 15 (1960) 316.

71. R.A. Peck Jr. Phys. Rev. 123 (1961) 1738.

72. C.B. Fulmer and B.L. Cohen, Phys. Rev. 112 (1958) 1672.

73. C.B. Fulmer and C.D. Goodman, Phys. Rev. 117 (1960) 1339.

74. R. Sherr and F.P. Brady, Phys. Rev. (to be published).

75. P.H. Stelson and C. Goodman, Phys. Rev. 82 (1951) 69.

76. B.G. Whitmore and G.E. Dennis, Phys. Rev. 84 (1951) 296.

77. E.R. Graves and L. Rosen, Phys. Rev. 89 (1953) 343.

78. L. Rosen and L. Stewart,Phys. Rev. 99 (1955) 1052.

79. W. Swenson and N. Cindro, Phys. Rev. 123 (1961) 910.

80. I. Kumabe, A.D. Poularikas, I.L. Preiss, D.G. Gardner and R.W. Fink, Phys. Rev. 117 (1960) 1568.

81. D.R. Koehler and W.L. Alford, Phys. Rev. 119 (1960) 311.

82. W.H. Sullivan, Trilinear Chart of Nuclides, A.E.C., U.S.A. January 1957.

83. M.L. Halbert, Phys. Rev. 107 (1957) 647.

84. S. Bashkin, R.R. Carlson, R.A. Douglas and J.A. Jacobs, Phys. Rev. 109 (1958) 434.

85. A.R. Quinton, C.E. Anderson and W.J. Knox, Phys. Rev. 115 (1959) 886.

86. W. Whaling, Handbuch der Physik, edited by S. Flugge (Spruiger-Verlag, Berlin, 1958), Vol 34, p.210 &213.

87. L.R.B. Elton and L.C. Gomes, Phys. Rev. 105 (1957)1027.

88. B.L. Cohen, Phys. Rev. 105 (1957) 1549.

89. B.L. Cohen and A.G. Rubin, Phys. Rev. 111 (1958) 1568.

90. J.L. Yntema and B. Zeidman, Phys. Rev. 114 (1959) 815.

91. B.L. Cohen, Phys. Rev. 116 (1959) 426.

92. D.R. Sweetman and N.S. Wall, Proc. of the Inter. Conf. on Nuc. Physics, Paris July 1958 (Compiled by Gugenberger) p. 549.

93. H.W. Fulbright, N.O. Lassen and N.O. Roy Poulsen, Mat. Fys. Medd, Dan. Vid. Selsk, 31 (1959) No. 10.

94. D.K. McDaniels, J.S. Blair, S.W. Chen and G.W. Farwell, Nuc. Phys. 17 (1960) 614.

95. M. Grut, D.R. Sweetman and N.S. Wall, Nuc. Phys, 17 (1960) 655.

96. B.L. Cohen and R.E. Price, Phys. Rev. 123 (1961) 283.

97. J.S. Blair, Phys. Rev. 115 (1959) 928.

98. T. Tamura and T. Terasawa, Progr. Theoret. Phys. Japan, 26 (1961) 285.

99. F.L. Ribe, Phys. Rev. 103 (1956) 741.

100. P.C. Gugelot, Phys. Rev. 93 (1954) 425.

101. N.O. Lassen and V.A. Sidorov, Nuc. Phys. 19 (1960) 579.

102. F.S. Houck and J.M. Miller, Phys. Rev. 123 (1961) 231.

103. I. Dostrovsky, P. Rabinowitz and R. Bivins, Phys. Rev. 111 (1958) 1659.

104. G.M. Marcazzan, E. Menichella Setta and F. Tonolini, Nuovo Cim. 20 (1961) 903.

105. S.J. Bame Jr. E. Haddad, J.E. Perry Jr. and R.K. Smith, Rev. Sci. Instr. 28 (1957) 997.

106. A.B. Lillie, Phys. Rev. 87 (1952) 716.

107. J. Heidmann and H.A. Bethe, Phys, Rev. 84 (1951) 274.

108. S. Yasumi, Jour Phys. Soc. Japan, 12 (1957) 443.

109. Grundl Henkel and Perkins, Phys. Rev. 109 (1958) 425.

110. A. Poularikas and R.W. Fink, Phys. Rev. 115 (1959) 989.

111. S.K. Mukherjee, A.K. Ganguly and N.K. Majumdar, Proc. Phys. Soc. 77 (1961) 508.

112. P. Strohal, N. Cindro and B. Eman, Rutherford Jubilee Inter. Conf. Manchester, Sep. 1961.

113. L. Colli, U. Facchini and S. Micheletti, Nuovo Cim. 5 (1957) 502.

114. D.H. Wilkinson, Phil Mag., 4 (1959) 215.
Proc. of the Kingston Conf. on Nuc. Structure, 1960, University of Toronto press, (Edited by D.A. Bromley and E.W. Vogt) P. 20; Rutherford Jubilee Inter. Conf. Manchester, Sept. 1961.

115. R.G. Moore Jr. Revs. Mod Phys. 32 (1960) 101.
A.M. Lane and R.G. Thomas, Revs. Mod Phys. 30 (1958) 257.
G.E. Brown, Revs. Mod Phys. 31 (1959) 893.
B.B. Kinsey, Handbuch der Physik (Edited by Flugge) Springer-Verlag Berlin 1957, Vol. 40, p. 202.
K.J. Le Couteur, Nuclear Reactions, Vol 1, 1959, (Edited by Endt and Demeur) p. 318.
P.C. Gugelot, ibid, p. 391.
T. Ericson (ref. 45).

116. S.T. Butler, Phys. Rev. 106 (1957) 272.

117. S. Hawakawa and S. Yoshida, Progr. Theoret Phys. Japan, 14 (1955) 1.

118. C.A. Levinson and M.K. Banerjee, Ann. Phy, 2 (1957) 471; 2(1957) 499; 3(1958) 67.

AUTHOR INDEX

Cohen and Rubin; 1958 (ref. 89).

Coleman et al; 1959 (ref. 51).

Colli et al; 1957;58;59;60;61 (ref. 113;63;64;65;66;67;68;69).

Crut et al; 1960 (ref. 95).

Dostrovsky et al; 1958 (ref. 103).

Elton and Gomes; 1957 (ref. 87).

Ericson; 1960 (ref. 45 and 115).

Ericson and Strutinski; 1958;58/59 (ref. 43;44).

Fermi; 1950 (ref. 20).

Fermi and Amaldi; 1935 (ref. 1).

Feshback et al; 1947;53;54 (ref. 13;11).

Feshbach and Weisskopf; 1949 (ref. 14).

Fox and Albert; 1961 (ref. 48).

Frisch et al; 1936 (ref. 1).

Frisch and Placzek; 1936 (ref. 1).

Fulbright et al; 1959 (ref. 93).

Fulmer and Cohen; 1958 (ref. 72).

Fulmer and Goodman; 1960 (ref. 73).

Graves and Rosen; 1953 (ref. 77).

Grundl et al; 1958 (ref. 109).

Gugelot; 1954 (ref. 100).

Gugelot; 1959 (ref. 115).

Hafstad and Tuve; 1935 (ref. 1).

Halbert; 1957 (ref. 83).

Hauser and Feshbach; 1952 (ref.42).

Hayakawa et al; 1955 (ref. 26).
Hayakawa and Yoshida; 1955 (ref. 117)
Heidmann and Bethe; 1951 (ref. 107).

Houck and Miller; 1961 (ref. 102).

Igo; 1959 (ref. 17).

Jack and Ward; 1960 (ref. 62).

Kapur and Peierls; 1938 (ref. 8).

Kinsey; 1957 (ref. 115).

Koehler; 1960 (ref. 81).

Kohman; 1952 (ref. 20).

Kumabe et al; 1957;58 (ref. 35;36).

Kumabe; 1958 (ref. 37).
Kumabe and Fink; 1960 (ref. 70)
Kumabe et al; 1960 (ref. 80).

Lane et al; 1955 (ref. 12).

Lane and Thomas; 1958 (ref. 115).

Lang and Le Couteur; 1954 (ref. 21).

Lassen and Roy Poulsen; 1958 (ref. 47).

Lassen and Sidorov; 1960 (ref. 101).

Le Couteur; 1959 (ref. 115).
Levinson and Banerjee; 1957,58 (ref. 118)
Lillie; 1952 (ref. 106).

Marcazzan et al; 1961 (ref. 104).

March and Morton; 1958 (ref. 56;57;58).

McDaniels et al; 1960 (ref. 94).

Moon and Tillman; 1935 (ref. 1).

Moore; 1960 (ref. 115).

Mukherjee et al; 1961 (ref. 111).

Nereson and Darden; 1953;54 (ref. 10).

Newton; 1956 (ref. 22).

Paul and Clark; 1953 (ref. 49).

Peck Jr; 1961 (ref. 71).

Peterson; (ref. 46).

Poularikas and Fink; 1959 (ref. 110).

Quinton et al; 1959 (ref. 85).

Ribe;1956 (ref. 99).

Ribe and Davis; 1955 (ref. 33).

Ribe and Seagrave; 1954 (ref. 34).

Robertson; 1961 (ref. 40).

Robertson and Ward; 1959 (ref. 39).

Shapiro; 1953 (ref. 54).

Sherr and Brady; (ref. 74).

Stelson and Goodman; 1951 (ref. 75).

Storey et al; 1960(ref. 32).

Strohal et al; 1961 (ref. 112).

Sullivan, 1957 (ref. 82).

Sweetman and Wall; 1958 (ref. 92).

Swenson and Cindro; 1961 (ref. 79).

Tamura and Terasawa; 1961 (ref. 98).

Weigold; 1960 (ref. 52).